



THE UNIVERSITY OF
WAIKATO
Te Whare Wānanga o Waikato

Research Commons

<http://researchcommons.waikato.ac.nz/>

Research Commons at the University of Waikato

Copyright Statement:

The digital copy of this thesis is protected by the Copyright Act 1994 (New Zealand).

The thesis may be consulted by you, provided you comply with the provisions of the Act and the following conditions of use:

- Any use you make of these documents or images must be for research or private study purposes only, and you may not make them available to any other person.
- Authors control the copyright of their thesis. You will recognise the author's right to be identified as the author of the thesis, and due acknowledgement will be made to the author where appropriate.
- You will obtain the author's permission before publishing any material from the thesis.

Field data Collection for Implementation of Supercapacitor Assisted LED Lighting (SCALED)

A thesis

submitted in partial fulfilment

of the requirements for the degree

of

Master of Engineering

at

The University of Waikato

by

TENZIN NORBU



THE UNIVERSITY OF
WAIKATO
Te Whare Wānanga o Waikato

2018

Abstract

With the increasing impact of global warming, climate change is becoming the biggest threat for all life on our planet. The conventional way of generating electricity from the burning of fossil fuels releases significant amounts of carbon dioxide to the atmosphere, which contributes to the rise in the earth's temperature. Moreover, fossil fuels are being consumed very rapidly and we now have limited resources, which need to be monitored to face future energy demands. The development of renewable energy sources, such as solar power, is a rapidly growing technology. With the extensive research and investment in this industry at present, in the near future solar power will be one of our leading renewable energy sources. Furthermore, as solar panels directly produce direct current (DC), they can be directly tied to a DC microgrid without requiring any power converter, thereby minimizing losses and increasing efficiency.

The supercapacitor assisted light emitting diode (SCALED) converter is one of the new circuit techniques under development for low voltage light emitting diode (LED) systems at the University of Waikato. In this circuit, an LED is connected in series with the supercapacitor bank forming part of a resistor-capacitor (RC) charging loop. This is to avoid energy losses in the RC charging loop, which can create, in the worst case, a 50% loss. As the commonly used 12 V LEDs are internally DC operated devices, SCALED will be applicable in DC microgrids, which are the emerging technology in low voltage distribution systems.

The groundwork for this project requires various solar-related field data collection and simulations for the successful implementation of this innovative technique. Unlike a conventional power supply, solar power output directly depends on the solar irradiance level, which is very unpredictable. Given the unique behaviour of solar panel output, starting with a near constant current behaviour and changing over to a practical voltage source with an approximately constant array resistance, combining a supercapacitor bank and an LED lamp will be a challenge in developing the SCALED topology. In addition, proper field measurements and analysis of these characteristics are essential to develop more efficient and reliable SCALED circuits for DC microgrid applications.

Acknowledgements

Firstly, I would like to thank my parents for their unwavering support and help in bringing me up with so much love and care, and my wider family, for your moral support as I pursued my master's in engineering. Your ceaseless effort will be remembered throughout my life.

I would also like to express my immense gratitude to my thesis supervisor, Associate Professor Nihal Kularatna of the Faculty of Science and Engineering at the University of Waikato. It is due to his consistent effort and guidance that I have had the opportunity to complete this thesis. He has been very open and approachable, clarifying any questions and doubts I had, which made me comfortable throughout my study period.

I would also like to acknowledge Mrs. Margaret Bellingham from NIWA for providing me the solar radiation data and helping me to register for online database access. My thanks go also to Seema Singh for assisting me with technical difficulties that arose while accessing the database.

In addition, I thank Dr Jayathu Fernando for always being available for discussions and assistance, and Dilini Jayananda, who is working on the same project sharing a research load; her guidance as a PhD student is greatly appreciated

My thanks also go to Benson Chang, laboratory technician, for his consistent support in making the PCB board for the project, and to our faculty administrator Mary Dalbeth, and librarian Cheryl Ward for their support and guidance.

Finally, we are very grateful to the Ports of Auckland for letting us carry out measurements and providing the opportunity to demonstrate the initial SCALED circuit for DC microgrid application during their open day festival held in January 2018.

Table of Contents

Abstract	i
Acknowledgements	iii
Table of Contents	v
List of Figures	xi
List of Tables.....	xv
Nomenclature	xvii
Chapter 1: Introduction	1
1.1 Introduction	3
1.2 Objective	4
1.3 Thesis outline	5
Chapter 2: Background	9
2.1 Supercapacitor	11
2.1.1 Supercapacitor as energy storage device.....	12
2.1.2 Supercapacitor application	14
2.1.3 Supercapacitor-assisted topologies developed at University of Waikato.....	15
2.1.4 Supercapacitor assisted LED (SCALED)	16
2.1.5 SCALED techniques for DC microgrid	16
2.2 LED lamp	18
2.2.1 LED driver.....	19
2.2.2 LED lamp characteristic.....	20
2.3 New Zealand climate overview	22
2.3.1 Sunshine hour	22
2.3.2 Hamilton’s climate	23
2.3.3 Solar power in New Zealand.....	23
2.4 Solar energy.....	23
2.4.1 Solar cell.....	23

2.4.2	Photovoltaic module	24
2.4.3	Equivalent circuit of a solar PV cell	25
2.4.4	Solar PV module specification	27
2.4.5	PV module output curves.....	29
2.4.6	Maximum power point tracking (MPPT)	29
2.5	ELGAR TerraSAS PV simulator.....	31
2.5.1	Product overview	31
2.5.2	User interface.....	32
2.5.3	Simulator block diagram.....	33
2.5.4	Software.....	33
2.5.5	Basic I-V curve simulation	34
2.5.6	Irradiance and temperature profile.....	34
2.5.7	PV array modeling.....	35
2.6	DC microgrid	36
2.6.1	Application of DC microgrid.....	36
Chapter 3: Solar Data Collection.....		39
3.1	Solar irradiation data.....	41
3.2	Solar radiation and the earth's atmosphere.....	41
3.3	Measurement of solar irradiance.....	42
3.3.1	NIWA Solar radiation database	43
3.3.1.1	Obtaining solar irradiance data from NIWA	45
3.3.1.2	Unit conversion	48
3.3.2	Measurement using a solar power meter	48
3.4	Comparison between the measured irradiance data and the data from NIWA database	49
3.5	Creating irradiance-temperature profiles in the PV simulator.....	52
3.5.1	Modelling of irradiance-temperature profile in PV simulator	53
3.5.2	Creating an I-V curve in the PV simulator	54
3.5.3	PV array I-V curve.....	55

3.6	NIWA SolarView tool.....	57
3.7	Installation of 1.12 kW solar array.....	58
3.8	Energy storage for RE sources.....	61
3.9	Charging SC bank directly from solar power.....	61
Chapter 4: Energy Storage Devices & Supercapacitors.....		67
4.1	General overview.....	69
4.1.1	Impact of the open circuit voltage and internal resistance of an energy source.....	69
4.1.2	Maximum power transfer.....	71
4.1.3	Different types of ESDs.....	71
4.1.4	Technical specifications of ESDs.....	74
4.2	Rechargeable battery technology overview.....	75
4.2.1	Battery charging and discharging behavior.....	75
4.3	Supercapacitor.....	79
4.3.1	Supercapacitor charging and discharging behavior.....	81
4.4	Hybrid capacitor.....	84
4.5	Battery capacitor.....	85
4.6	Comparison between different types of SCs.....	86
4.6.1	Comparison of discharge current and voltage characteristics of different types of SCs.....	87
4.6.1.1	Discharge characteristics of SCs.....	88
4.6.1.2	Discharge characteristics of hybrid capacitor.....	89
4.6.1.3	Discharge characteristics of battery capacitor.....	89
4.6.2	Battery capacity versus SC capacity.....	91
Chapter 5: SCALED Circuit Concept Development and Initial Performance Test.....		95
5.1	Circuit concept development.....	97
5.2	Analysis of the charging behaviour of a capacitor.....	99
5.3	Inserting a useful resistance in the RC loop.....	103
5.4	SCALED circuit topology configuration.....	105

5.4.1	Basic circuit operation	106
5.4.2	Solar LED technique.....	107
5.4.3	SCALED circuit with solar LED technique	108
5.4.4	Ultracapacitor module from LS Mtron	109
5.5	Initial circuit testing	110
5.6	Port of Auckland DC microgrid research project	114
Chapter 6: Conclusion and Future Development		119
6.1	Conclusion	121
6.2	Future development	122
References		125
Appendices		129
7.1	Mean daily global radiation in mega jules per square meter of different places of New Zealand (source: NIWA).....	131
7.2	Mean Monthly total sunshine hours of various places of New Zealand (source: NIWA).....	133
7.3	Solar irradiance data measured at the University of Waikato using solar power meter from 10/12/2017 to 15/12/2017	135
7.4	Solar Irradiance data measured using solar power meter on 4/1/2018 (rainy day).....	138
7.5	Daily global solar radiation from 10/12/2017 to 15/12/2017 (source: NIWA).....	139
7.6	Rainy day solar irradiance data on 4/1/2018 (source: NIWA)	143
7.7	University of Waikato hourly irradiance data of an average year (source: NIWA).....	145
7.8	University of Waikato hourly irradiance data of an average season of an average year (source: NIWA)	154
7.9	SCALED circuit schematic.....	156
7.10	PCB layout (top layer)	157
7.11	PCB layout (bottom layer).....	157

List of Figures

Figure 2-1: Comparison of SCs and electrolytic capacitors in terms of energy and sizes	11
Figure 2-2: Relative performance in energy and power of different ESDs [4].....	13
Figure 2-3: Comparison of the rate of change of ESR of an SC and a type AA cell with discharge [3].....	14
Figure 2-4: Typical solar PV system for residential application.....	17
Figure 2-5: (a) SCALED topology concept block diagram (b) Pictorial view [11]	18
Figure 2-6: A simple LED device structure	19
Figure 2-7: Typical LED luminaire driver circuit with transient and surge energy protection devices [14]	19
Figure 2-8: A low voltage (12V) LED lamp package [15]	20
Figure 2-9: V-I characteristics of 5 W, 12 V, type: LDR16 LED lamp.....	21
Figure 2-10: Voltage vs luminance characteristics of 5 W, 12 V type: LDR16 LED lamp	21
Figure 2-11: New Zealand mean annual sunshine hours 1971 – 2000 [16].....	22
Figure 2-12: Silicon solar cell components [18]	24
Figure 2-13: Solar PV module [19].....	25
Figure 2-14: Electrical equivalent circuit of a solar cell (a) Open circuit voltage equivalent, (b) Short circuit equivalent	25
Figure 2-15: Equivalent circuit of a practical PV cell.....	26
Figure 2-16: Irradiance and temperature in the field affect instantaneous module output [21]	29
Figure 2-17: General configuration of a solar PV system with an MPPT controller	30
Figure 2-18: (a) The typical I-V characteristics curve. (b) I-V and P-V characteristic curves	31
Figure 2-19: ELGAR TerraSAS standalone PV simulator	32
Figure 2-20: System control tabs from the main screen	32
Figure 2-21: PV Simulator block diagram [23]	33
Figure 2-22: Simple three-steps basic I-V curve simulation.....	34

Figure 2-23: (a) Solar irradiance create profile table (b) Dynamic irradiance profile display	35
Figure 2-24: DC microgrid configuration [26].....	36
Figure 2-25: DC microgrid application [26]	37
Figure 2-26: (a) Installation and appliances today (b) Installation and appliances in the future, using a DC microgrid [26]	37
Figure 3-1: Map showing the amount of solar energy in hours received each day [1].....	41
Figure 3-2: Scattering of direct-beam solar radiation from the sun by the atmosphere [28]	42
Figure 3-3: Mean daily global radiation (W/m^2) in a range of New Zealand cities in an average year [16]	44
Figure 3-4: Mean daily sunshine hours in a range of New Zealand locations in an average year [16]	45
Figure 3-5: Climate database web-based application (CliFlo) login screen.....	45
Figure 3-6: Database query screen	46
Figure 3-7: Sample hourly global radiation data from Ruakura 2 Ews climate station.....	47
Figure 3-8: Sample sunshine hours data for Ruakura 2 Ews climate station	48
Figure 3-9: Solar power meter TM-206	49
Figure 3-10: Percentage variance between NIWA solar radiation data and manually recorded data on 10.12.2017, in cloudy weather	50
Figure 3-11: Percentage variance between NIWA solar radiation data and manually recorded data on 12.12.2017, in sunny weather	51
Figure 3-12: Percentage variance between NIWA solar radiation data and manually recorded data on 4.1.2018, in rainy weather.....	51
Figure 3-13: Sample irradiance-temperature profile on 1.1.2018	53
Figure 3-14: (a) Sample irradiance profile template of PV simulator (b) Sample irradiance curve created in PV simulator.....	54
Figure 3-15: (a) Screenshot of the simulator showing entry of PV panel data to create an I-V curve (b) The I-V curve and power curve of a 280 W Mitsubishi MLE series PV module.....	55
Figure 3-16: (a) PV Array programming for creating a PV array I-V curve (b) PV array I-V and power curve	56
Figure 3-17: PV Simulator system control user interface	56

Figure 3-18: SolarView address selection screen	57
Figure 3-19: SolarView output showing the cumulative energy in kWh/m ² showing the path of the sun.....	58
Figure 3-20: Solar panel configuration diagram	59
Figure 3-21: (a) PV panel configuration to get total output voltage of 96 V (b) Configuration at the output side to get total output voltage of 48 V	60
Figure 3-22: (a) 1.12 kW solar PV array installed at University of Waikato (b) Circuit breakers and isolators installed on the output side.....	60
Figure 3-23: Charging of 50.4 V, 166 F SC bank directly from solar PV array output.....	62
Figure 3-24: The charging voltage, charging current and corresponding irradiance level curves.....	64
Figure 4-1: (a) ESD represented by a constant voltage source and fixed internal resistance, (b) Closed circuit formed by the external load R_L [3]....	70
Figure 4-2: Energy storage technologies (source : EIA).....	72
Figure 4-3: Typical discharge curve of a rechargeable batteries [3].....	76
Figure 4-4: 12 V, 12 Ah lead acid Battery charging current and voltage characteristics	78
Figure 4-5: Discharging current and voltage characteristics of a lead acid battery using 20 W LED bank as load.....	79
Figure 4-6: Constructional difference between traditional capacitors and supercapacitors [4]	80
Figure 4-7: Distribution of ions in charged and discharged capacitor	81
Figure 4-8: Typical discharge characteristics of SCs.....	82
Figure 4-9: SC bank assembled using 16 SCs, each of 2.7 V, 1500 F.....	82
Figure 4-10: Supercapacitor charging voltage and current characteristics	83
Figure 4-11: SC discharging voltage and current characteristics using 20 W LED bank as load	84
Figure 4-12: Different SCs and batteries in terms of energy and power density [4]	85
Figure 4-13: Three different types of SCs.....	86
Figure 4-14: Experimental set up to obtain the discharge characteristics of different types of SCs	88
Figure 4-15: Discharge characteristics of 3000 F, 2.7 V, type: LSUC SC	88

Figure 4-16: Discharge characteristics of 7500 F, 2.8 V, type: ESD CAP CL hybrid capacitor	89
Figure 4-17: Discharge characteristics of 40000 F, 2.7 V, type: ESD CAP CB battery capacitor.....	90
Figure 4-18: Graph showing discharge energy in Wh against voltage of all three types of SCs	91
Figure 4-19: Comparison of the battery parameters and SC parameters.....	92
Figure 5-1: A basic RC circuit.....	97
Figure 5-2: Capacitor voltage and loop current versus time [11].....	98
Figure 5-3: (a) Parasitic resistance R_p in a simple RC circuit (b) R_p Broken down into three parts consisting of source internal resistance r_s , loop resistance r_l and series resistance (ESR) of the capacitance r_c [11]..	99
Figure 5-4: Capacitor charging circuit [11].....	99
Figure 5-5: Partial capacitor charging curve (bold curve) from time t_1 to t_2 [11]	101
Figure 5-6: (a) Insertion of a useful resistive load in the capacitor charging loop to increase the charging efficiency. (b) An additional switch to prevent overcharging of the capacitor [11].....	104
Figure 5-7: Overall efficiency of powering a useful load within a capacitor charging loop [11].....	105
Figure 5-8: (a) Initial SCALED circuit block diagram. (b) First SCALED prototype circuit diagram.....	106
Figure 5-9: (a) Block diagram of SC and LED arrangement. (b) Truth table of control signals [31]. (c) Second version of SCALED circuit topology with two identical SC and LED banks.....	108
Figure 5-10: Preliminary version of PCB developed for initial testing.....	109
Figure 5-11: 166 F 50.4 V Ultracapacitor from LS Mtron with specifications [6]	109
Figure 5-12: SCALED circuit testing set-up for initial testing	110
Figure 5-13: Preliminary testing result showing SC and LED banks voltage characteristics	113
Figure 5-14: University of Waikato SCALED project team	114
Figure 5-15: 40 ft container with DC microgrid research project prototype on display during 2018 annual POAL open day.....	115
Figure 5-16: POAL's DC microgrid research project highlighted in world ports sustainability program [32].....	116

List of Tables

Table 2-1: Comparison of typical electrolytic capacitor and SCs for their ESR values and other useful specifications [5]	12
Table 2-2: Comparison of the parameters between energy storage technologies [4]	13
Table 2-3: Module specification of Mitsubishi MLE series PV panel.....	28
Table 3-1: Irradiance-temperature data on 1.1.2018 (source: NIWA).....	52
Table 3-2: Measurement data of charging current, charging voltage and irradiance level	62
Table 4-1: 12 V, 12 Ah lead acid battery charging current and voltage measurement data	77
Table 4-2: 12 V, 12 Ah lead acid battery discharging current and voltage measurement data	78
Table 4-3: SC charging current and voltage measurement data	83
Table 4-4: SC discharging current and voltage measurement data.....	84
Table 4-5: Comparison of three different types of SCs	87
Table 4-6: Cumulative hourly discharge energy in Wh of all three types of SCs	90
Table 5-1: Measurement data of SC banks and LED banks voltages	111

Nomenclature

AC	Alternating Current
DC	Direct Current
DOD	Depth of Discharge
ESD	Energy Storage Device
EDLC	Electrochemical double-layer capacitor
ETEE	End to End Efficiency
EV	Electric Vehicle
Li-ion	Lithium Ion
LED	Light Emitting Diode
MOSFET	Metal-Oxide-Semiconductor Field-effect Transistor
MPPT	Maximum Power Point Tracking
NIWA	National Institute of Water and Atmospheric Research
PV	Photovoltaic
PCB	Printed Circuit Board
POAL	Ports of Auckland Limited.
RE	Renewable Energy
RC	Resistor-Capacitor circuit
SC	Supercapacitor
SOC	State of Charge

Chapter 1

Introduction

1.1 Introduction

With the impact of climate change becoming increasingly evident, energy generation from clean renewable energy sources is developing rapidly, and there is a particular interest in solar energy, which has become very popular in recent years. Solar energy is abundant, and findings have shown that the solar energy radiated from the sun in one and half hours is enough to meet the energy requirements of the whole world for a year [1] . Most of our household appliances are powered internally by DC, which requires various power converter stages that incur huge energy losses. Solar PV modules produce DC, which could be used directly to power certain loads without requiring any power converters, thus eliminating energy losses. Over the past few years, the cost of solar PV modules has decreased while their efficiency has increased, making solar power more affordable. This is mainly due to continuous developments in solar cell technology.

Solar energy in New Zealand had barely begun development prior to 2013 and even now, solar energy generation is less than 0.1% of the country's total electricity generation [2] . This is mainly because of scepticism about solar power systems and a lack of understanding of solar technology. The cost of installation of a PV system is also a major factor, along with the availability of reliable conventional energy generation systems such as geothermal and hydro power.

The intermittent nature of solar power means that storage devices such as batteries and supercapacitors play a vital role in the reliable operation of a solar power system. Therefore, it is very important to carry out a detailed study and analysis of the solar irradiance data for locations where solar PV modules are to be installed. Solar irradiance data were obtained from NIWA, which maintains the national climate database for New Zealand. As the data currently refers only to the closest climate station, hourly solar irradiance data was also measured manually at the University using a solar power meter to compare readings with the NIWA database to get more reliable data. Automated recording at this site was not possible as an automated data logger was not available. The data obtained from NIWA was found to be reliable enough to use for this project. Field data collection is an enormous manual task, in which periodic readings need to be obtained throughout the day, often in harsh environments.

Most solar PV panels have a module efficiency of only about 20%. Losses across other components in the PV system, such as the power converters, further reduce the end-to-end efficiency. However, the majority of household appliances work on DC and the power produced by a PV array is DC. Therefore, this project is mainly focused on eliminating the converters and making the DC available at load directly, thereby increasing the overall efficiency and making solar power systems more economical. As this project involves a team of researchers and clients from industries, my research covers only the field data collection and analysis required for the implementation of this project.

1.2 Objective

Solar energy is the most abundant renewable energy source in the world. Tapping into this renewable energy and making use of the emerging supercapacitor-based energy storage devices can provide a way to boost the usage of solar power. The overall objective of this project is to integrate SCALED into DC microgrid applications, which is a rapidly advancing technology. Making use of supercapacitors as energy storage elements is expected to radically increase the efficiency of solar PV systems.

The objective of my thesis was to conduct an accurate study, analysis and simulation of solar irradiance data, which is crucial for the implementation of this project. This is done by measuring solar irradiance on an hourly basis using a pyranometer, followed by modelling in a solar PV simulator to demonstrate the potential output of a physical solar terrestrial PV array. Solar data was also obtained from NIWA's database. The comparative analysis carried out on the solar data obtained from NIWA and the measured data using a solar power meter showed that NIWA's data was reliable and accurate. This further refined the accuracy and provided authentication of the irradiance data. This also provides a reliable basis for further testing and development of similar circuit topologies in a totally renewable environment, which is a growing area of interest worldwide.

1.3 Thesis outline

Chapter 1: Introduction.

This chapter introduces the main aim and objectives of this project. The threat of global climate change means it is high time to explore alternative renewable energy sources with a view to improving efficiency and reliability. As this project involves a team of researchers, my part in the project is briefly explained.

Chapter 2: Background.

This chapter provides a brief background on the supercapacitor and supercapacitor assisted circuit topologies that are being developed at the University of Waikato. The DC microgrid, LED characteristics, an overview of solar PV systems, a New Zealand climate overview, solar PV simulators and maximum power point tracking are also briefly covered in this chapter.

Chapter 3: Solar data collection and analysis.

This chapter details the ground work of the project, which includes the study of solar data collection, analysis and simulations. The procedures involved in obtaining irradiance data from NIWA's online database are explained. In the latter part of the chapter, the installation of a 1 kW solar PV array guided by NIWA's solar view tool is also covered. Finally, the charging characteristics of an SC when charged directly from the solar array are demonstrated, which are essential to this project.

Chapter 4: Energy storage devices and supercapacitors.

Here, the fundamentals of energy storage devices are explained with brief descriptions of various ESDs. Batteries are one of the oldest energy storage technologies and their popularity is growing rapidly in many applications. In contrast, supercapacitors are a rapidly emerging technology in energy storage technology and have already earned a place in numerous applications. The charging and discharging behaviour of both rechargeable batteries and supercapacitors are also explained. The final section of the chapter discusses the latest hybrid capacitor and its advantages over supercapacitors.

Chapter 5: SCALED circuit concept development and initial performance test.

The development of the SCALED circuit is discussed in this chapter. The initial circuit topology is tested, and observations are recorded and explained. The demonstration of this circuit prototype during the open day staged by the Ports of Auckland is also briefly covered in the final part of this chapter.

Chapter 6: Conclusion and future development.

Renewable energy sources in New Zealand include hydro, wind, geothermal, solar, biomass, biogas and liquid biofuels. Solar is currently only a small portion (0.2%) of total generation from renewable energy sources. Most places in New Zealand receive an average of at least 5 sunshine hours per day, which is good enough to install solar PV systems. The use of PV systems has been increasing rapidly in recent years.

A team of researchers at the University of Waikato is working on developing supercapacitor-assisted power converters and SCALED is one of the latest topologies under development. The team is currently working with the Ports of Auckland and an initial version of the circuit was successfully demonstrated at POAL's open day 2018 as an illustration of POAL's sustainability programme. This project looks at designing new types of MPPT charge controllers that are well-matched with SC and Solar PV arrays. This project has huge potential, with clients from many industries working together to develop a suitable technology for sustainable future energy sources.

Chapter 2

Background

2.1 Supercapacitor

Electrolytic capacitors are used in well-known applications such as DC blocking, filtering, temporary energy storage and building tuned circuits [3]. Newer families of capacitors called supercapacitors (SCs) or ultracapacitors are an emerging technology with exceptionally high power characteristics and longer useful lifetimes than conventional energy storage technologies such as lithium batteries [4]. Their capacitance value typically varies from 0.2 F to 7500 F, with relatively low voltages from 0.7 V to 4 V. With their larger energy density compared to other normal capacitors, SCs are mostly used as ESDs in many applications.

Figure 2-1 shows the comparison between SCs and conventional electrolytic capacitors in terms of their important parameters. It displays the value of the energy stored in each of the capacitors in comparison with their physical dimensions.



Figure 2-1: Comparison of SCs and electrolytic capacitors in terms of energy and sizes

The energy stored in capacitors is determined using the following equation:

$$E = \frac{1}{2} CV^2 \quad (2-1)$$

Where E - Energy stored in capacitor

C - Capacitance value of the capacitor

V - DC Voltage rating of the capacitor

Table 2-1: Comparison of typical electrolytic capacitor and SCs for their ESR values and other useful specifications [5]

ENERGY STORAGE LIMIT	CAPACITOR TYPE	MANUFACTURER	PARAMETERS			
			CAPACITANCE (μF)	TERMINAL VOLTAGE (V)	SHORT CIRCUIT CURRENT (A)	ESR (m Ω)
Less than 1J	Electrolytic	RSS	2200 μF	16	104	153
1-5 J	Supercap	Maxwell	1 F	2.7	3.85	700
		Cap-xx	2.4 F	2.3	115	20
	Electrolytic	Cornell Dubilier	2200 μF	50	704	71
5-50 J	Supercap	Maxwell	10 F	2.5	14	180
		Cap-xx	1.2 F	4.5	112.5	40
		Nesscap	10 F	2.3	33	70
	Electrolytic	Cornell Dubilier	82,000 μF	16	1441	11.1
		VICOR	270 μF	200	325	614
Above 50 J	Supercap	Maxwell	350 F	2.7	840	3.2
		Nesscap	120 F	2.3	144	16

2.1.1 Supercapacitor as energy storage device

The comparison between the energy density in Watthours per kg (Wh/kg) and power density in Watts per kg (W/kg) explains exactly where each of these ESDs lies on the graphical plot commonly known as a Ragone plot, as shown in Figure 2-2. SCs fall exactly in the middle of the diagonal line from the top left corner to the bottom right corner, showing their energy and power density values lie between those of batteries and electrolytic capacitors.

The complementary nature of batteries and SCs gave rise to new improved and cost-effective ESDs called hybrid capacitors, which occupy the space towards the upper right corner of the Ragone plot, as shown in Figure 2-2.

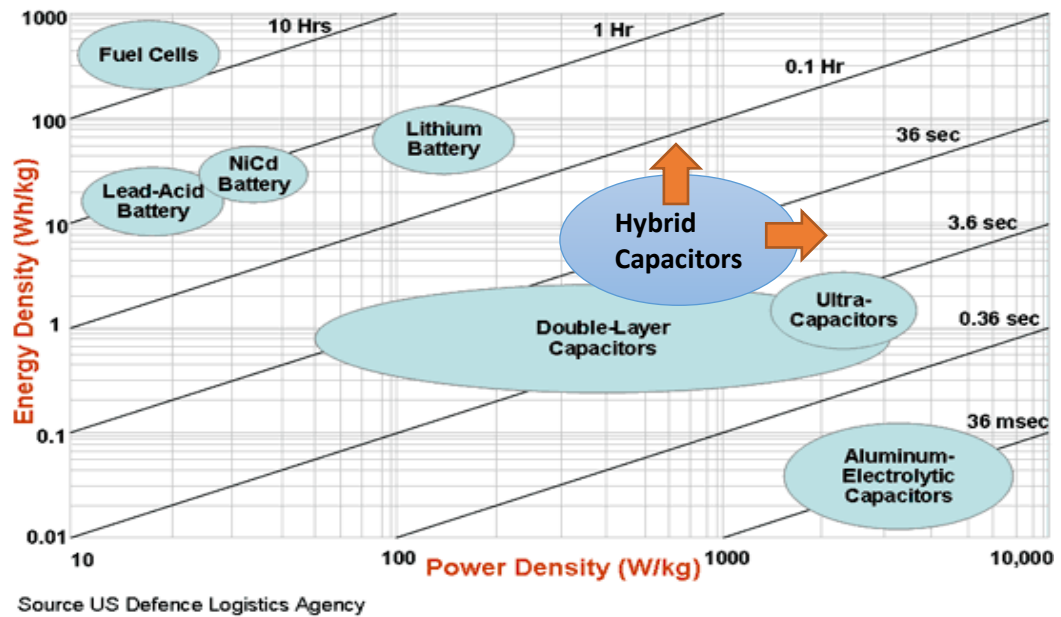


Figure 2-2: Relative performance in energy and power of different ESDs [4]

Table 2-2 shows the difference between ESDs in terms of their power density, energy density, cycles and temperature range. Extensive research is being conducted on hybrid capacitors and recently SAMWHA Capacitors from South Korea developed a high energy density battery capacitor of capacitance 40000 F with an energy density of 37 Wh/kg. The characteristics of this new, very high energy density battery capacitor are briefly covered in later chapters.

Table 2-2: Comparison of the parameters between energy storage technologies [4]

ESD type	Power density max (kW/kg)	Energy density max (Wh/kg)	Cycles	Temperature range
Li-ion battery	3	200	500 - 1000	0 to 60
Supercapacitor	10	10	1000000	-40 to 80
Hybrid SC	5	25	>10000	-20 to 60

Another important feature of SCs is their lower ESR compared to batteries and normal electrolytic capacitors. More interestingly, the ESR of SCs reduces as the capacitance value increases. Their ESR remains relatively constant over the discharge period and throughout the life span [3]. As a result, they can deliver higher power to the load than an electrochemical battery, where ESR keeps increasing with discharge as shown in Figure 2-3. The graph in Figure 2-3 demonstrates the change in ESR when both the devices are discharged at an approximate current of 1 A.

Even a small SC with a capacitance of 0.6 F could maintain an almost constant ESR of around 80 mΩ throughout its discharging period. In contrast the AA energizer cell shows an increasing ESR with an increasing depth of discharge.

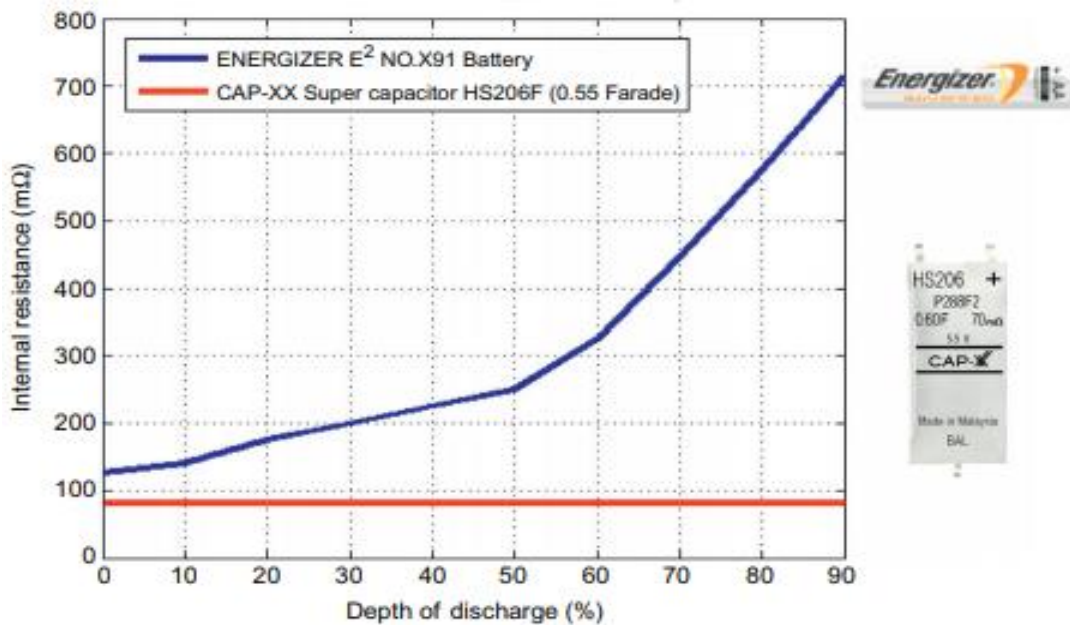


Figure 2-3: Comparison of the rate of change of ESR of an SC and a type AA cell with discharge [3]

2.1.2 Supercapacitor application

Some of the most prominent applications of SCs include [6]

1. Hybrid electric vehicle (HEV): To recapture braking energy and compensate peak power load thereby increasing efficiency, reliability and safety system of vehicle.
2. Fuel cell electric vehicle (FCEV): Compensate output load of the fuel cell by providing peak power.
3. Hybrid harbor crane: Regenerate the energy while lowering the container and provide output load compensation during the lifting of container.
4. Power quality solution: Increase power quality by fast reacting short term backup.
5. Photovoltaic and solar light: Provide energy for motor used in heliostats. Store energy generated from the sun during daytime and provide energy for lighting during night time.
6. Wind turbine: Increase the reliability of the pitch system by providing emergency power.

2.1.3 Supercapacitor-assisted topologies developed at University of Waikato

A research team in the school of Science and Engineering at University of Waikato has been developing SC-assisted electronic circuit topologies for almost a decade. Gradually, the team started to build some novel circuit topologies from basic theoretical concepts through to practical implementation. The circuit topologies developed so far are listed below:

1. SCALDO (Supercapacitor assisted low dropout regulator)
2. SCASA (Supercapacitor assisted surge absorber)
3. SCATMA (Supercapacitor assisted temperature modification apparatus)
4. SCAHDI (Supercapacitor assisted high density inverter)

The above circuit topologies are briefly explained as follows:

SCALDO was one of the very first applications developed by combining a low dropout linear voltage regulator with an SC or an array of SCs, achieving a significant improvement in the ETEE. This was granted a US patent in 2011. This successful technique provided a gateway to the development of many other SC-assisted applications.

One important application relies on the fact that SCs are capable of absorbing very high surges. This is due to their combination of large continuous energy ratings and very large time constants, allowing them to be used in surge protection circuits [7]. This circuit topology, named SCASA, has better surge handling capability than traditional surge protectors.

SCATMA is an instant water heating technique based on the use of stored SC energy to overcome the delayed delivery of hot water in domestic water systems [8]. This application makes use of the SC's feature of high power density, which enables it to deliver high levels of power for short periods.

SCAHDI was developed by placing a resistive inverter load in the capacitor charging loop to produce a high-density inverter [9]. This is done by splitting the inverter into two smaller inverters powered by putting them in series with discharged SC banks. This configuration allows the recovery of the fundamental energy loss that occurs during capacitor charging, thus increasing the overall efficiency. The total output of the system is the sum of the outputs from the two individual inverters.

2.1.4 Supercapacitor assisted LED (SCALED)

SCALED is one of the byproducts of the above supercapacitor-assisted circuit applications, which has led to another novel application in DC microgrid technology. As many domestic electrical appliances operate internally on DC, a locally operated DC microgrid using a renewable energy source such as solar power is a potential alternative to a traditional electricity supply. As an example, 12 V LED lamp arrays can be powered by a DC bus [10]. Inverter-driven white goods and air conditioners are other examples which encourage the use of DC microgrids at home. Recent solar technologies propose using SCs in parallel with battery banks to reduce the strain of large current extraction from the battery bank under heavy load conditions [9]. SC-based energy storage is also used to stabilize short-term power fluctuations due to the intermittent nature of solar energy supplies.

The concept of recovering significant amounts of energy loss by using a useful load like an LED in a capacitor charging loop is a new application, where the SC acts as a lossless dropper in the circuit. One early example of this is SCALDO, where an SC is placed in series with the input of a low dropout voltage regulator, producing a substantial improvement in ETEE. This same concept is applied to SCALED in building an efficient SC-assisted low voltage LED lighting system powered by solar energy.

2.1.5 SCALED techniques for DC microgrid

The existing solar PV systems for residential applications consist of the components shown in Figure 2-4. The ETEE is determined by the product of the individual efficiencies of each component, such as the charge controller, inverter and internal DC-DC converters in the various loads [11]. Rechargeable batteries are commonly used as energy storage systems in solar energy systems, as shown in Figure 2-4. The main advantage of a supercapacitor is that it can provide a quick burst of power with its fast charging and discharging capability, which enables it to handle peak power demands. In contrast, batteries are characterized by relatively slow charge and discharge with a continuous source of power. In addition, supercapacitors are very reliable and have a lifespan of millions of cycles.

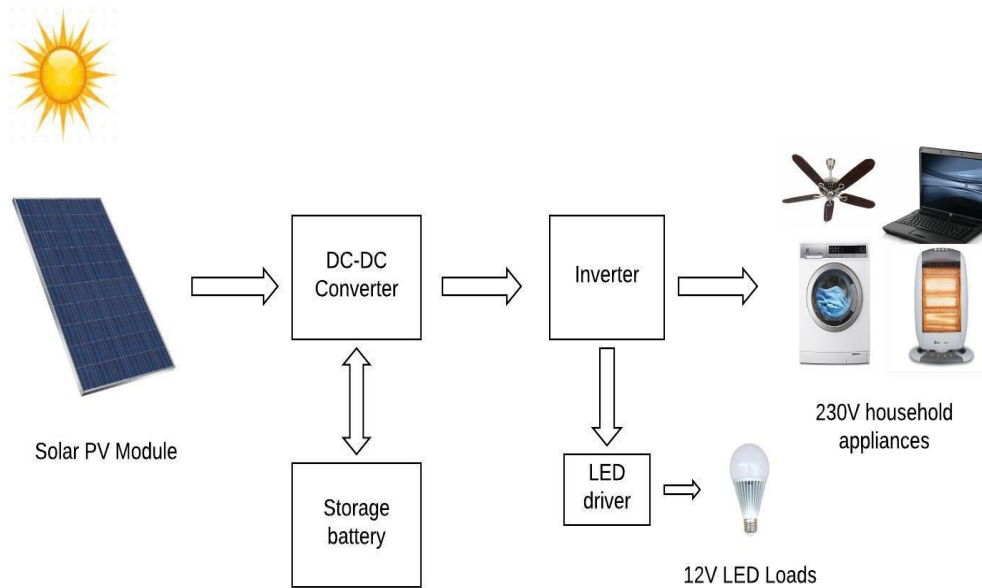


Figure 2-4: Typical solar PV system for residential application

Commercially available 12 V LED lamps can operate over a wide range of input voltages, maintaining the same brightness. This useful property can be combined with an SC bank in a DC microgrid environment fed by solar power to achieve high ETEE [11].

This arrangement is demonstrated in a simplified block diagram as shown in Figure 2-5 (a). Figure 2-5 (b) gives a pictorial representation of the SCALED circuit where the SC bank is connected in series with the LED load fed from the solar power source. The SC bank is used as the buffer to maintain the voltage in the LED's operating range during fluctuations in solar power. The loop resistance (R_L) here is the LED load making use of the energy which otherwise would be lost in the loop resistance.

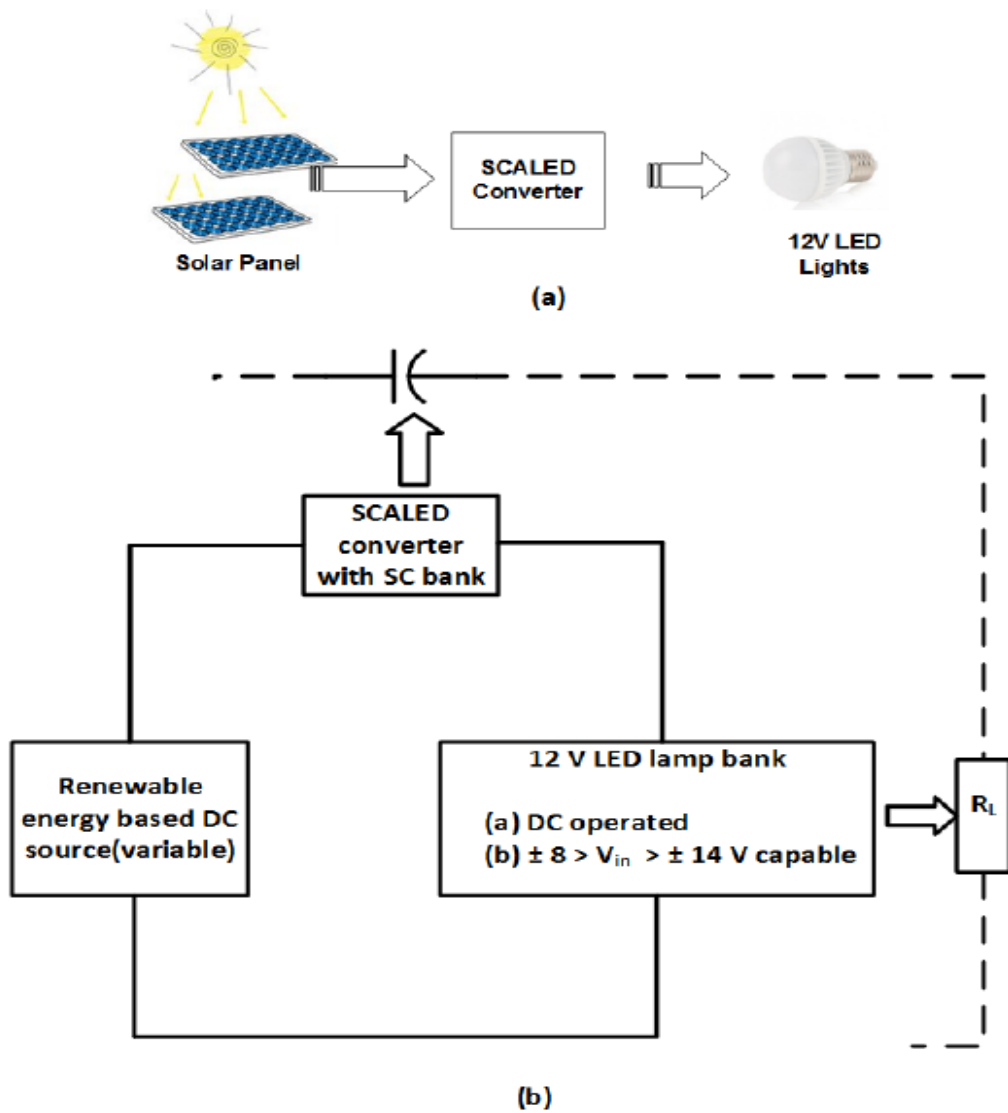


Figure 2-5: (a) SCALED topology concept block diagram (b) Pictorial view [11]

2.2 LED lamp

An LED lamp is a solid state light-emitting source comprised of a substrate base, a P-N junction diode and a protective glass or plastic enclosure, which emits light through a phenomenon called electroluminescence [12]. A simple LED device structure showing different layers with the direction of emitted light is shown in Figure 2-6.

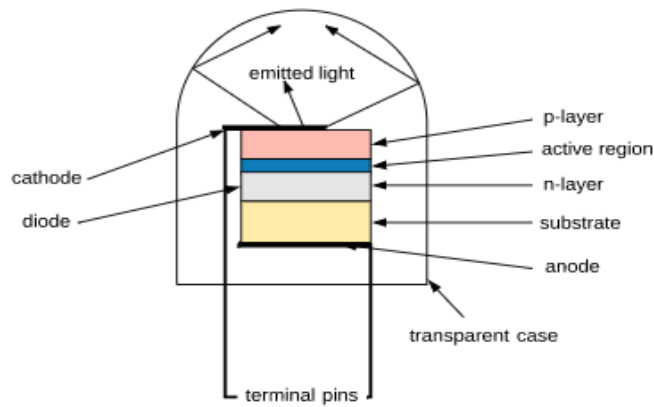


Figure 2-6: A simple LED device structure

Unlike traditional incandescent and fluorescent lamps, LED lamps are very efficient, with very low energy consumption and lifespans of over 10,000 hours. Moreover, they give instant brightness without needing to warm up like other conventional high-power lamps. In addition, their minimal maintenance and reducing cost makes them increasingly suitable for use and acceptance in the market [13].

2.2.1 LED driver

Nowadays, with the availability of LED lamps compatible with both AC and DC sources, they have become even more reliable, flexible and popular. This has been made possible by using a driver circuit that drives the lamp according to the source. A retrofit 230 V AC commercial LED lamp driver circuit is demonstrated in Figure 2-7 consisting of various components as explained.

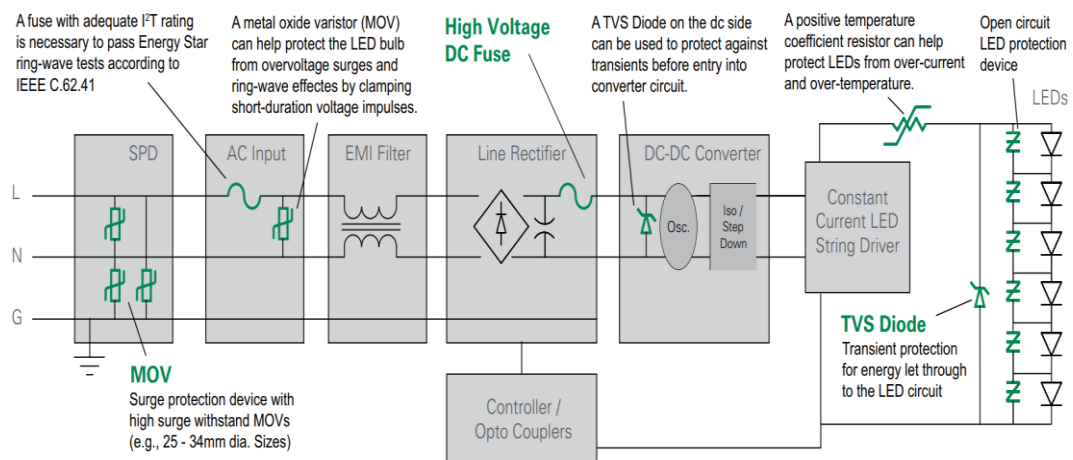


Figure 2-7: Typical LED luminaire driver circuit with transient and surge energy protection devices [14]

This LED driver regulates the output current that is delivered to the LED as the voltage varies. LED drivers are either based on an integrated circuit linear regulator or on a bipolar junction or field effect transistor operating in the linear region.

Figure 2-8 shows a typical low voltage LED driver circuit. The internal circuitry makes this lamp work with both AC and DC.

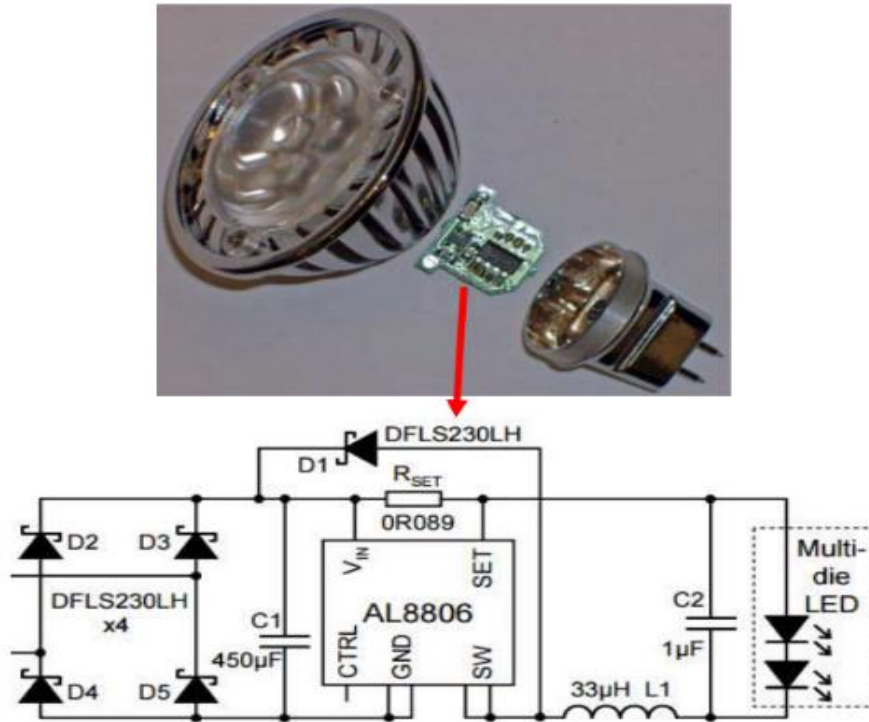


Figure 2-8: A low voltage (12V) LED lamp package [15]

2.2.2 LED lamp characteristic

A typical commercially available low voltage LED lamp (LDR16) was tested to obtain its performance characteristics. Figure 2-9 shows the V-I characteristics curve, where there is an approximately constant current region after initially drawing a high current. This current is limited by the driver circuit, which avoids damage to the bulb due to overheating.

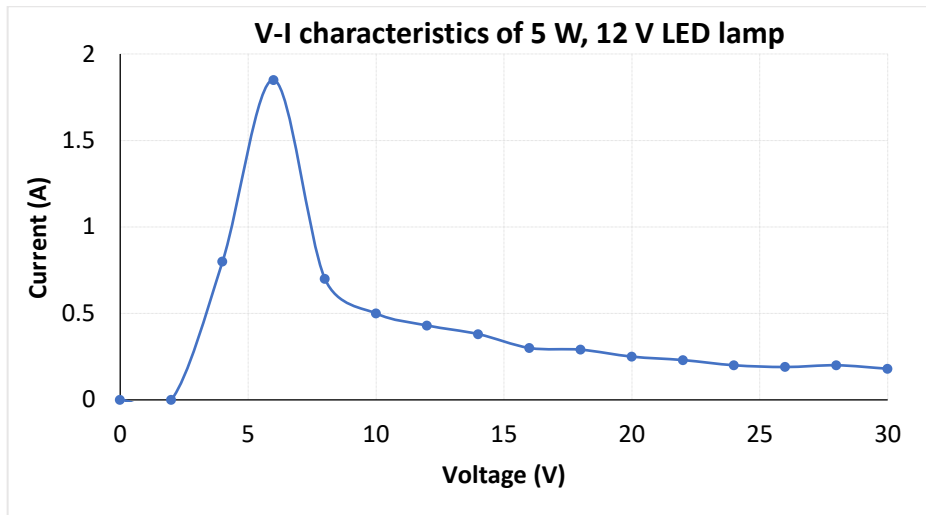


Figure 2-9: V-I characteristics of 5 W, 12 V, type: LDR16 LED lamp

Figure 2-10 shows the voltage against luminance curve, where there is a constant brightness region. As the applied voltage increases, the lamp brightness increases proportionally until it reaches a certain voltage and then settles down to a constant brightness regardless of further increase in voltage. The graph shows that LED lamps come with the useful performance characteristics of a wide range of constant current, and a constant brightness region which is of particular interest to this project.

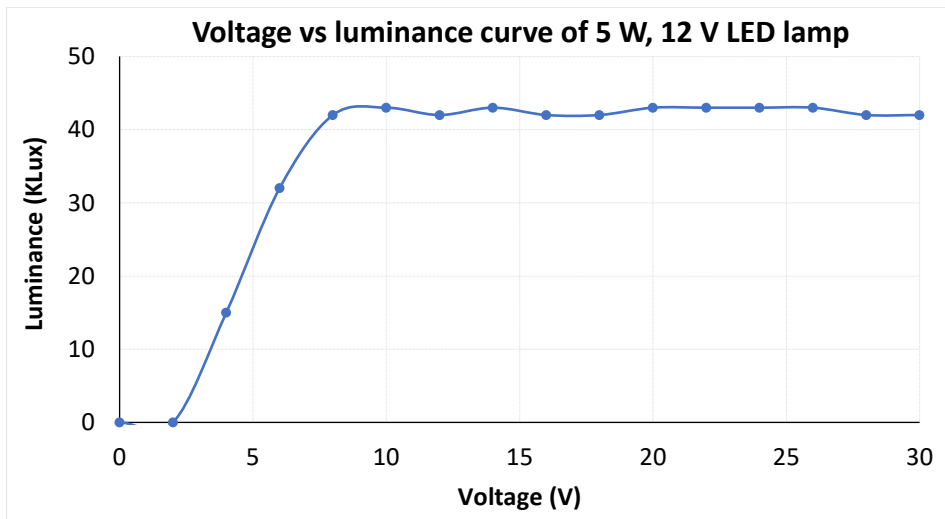


Figure 2-10: Voltage vs luminance characteristics of 5 W, 12 V type: LDR16 LED lamp

2.3 New Zealand climate overview

The climate of New Zealand is complex and varies from warm subtropical in the far north to cool temperate in the far south, with severe alpine conditions in the mountainous areas [16]. The country has four seasons with colder winters in the south, wet winters in the northern and central regions and warm, often dry summers. Most areas in the country receive between 600 mm and 1600 mm of rainfall annually. The mean annual temperature ranges from 10°C in the lower South Island to 16°C in the North Island. The temperature drops to below freezing point in mountainous areas and in the South Island, with some snow during the winter. The country's warmest month is usually January and the coldest is July, with very frequent changes in weather on a daily basis.

2.3.1 Sunshine hour

Sunshine hour is defined as the duration of sunshine in a given period at a given measurement panel. Sunshine hours are calculated depending on the angle of the sun, so an hour of sunshine during the morning may count as only half a sunshine hour. Most places in New Zealand record at least 2000 sunshine hours per year. This gives an average of 5 sunshine hours per day, which makes the installation of solar electric power systems feasible. Figure 2-11 shows the country's mean annual sunshine hours for 1971-2000. This is calculated from historical data recorded by NIWA at various stations throughout the country.

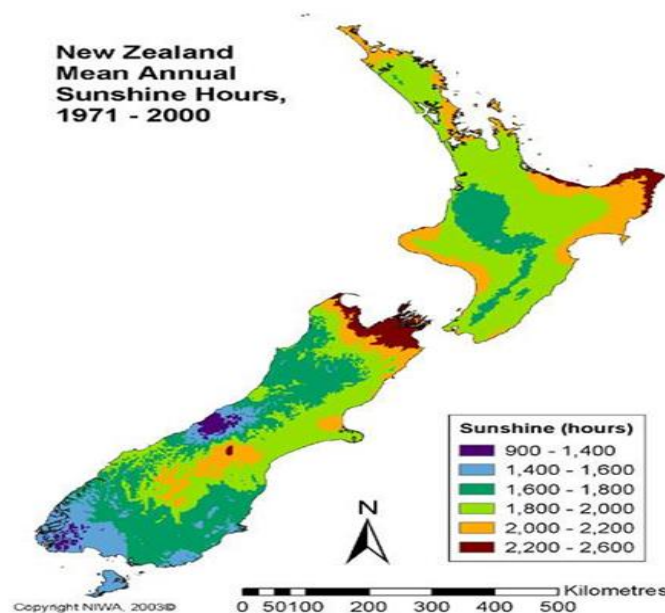


Figure 2-11: New Zealand mean annual sunshine hours 1971 – 2000 [16]

2.3.2 Hamilton's climate

Hamilton is in the Waikato region, which is in the Central North Island climate zone. It exhibits a range of climates due to the different landscapes in the region [17]. Summer is mostly warm and dry with temperatures ranging from 21°C to 26°C and sometimes exceeding 30°C [16]. Winters are mostly cool with temperatures ranging from 10°C to 14°C. The average annual sunshine in this region ranges from 2000 hours to 2100 hours. The area also receives plenty of rainfall throughout the year.

2.3.3 Solar power in New Zealand

Solar power generation in New Zealand was only 0.2% of the total renewable energy in 2016 [2], which is very low compared to other countries. This is mainly because of the high price of installation of PV systems and public scepticism about solar technology. However, more recently, with soaring prices for conventional electricity and reduction in the cost of PV panels, there has been a steady growth in the use of solar PV panels and this growth is expected to accelerate in years to come. Climate scientists from NIWA have found that solar power systems are viable, and it is worth investing in installation in all regions of New Zealand. This is based on their analysis of decades of available solar irradiance data.

2.4 Solar energy

Solar energy is the most abundant renewable energy source available on earth. The amount of solar energy that strikes earth in one and half hours is enough to power the whole world for one year [1]. The most common way to harness this renewable energy is through PV capture, which was invented more than half a century ago. Early developments in PV technology were not impressive because of the very high cost of manufacture, and the limited efficiency of early PV cells. With recent developments in the technology and decreasing costs for PV modules, solar energy has now become one of the most promising alternative renewable energy sources, which is of interest to many developers worldwide. Moreover, since solar power systems have no moving parts, their maintenance costs are very low, with a normal life span of around 30 years.

2.4.1 Solar cell

Solar cells are made up of semiconductor materials and come in different shapes and sizes. The silicon solar cell is made up of N-type (negative) and P-type

(positive) components, with two conductor plates at the top and the bottom as shown in Figure 2-12. When solar energy strikes the cell, the free electrons from the N-type layer are knocked off and travel to the P-type layer, creating an electron hole in the region. This electron hole is filled when an external circuit is completed, making current flow through the circuit.

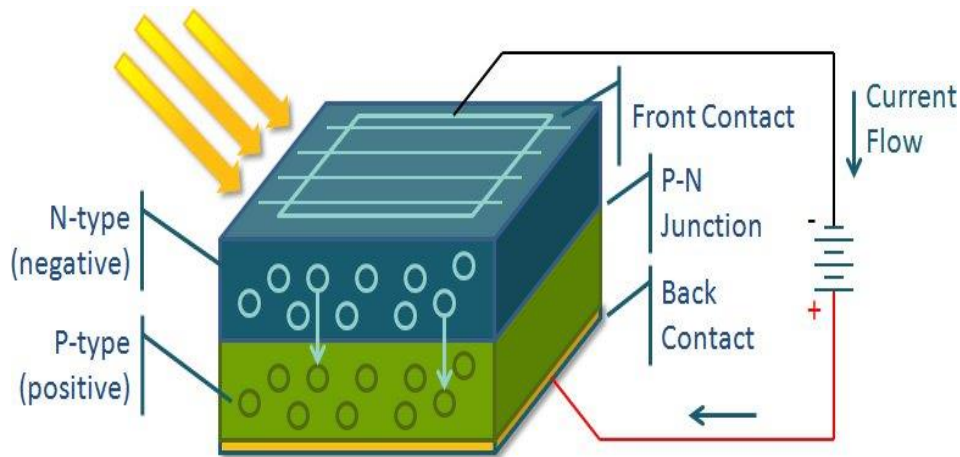


Figure 2-12: Silicon solar cell components [18]

2.4.2 Photovoltaic module

The silicon solar cells explained above are electrically connected in various combinations to make a solar panel, also known as a PV module. PV modules come in different shapes and sizes, as shown in Figure 2-13. The cells are connected either in series or in parallel, depending on the required power output of a module. Modules can be classified into two types depending on the materials used in their construction and are referred to as monocrystalline and polycrystalline PV modules. Several PV modules make a solar array, which makes up a solar electric power system.



Figure 2-13: Solar PV module [19]

2.4.3 Equivalent circuit of a solar PV cell

PV cells are basically a PN junction diode where, as the sunlight (photon) strikes it, electron hole pairs are generated and current starts flowing [20]. An ideal solar cell can be represented by an equivalent electrical circuit with a single diode in parallel with a current source as shown in Figure 2-14 (a) and Figure 2-14 (b). The three parameters are:

- I_{ph} - Photo generated current
- I_D - Diode equivalent current
- V_{oc} - Open circuit voltage

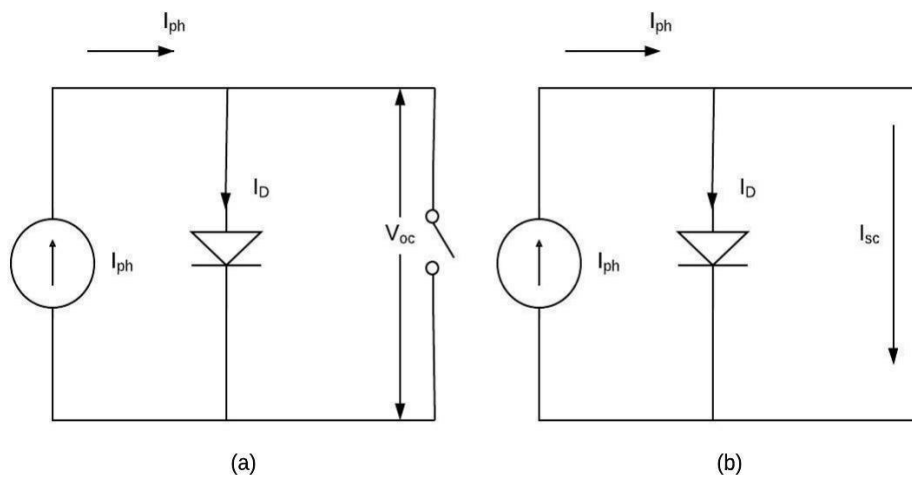


Figure 2-14: Electrical equivalent circuit of a solar cell (a) Open circuit voltage equivalent, (b) Short circuit equivalent

In practice, none of the solar cells are ideal as the generation of electricity depends on many factors, including the flux of incident light, the temperature of the PV cell, the bandgap energy of the cell, the reflectance of the surface, and the electron-hole recombination rate. Therefore, the non-ideal PV cell can be represented as an extended equivalent circuit from that shown in Figure 2-14 with the addition of a series resistance R_s and the shunt resistance R_{sh} shown in Figure 2-15.

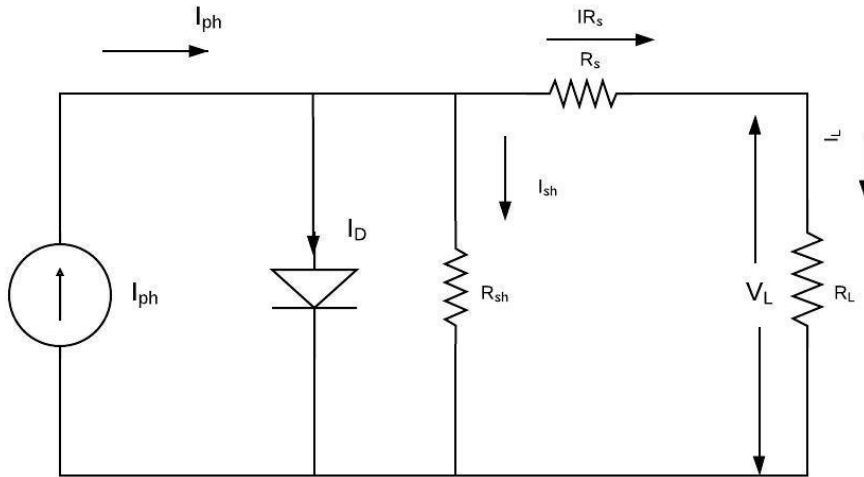


Figure 2-15: Equivalent circuit of a practical PV cell

R_s represents the resistance of the bulk material and also the resistance between the bulk material and the metal conductor

R_{sh} represents the recombination of the electron hole pair before reaching the load

I_{ph} is directly proportional to the solar radiation, therefore the voltage and current relationship seen by the load will be given by:

Ignoring I_{sh} , as this has minimal effect on the photo generated current,

$$I_{ph} - I_D = I_L \quad (2-2)$$

$$I_D = I_0 \left(e^{\frac{qV_D}{NkT}} - 1 \right) \quad (2-3)$$

Using Equation 2-3 in Equation 2-2

$$I_{ph} - I_0 \left(e^{\frac{qV_D}{NkT}} - 1 \right) = I_L \quad (2-4)$$

$$I_{ph} - I_0 \left(e^{\frac{q(R_S I_L + V_L)}{NkT}} - 1 \right) = I_L \quad (2-5)$$

$$\ln \left(\frac{I_{ph} - I_L}{I_0} + 1 \right) = \frac{q(R_S I_L + V_L)}{NkT} \quad (2-6)$$

$$(R_S I_L + V_L) = \frac{NkT}{q} \ln \left(\frac{I_{ph} - I_L}{I_0} + 1 \right) \quad (2-7)$$

$$V_L = \frac{NkT}{q} \ln \left(\frac{I_{ph} - I_L}{I_0} + 1 \right) - R_S I_L \quad (2-8)$$

For open circuit, $I_L = 0$,

$$V_{oc} = \frac{NkT}{q} \ln \left(\frac{I_{ph} - I_L}{I_0} + 1 \right) \quad (2-9)$$

Open circuit voltage will not reduce much as it is directly proportional to the logarithm of I_{ph} as shown in the Equation 2-9.

Taking the case with shunt resistance R_{sh} , the complete equation for a PV cell relating V_L and I_L can be represented as:

$$I_{ph} - I_D - I_{sh} = I_L \quad (2-10)$$

$$I_{ph} - I_0 (e^{AV_D} - 1) - \frac{V_D}{R_{sh}} = I_L, \quad \frac{q}{NkT} = A \quad (2-11)$$

$$I_{ph} - I_0 (e^{A(R_S I_L + V_L)} - 1) - \frac{(R_S I_L + V_L)}{R_{sh}} = I_L \quad (2-12)$$

2.4.4 Solar PV module specification

Solar panels specifications are obtained under two conditions; Standard Test Conditions (STC) and Normal Operating Cell Temperature (NOCT) [18]. All solar panels are tested under same STC, which involves a light intensity of 1000 watts per square meter and a temperature of 25°C.

NOCT is a more realistic set of test conditions with a light intensity of around 800 W/m² and an average temperature of around 20°C. This gives the performance of a solar panel when it is installed and when starting to use the power generated from

it. Table 2-3 shows the module specifications for the Mitsubishi MLE series PV module.

Table 2-3: Module specification of Mitsubishi MLE series PV panel

Model name:	PV-MLE280HD2
Cell type:	Monocrystalline Silicon, 78 mm x 156 mm
Number of cells:	120 cells
Maximum power rating (P_{max}):	280 W
Warranted minimum P_{max} :	280 W
PV USA test condition rating (PTC):	252.1 Wp
Open circuit voltage (V_{oc}):	38.6 V
Short circuit current (I_{sc}):	9.37 A
Maximum power voltage (V_{mp}):	32.4 V
Maximum power current (I_{mp}):	8.68 A
Module efficiency:	16.9 %
Aperture efficiency:	19.5 %
Tolerance of maximum power rating:	-0/+5 %

Each of the PV module specifications is briefly described as follows.

Open circuit voltage (V_{oc}): V_{oc} is the voltage measured across the solar panel output terminal when there is no load connected to it. This is measured under STC and is very important in estimating the solar module requirements for specific purposes.

Short circuit current (I_{sc}): I_{sc} is the amount of current that the solar panel produces when the output terminals are short circuited. This is also a very important parameter to determine whether the connected devices can handle the current produced.

Maximum power point (P_{max}): P_{max} is the maximum power produced by the solar panel when the voltage and current are at their maximum values.

Maximum power point current (I_{mpp}): I_{mpp} is the maximum current produced by a solar panel at its maximum power output.

Maximum power point voltage (V_{mpp}): V_{mpp} is the maximum voltage that the solar panel can produce to get the maximum power output.

PV USA test condition rating (PTC): PV USA stands for Photovoltaic for Utility Scale Applications. This test is carried out with a cell temperature of around 45 °C, which is a typical operating cell temperature.

Module efficiency: This is the actual amount of energy that is converted to electricity from the total solar energy that strikes the PV module. It is an important parameter to be considered while installing the PV system to calculate the amount of energy generated over the operating period.

Aperture efficiency: This refers to the ratio of output power to the solar power that strikes the panel aperture.

2.4.5 PV module output curves

The manufacturer’s datasheet also provides the electrical performance I-V characteristics curve, which is dependent on both irradiance and temperature, as shown in Figure 2-16. As the temperature of the PV panel increases, the output voltage decreases. The solar irradiance doesn’t have much impact on the output voltage of the PV module, but the output current is directly proportional to the irradiance value.

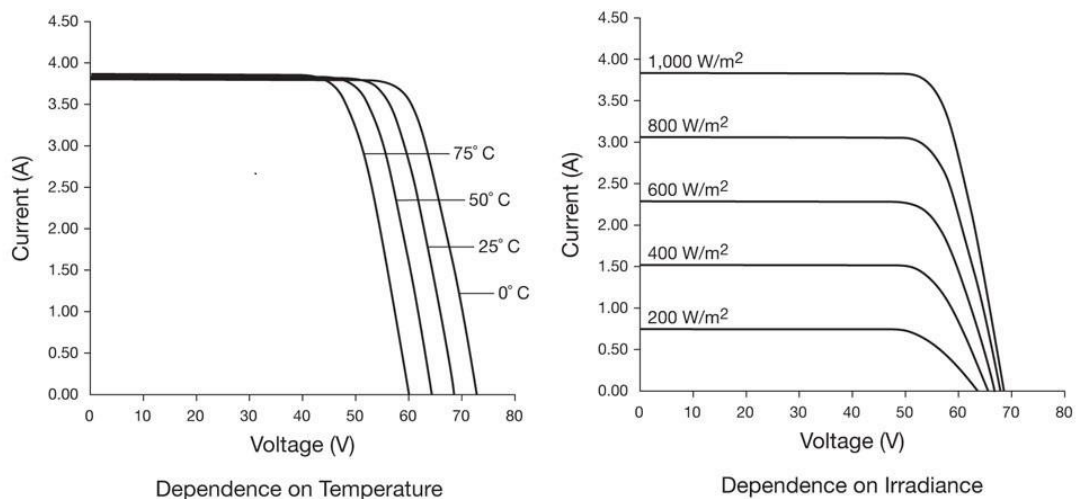


Figure 2-16: Irradiance and temperature in the field affect instantaneous module output [21]

2.4.6 Maximum power point tracking (MPPT)

The power output from a solar array is a function of the product of the voltage and the current, which depends on solar radiation, temperature and array voltage [22]. As the load connected to the solar output needs to be always powered optimally, it is very important to ensure that the PV module produces the maximum possible

power. Early attempts to achieve this used electromechanical fixture; single or double axis trackers which track the direction of the sun. With developments in technology, tracking is now done automatically using electronic devices. Figure 2-17 shows the general configuration of a PV system with an MPPT controller.

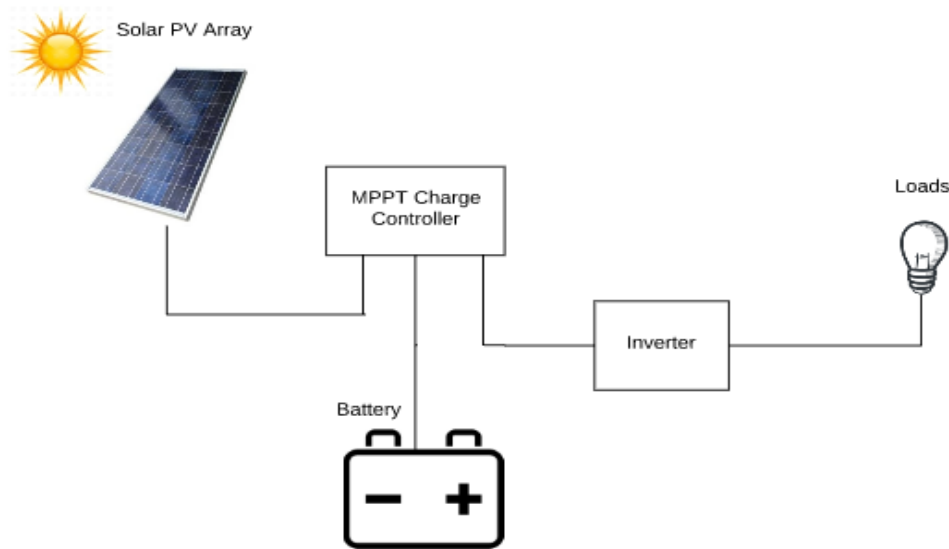


Figure 2-17: General configuration of a solar PV system with an MPPT controller

MPPT is currently the most popular technology offered by many charge controllers. It is also the most sophisticated and expensive solar charge controller. It tracks the output of the solar array and adjusts itself so that the output is always maximum [18]. Figure 2-18 illustrates a typical I-V curve for a PV module at different levels of irradiance, showing the position of the maximum short circuit current (I_{sc}), maximum open circuit voltage (V_{oc}) and maximum power output point (P_{max}). The maximum power point occurs at the knee region where the product of corresponding current and voltage values is at a maximum. At this point, the corresponding voltage and current is called the voltage at maximum power point (V_{mp}) and current at maximum power point (I_{mp}).

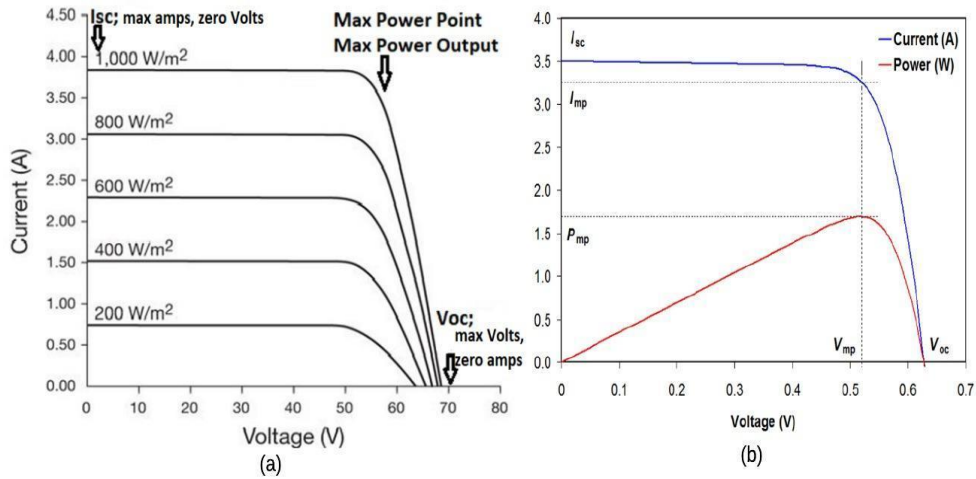


Figure 2-18: (a) The typical I-V characteristics curve. (b) I-V and P-V characteristic curves

This method of extracting maximum power increases the performance of the module by about 30% compared to other charge controllers without MPPT [18]. This technique can also take higher voltages from the solar PV array thereby requiring a smaller cable due to the reduced current at higher voltages. With these advantages, it is worth having a PV system with an MPPT charge controller.

2.5 ELGAR TerraSAS PV simulator

2.5.1 Product overview

The Elgar TerraSAS series Photovoltaic Simulator from AMETEK Programmable Power is specifically designed to emulate the dynamic electrical behaviour of a terrestrial PV solar panel array for DC microgrids, energy storage and inverter test applications [23]. It consists of a high-performance, programmable DC power supply with a state-of-the-art single standalone unit offering low output capacitance and high closed loop bandwidth to keep up with the advanced MPPT algorithms. Power supplies are available in 850 W, 5 kW, 10 kW, and 15 kW increments, and 600 V and 1000 V units are available in 5 kW, 10 kW and 15 kW versions depending on the short circuit current (I_{sc}) requirements. Many models can be also connected in series to handle higher voltage tests. The Figure 2-19 shows the standalone TerraSAS PV simulator ETS 600/8, which was used for the simulation for this project.



Figure 2-19: ELGAR TerraSAS standalone PV simulator

2.5.2 User interface

The simulator front panel displays only the status indication and on/off switch. The user interacts with the simulator through a remote ethernet connection. A single software operated from a desktop or laptop can control up to 48 simulators at a time. Figure 2-20 shows the TerraSAS simulator user interface with control buttons and selections on the right-hand side and the irradiance profile and PV curve on the left-hand side. This provides a very simple and user-friendly interface with which to select the required profiles and curves on a single window.

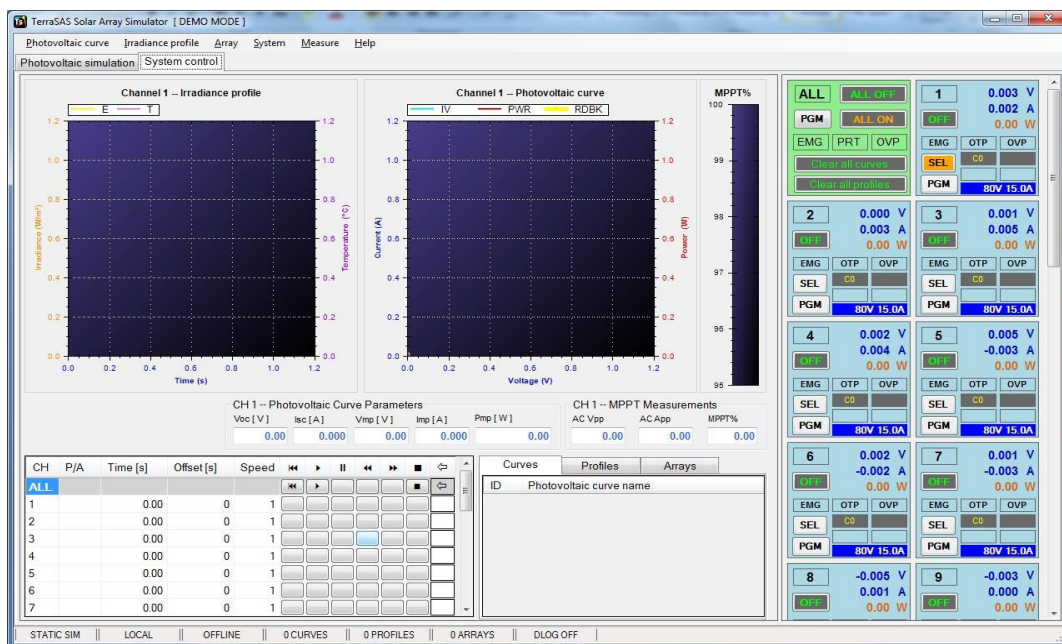


Figure 2-20: System control tabs from the main screen

The software allows modelling of the PV panel with data that is normally found in the manufacturer’s datasheet for solar panels. These parameters are V_{oc} , I_{sc} , V_{mp} , I_{mp} , β_v (voltage temperature coefficient) and β_p (power temperature coefficient) [24].

2.5.3 Simulator block diagram

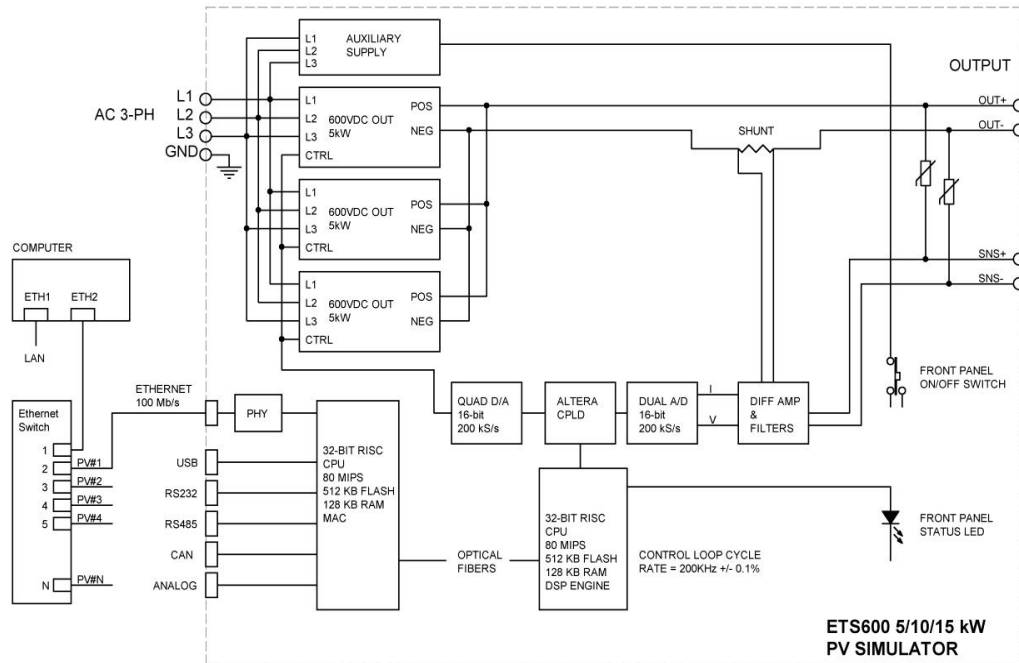


Figure 2-21: PV Simulator block diagram [23]

The simulator mainly consists of two 80 MIPS RISC microcontrollers. One processor interfaces with a 16-bit measurement and control system that monitors the source output voltage and current at 5 μ s intervals [23] as shown in the Figure 2-21. The other processor supports the ethernet interface, analog and digital input/output. In the PV simulator memory, an I-V curve is represented by 1,024 data pairs with each pair representing a single voltage/current point on the I-V curve. It interpolates 1,024 points in its curve memory with 16-bit accuracy. It then produces smooth voltage and current waveforms to the unit under test by interpolating between consecutive curves 128 times per second.

2.5.4 Software

The Simulator software offers following main features:

- Easily creates PV curves from manufacturer supplied data, based on the Sandia National Labs model.

- Easily creates irradiance/temperature profiles by entering ramp and dwell timing data.
- Has an intuitive drag-and-drop interface to easily assign curves and profiles to individual array elements, to support accurate modelling of array shadowing patterns
- Provides real-time control of standalone, desktop TerraSAS digital photovoltaic simulator units.
- Provides real-time control of TerraSAS digital photovoltaic simulator systems (up to 50 channels)

2.5.5 Basic I-V curve simulation

The Elgar TerraSAS user interface is simple to learn, as shown in Figure 2-22. The I-V curve is created by directly entering simple parameters available from the manufacturer’s datasheet. The curve can then be automatically saved in the software library and can be easily dragged to the channel tile. Clicking on the ON/OFF button on the channel tile will then execute the curve.

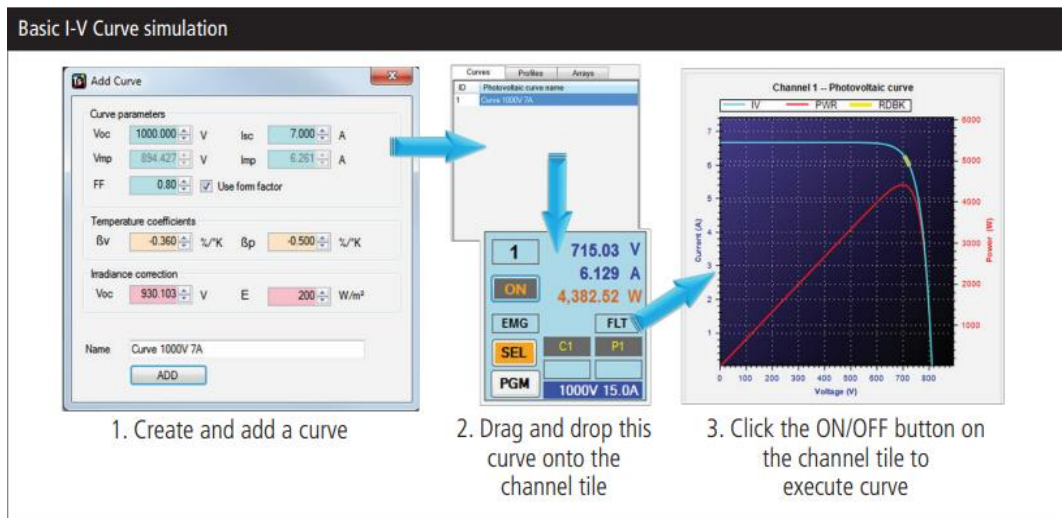


Figure 2-22: Simple three-steps basic I-V curve simulation

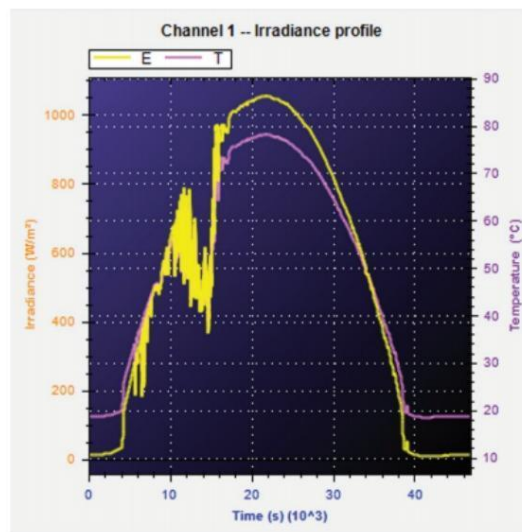
2.5.6 Irradiance and temperature profile

The irradiance profile is also created by entering the solar irradiance data with ramp time in the table, as shown in Figure 2-23 (a). It displays the irradiance and temperature in a unique and innovative way that enables dynamic performance profiles to be modelled, allowing complex test validation in any situation in a repeatable and reliable manner as shown in the Figure 2-23 (b).

	Line Number	Ramp Time	Ramp to Irradiance	Ramp to Temperature	Dwell Time	Dwell Irradiance	Dwell Temperature	Go to Line	Repeat Cycles
▶	1	0	0.0	0.00	300	100.0	25.00	0	0
	2	800	500.0	25.00	10	500.0	25.00	0	0
	3	800	100.0	25.00	10	100.0	25.00	2	2
	4	0	0.0	0.00	300	100.0	25.00	0	0
*	5	0	0.0	0.00	0	0.0	0.00	0	0

LOAD TABLE SAVE TABLE CREATE PROFILE INSERT ROWS ADD ROWS

(a)



(b)

Figure 2-23: (a) Solar irradiance create profile table (b) Dynamic irradiance profile display

2.5.7 PV array modeling

Multiple PV modules connected either in series or in parallel create a PV array. Elgar TerraSAS allows users to quickly define an array of PV panels and simulate real-world conditions, as illustrated in few steps below [24]:

1. Import module data from embedded Sandia database and create I-V curve
2. Build the array model by binding the desired curve and specifying the array size.
3. The effects of shadowing, aging and faulty modules can be previewed in real time. The resulting I-V curve can be dragged and dropped to any output for testing.

2.6 DC microgrid

To mitigate the effects of climate change, distributed generation and microgrids are seen as promising technologies to increase the renewable energy contribution to power markets [25]. A DC microgrid is analogous to a conventional AC grid system but with only DC power flowing throughout the entire grid. This will easily integrate locally generated power such as solar and wind energy directly to the DC microgrid, forming a local grid. With proper design and installation, a DC microgrid will be more reliable and flexible, with every component localized. The DC microgrid consist of a distributed generated RE source, microgrid loads, power converters and energy storage devices as shown in Figure 2-24.

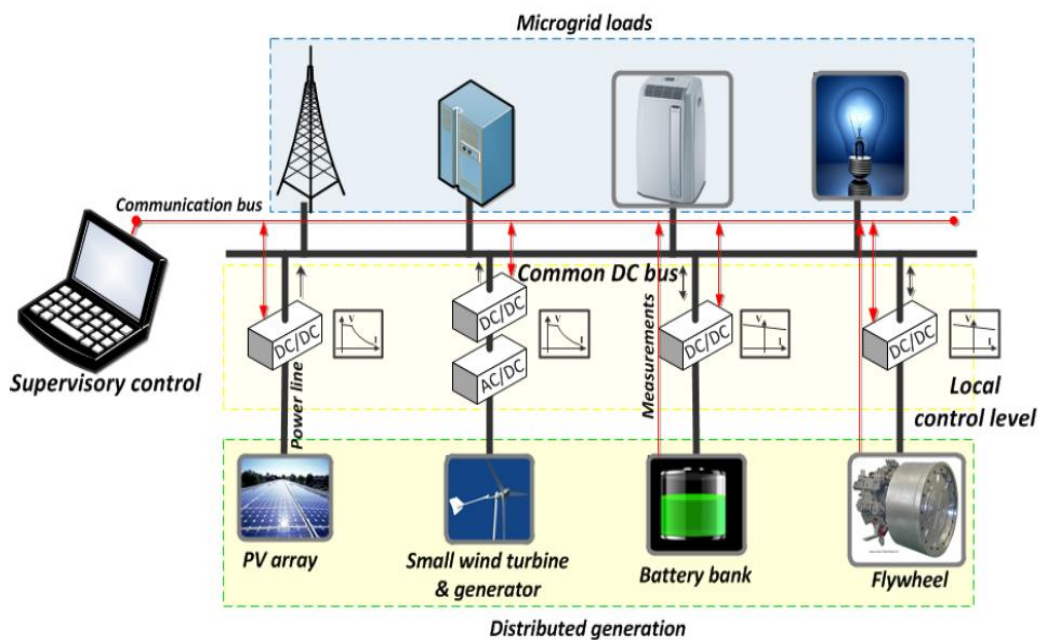


Figure 2-24: DC microgrid configuration [26]

2.6.1 Application of DC microgrid

The conventional application of DC microgrid is in distributed power systems, telecommunications, data centers and vehicular power systems. New applications include high efficiency households, renewable energy packs, hybrid energy storage systems and EV charging stations, as shown in Figure 2-25 [26]. Lately, the efficiency of household appliances has become of more interest to many people who are aiming to reduce their electricity costs.

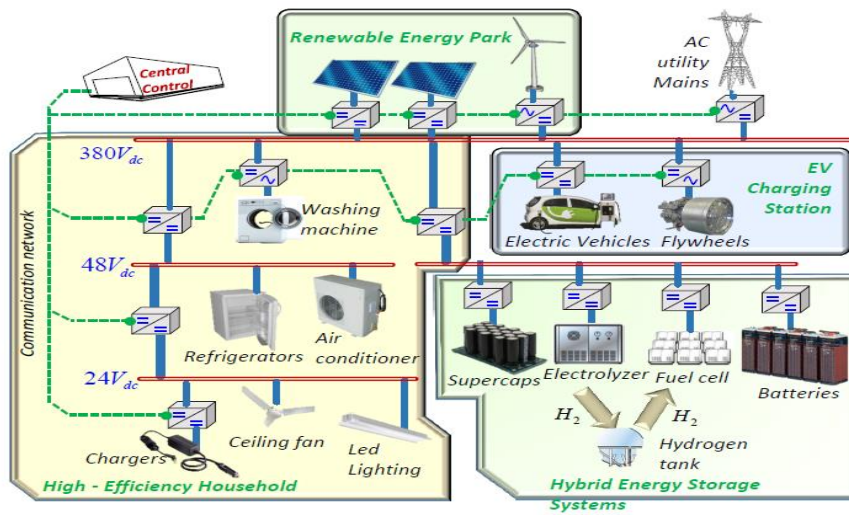


Figure 2-25: DC microgrid application [26]

Adopting DC microgrid will help to create highly energy-efficient households by eliminating the losses that occur in the AC-DC converters.

The installation of common modern appliances is shown in Figure 2-26 (a). Low voltage appliances use huge numbers of power adapters, where power losses occur.

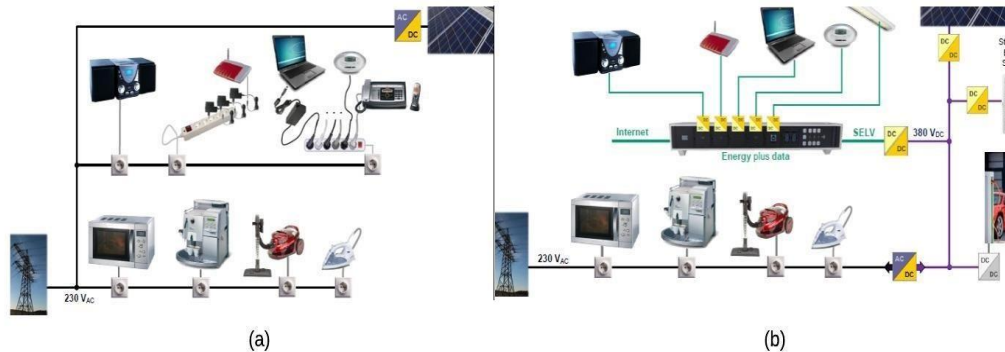


Figure 2-26: (a) Installation and appliances today (b) Installation and appliances in the future, using a DC microgrid [26]

However, with the system shown in Figure 2-27 (b), all low voltage appliances are connected to a single interface device, which is directly connected to the DC bus. In low voltage applications, DC microgrids will help to further improve efficiency by eliminating power converters, thereby increasing the ETEE of the system.

Chapter 3

Solar Data Collection

3.1 Solar irradiation data

Building and operating reliable solar energy systems requires information about solar irradiation in the region where the system is located [27]. Solar electric systems can operate in every part of the world. The only difference is that some parts of the world generate more energy than others due to the difference in solar energy received on the surface of the solar panels. Figure 3-1 shows the amount of solar energy in hours received each day on an optimally tilted surface during the worst month of the year, based on accumulated worldwide solar insolation data [1].

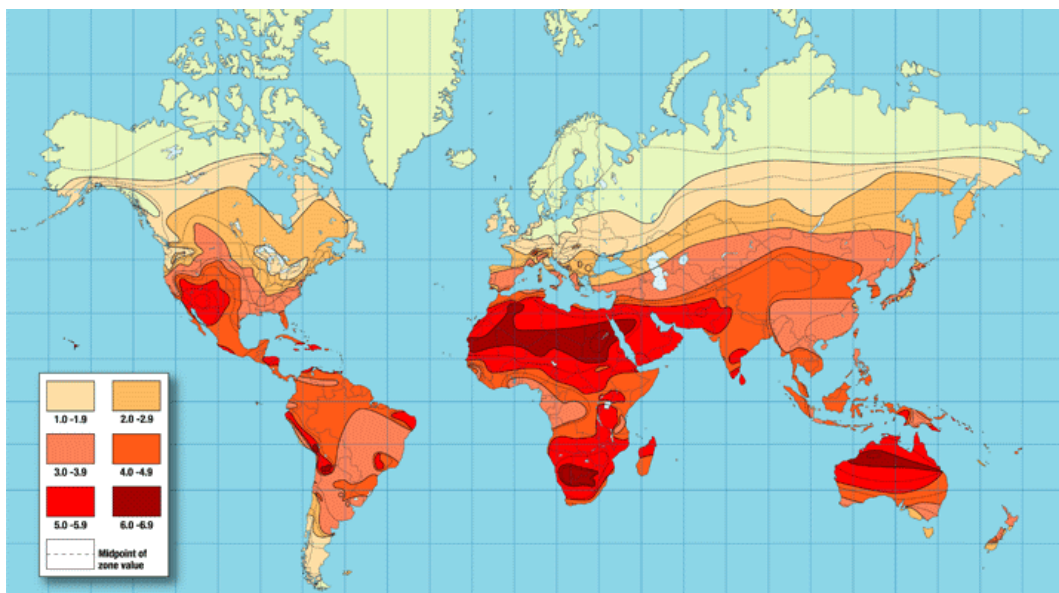


Figure 3-1: Map showing the amount of solar energy in hours received each day [1]

Reliable information on solar irradiance data is also very important for carrying out financial feasibility studies before installing solar power systems. After installation, the solar data is used to operate the system more efficiently and to achieve more efficient maintenance planning. Other factors, including the type and angle of roof and any objects nearby that can cause shadowing of the panel, must also be considered.

3.2 Solar radiation and the earth's atmosphere

The earth's atmosphere is a continuously variable filter for solar radiation reaching the surface [28]. Figure 3-2 illustrates the typical absorption of solar radiation by ozone, oxygen, water vapour and carbon dioxide [28]. Weather conditions such as cloud, storms and even a cloudless atmosphere can interfere with solar radiation absorption and scattering.

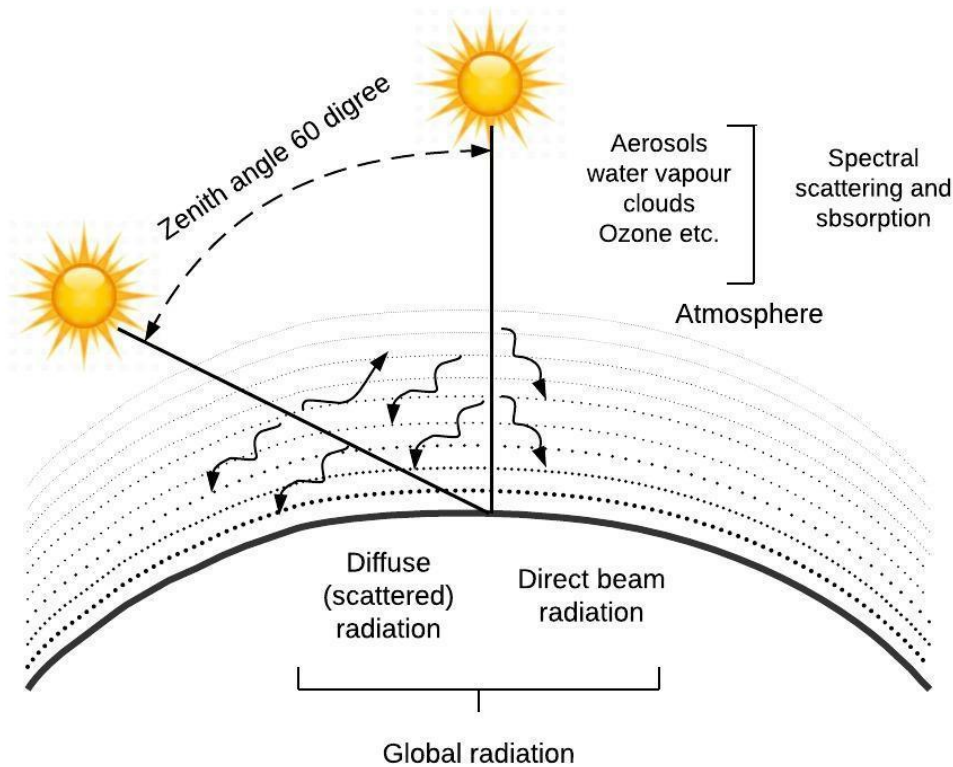


Figure 3-2: Scattering of direct-beam solar radiation from the sun by the atmosphere [28]

The solar radiation that is absorbed is converted into heat and raises the temperature of the absorber. The part of the incoming radiation that is scattered is mostly reflected back to the atmosphere, depending on the reflectivity and physical properties of the ground and atmospheric constituents, especially clouds [28]. Therefore, the radiant energy received at the earth's surface includes radiation from direct sunlight and from diffuse sources due to scattering.

3.3 Measurement of solar irradiance

Accurate measurements of incoming irradiance are essential in solar power plant project design and implementation [28]. The instruments required for the measurement of solar data are more complex and costly and analysis is also more complex compared to other climate data. Therefore, most countries have dedicated companies or government agencies to maintain their national climate data. In New Zealand, NIWA records and maintains national climate data, with a comprehensive

climate database dating back to the 1980s. These data are available online to the public in a variety of ways.

Instruments designed to measure any form of radiation are called radiometers [28]. Two types of radiometers used to measure global solar radiation are pyranometers and pyrhemometers. A solar pyranometer measures the global radiation flux density in watts per square metre. Pyrhemometers measures the direct normal irradiance. Most commonly used pyranometers are handheld devices that should be placed upright with the light sensor facing towards the sun.

For this project, solar irradiance data was recorded using a TENMARS solar power meter TM-206. The required solar irradiance data was also obtained from the NIWA database online. Then a comparative analysis was carried out using the two sources of data to determine which was the most reliable source of data for this project.

3.3.1 NIWA Solar radiation database

NIWA has recorded solar radiation data in New Zealand for decades, using a wide range of modern scientific instruments in climate stations located all over the country. Radiation is the amount of radiation energy received at the measuring instrument.

The climate database contains three types of visible solar radiation measurements [16]:

1. **Global:** This includes radiation from both direct sunlight and from diffuse (scattering) sources in the earth's atmosphere such as clouds.
2. **Diffuse:** Solar radiation that is not directly incident on the earth's surface. This is measured by a pyranometer mounted on a horizontal plane equipped with a shading ring that blocks the direct radiation from the sun.
3. **Direct:** Solar radiation that is directly incident on the earth's surface. This is measured by a normal incidence pyrhemometer equipped with a solar tracker that automatically points towards the sun.

NIWA solar data loggers measure instantaneous radiation in W/m^2 every 3 seconds and then calculate the average over the recording period (either ten minutes or one hour). This value is then converted to MJ/m^2 for importation into the database [16]. Figure 3-3 shows the mean daily global radiation in W/m^2 for an average year for

various places in New Zealand. The data are mean monthly values for the period (1981-2010) for locations having at least five complete years of data. The bar graph shows that most sites receive a mean daily global radiation of 150 W/m² in an average year.

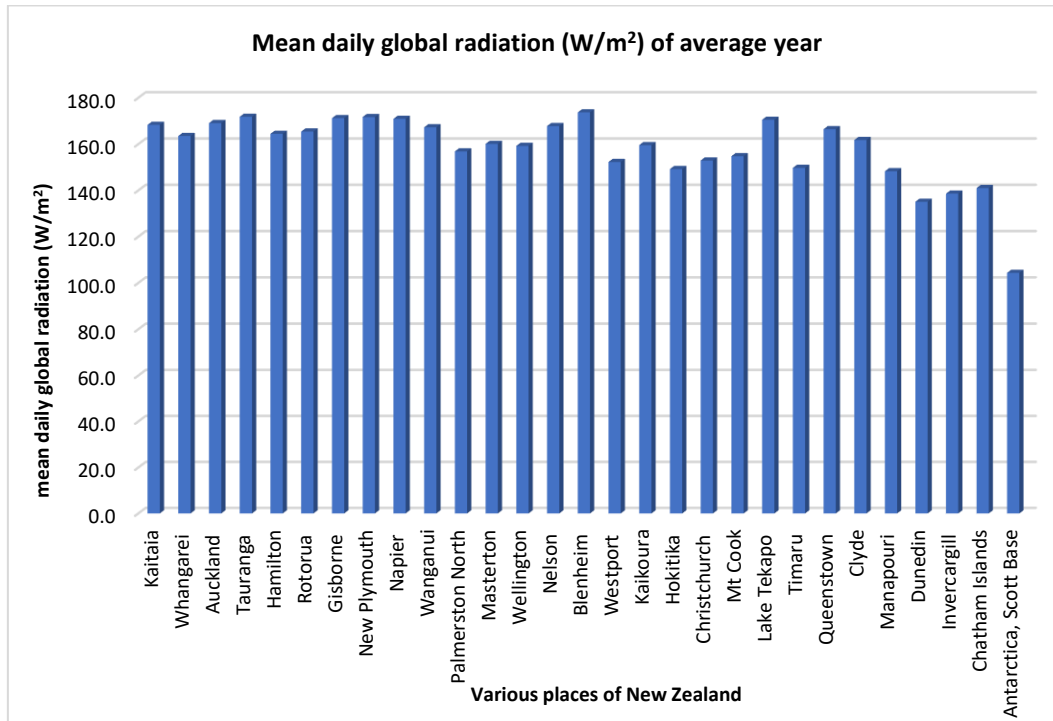


Figure 3-3: Mean daily global radiation (W/m²) in a range of New Zealand cities in an average year [16]

The corresponding daily sunshine hours for an average year in the same sites are shown in Figure 3-4. The data are mean monthly values for the period (1981-2010) for locations having at least 5 complete years of data. A sunshine hour is defined as the duration of bright sunshine received on the surface of the location. Sunshine hours are measured daily and hourly and the unit used is hours. Most sites in New Zealand have a mean daily of 5 sunshine hours, which shows that many places receive enough sunshine to make the installation of solar power systems feasible.

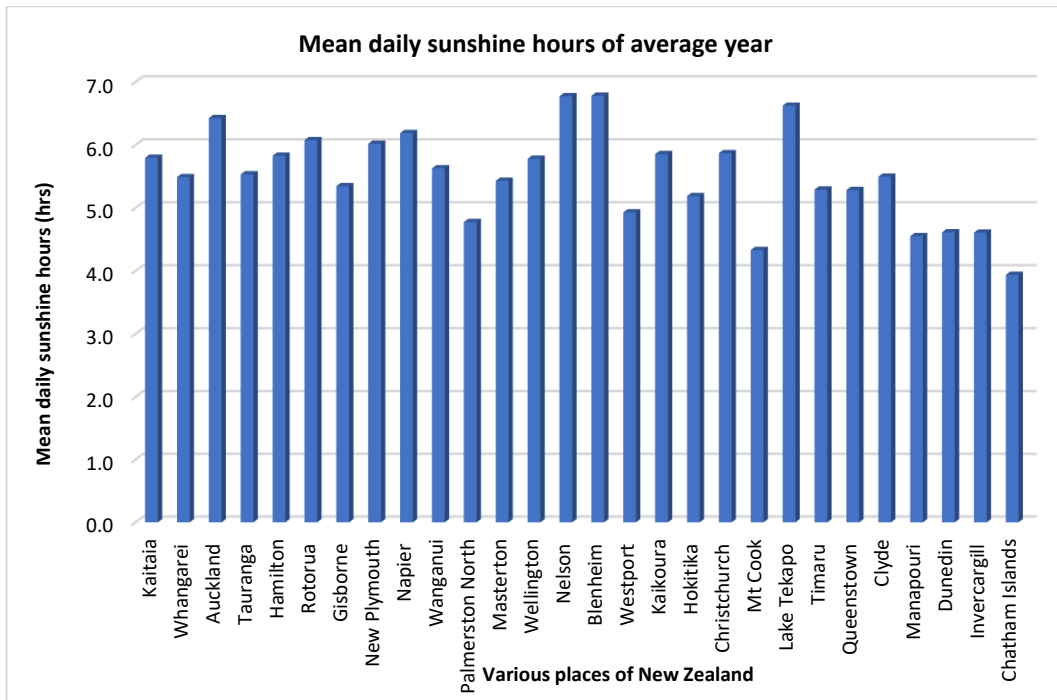


Figure 3-4: Mean daily sunshine hours in a range of New Zealand locations in an average year [16]

3.3.1.1 Obtaining solar irradiance data from NIWA

NIWA’s solar radiation data can be obtained from the online database. Registration is required for free climate data access through a web-based application system called CliFlo. The systems contain data from over 600 currently operating stations. The database link login screen for free access is shown in Figure 3-5.

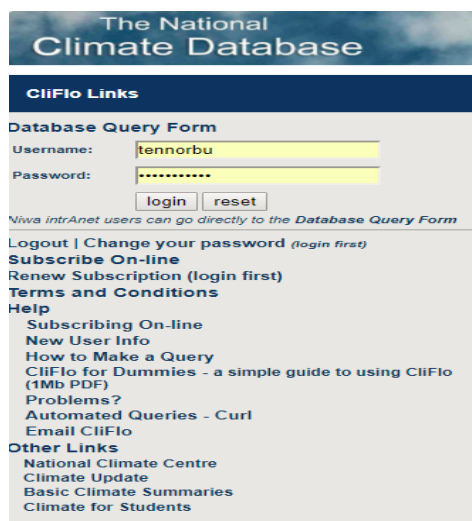


Figure 3-5: Climate database web-based application (CliFlo) login screen

After login, the database query page opens, where the necessary selection is made to obtain the daily global and hourly global irradiance values for the desired period,

as shown in Figure 3-6. The nearest station to the University of Waikato is Ruakura
2 Ews, .

The screenshot shows the 'Database Query' interface. At the top, there's a header for 'The National Climate Database' with the NAWA logo and navigation links like 'help', 'home', 'subscription', and 'query'. Below the header, there are buttons for 'Save Settings', 'Preview', and 'Send Query'. The main area is divided into four sections:

- 1. Datatype:** A dropdown menu shows 'Radiation' selected. Below it, 'Specify options' includes checkboxes for 'Daily', 'Hourly', 'Global', 'Diffuse', and 'Direct'. A 'Remove All Datatypes' button is also present.
- 2. Location:** A dropdown menu shows 'Station agent number(s): 26117'.
- 3. DateTime:** 'Start date (yyyy mm dd hh): 2018 01 01 00' and 'End date (yyyy mm dd hh): 2018 01 01 23'.
- 4. Format:** A dropdown menu shows 'NZST' selected.

At the bottom right, there's a 'logout' link and subscription details: 'Your subscription details: username=tennorbu Remaining rows = 1,745,878'.

Figure 3-6: Database query screen

By making the required selections and then clicking the send query button, the required data is obtained in the desired format as shown in Figure 3-7.

The details of the radiation data are as follows:

Field description:

Amount: MJ/m² – Total radiant energy accumulated during the period

Frequency: reporting frequency; “H” = hourly or “D” = daily

Type of radiation measured:

- G = Global
- F = Diffuse
- R = Direct

Station information:

Name	Agent Number	Network Number	Latitude (dec.deg)	Longitude (dec.deg)	Height (m)	Position Precision	Observing Authority
Hamilton, Ruakura 2 Ews	26117	C75734	-37.77567	175.30506	45	H	NIWA/AGRESEARCH

Note: Position precision types are: "W" = based on whole minutes, "T" = estimated to tenth minute, "G" = derived from gridref, "E" = error cases derived from gridref, "H" = based on GPS readings (NZGD49), "D" = by definition i.e. grid points. [For more info](#)

[Back to Database Query Form](#)

Radiation: Hourly Global

Station	Date (NZST)	Amount (MJ/m2)	Period (Hrs)	Type	Freq
26117	20180101:0000	0.0000	1	G	H
26117	20180101:0100	0.0000	1	G	H
26117	20180101:0200	0.0000	1	G	H
26117	20180101:0300	0.0000	1	G	H
26117	20180101:0400	0.0000	1	G	H
26117	20180101:0500	0.0000	1	G	H
26117	20180101:0600	0.0800	1	G	H
26117	20180101:0700	0.3600	1	G	H
26117	20180101:0800	0.7200	1	G	H
26117	20180101:0900	0.5400	1	G	H
26117	20180101:1000	0.9800	1	G	H
26117	20180101:1100	1.3900	1	G	H
26117	20180101:1200	1.4000	1	G	H
26117	20180101:1300	0.3300	1	G	H
26117	20180101:1400	0.3900	1	G	H
26117	20180101:1500	0.4700	1	G	H
26117	20180101:1600	0.4500	1	G	H
26117	20180101:1700	0.3300	1	G	H
26117	20180101:1800	0.2800	1	G	H
26117	20180101:1900	0.0800	1	G	H
26117	20180101:2000	0.0100	1	G	H
26117	20180101:2100	0.0000	1	G	H
26117	20180101:2200	0.0000	1	G	H

Figure 3-7: Sample hourly global radiation data from Ruakura 2 Ews climate station

Similar to the way global radiation is queried, sunshine hours are also obtained by selecting the required data types and locations. Sample data are shown in Figure 3-8.

The details of the sunshine data are as follows:

Field Descriptions:

Amount: Accumulated hours of bright sunshine during the period

Frequency: Reporting frequency; "H" = Hourly or "D" = daily.

Source of data; "D" = Daily climate, "H" = Hourly

The National Climate Database

Station information:

Name	Agent Number	Network Number	Latitude (dec.deg)	Longitude (dec.deg)	Height (m)	Position Precision	Observing Authority
Hamilton, Ruakura 2 Ews	26117	C75734	-37.77567	175.30506	45	H	NIWA/AGRESEARCH

Note: Position precision types are: "W" = based on whole minutes, "T" = estimated to tenth minute, "G" = derived from gridref, "E" = error cases derived from gridref, "H" = based on GPS readings (NZGD49), "D" = by definition i.e. grid points. [For more info](#)
[Back to Database Query Form](#)

Sunshine: Hourly				
Station	Date (NZST)	Amount (Hrs)	Period (Hrs)	Freq
26117	20180401:0000	0.0	1	H
26117	20180401:0100	0.0	1	H
26117	20180401:0200	0.0	1	H
26117	20180401:0300	0.0	1	H
26117	20180401:0400	0.0	1	H
26117	20180401:0500	0.0	1	H
26117	20180401:0600	0.0	1	H
26117	20180401:0700	0.1	1	H
26117	20180401:0800	1.0	1	H
26117	20180401:0900	1.0	1	H
26117	20180401:1000	1.0	1	H
26117	20180401:1100	1.0	1	H
26117	20180401:1200	1.0	1	H
26117	20180401:1300	1.0	1	H
26117	20180401:1400	1.0	1	H
26117	20180401:1500	1.0	1	H
26117	20180401:1600	1.0	1	H
26117	20180401:1700	1.0	1	H
26117	20180401:1800	0.9	1	H
26117	20180401:1900	0.0	1	H
26117	20180401:2000	0.0	1	H
26117	20180401:2100	0.0	1	H
26117	20180401:2200	0.0	1	H

Figure 3-8: Sample sunshine hours data for Ruakura 2 Ews climate station

3.3.1.2 Unit conversion

NIWA station data loggers measure the instantaneous radiation in W/m^2 every 3 seconds and then calculate the average over the recording period (either ten minutes or one hour) [16]. This is then converted into MJ/m^2 for importation into the database.

To convert from MJ/m^2 to W/m^2 :

$$Watts/m^2 = MJ/m^2 * 1000000 / \text{Number of seconds in the period}$$

To convert from W/m^2 to MJ/m^2 :

$$MJ/m^2 = W/m^2 * \text{Number of seconds in the period} / 1000000$$

3.3.2 Measurement using a solar power meter

The solar power meter TM-206 is a small, portable instrument that can be carried anywhere to measure irradiance as and when required. The ambient weather TM-206 solar power meter is shown in Figure 3-9. It measures the amount of solar power in watts that strikes a one-meter square space on the surface of the earth. This is the same unit with which the solar panels are tested under standard test

conditions. It has an accuracy of $\pm 5\%$ with an operating temperature range from 5°C to 40°C .



Figure 3-9: Solar power meter TM-206

Measurements were taken on the rooftop of ‘C’ Block at the University of Waikato, where the solar array was to be installed. As the panels must face north at the angle of latitude to get the most energy from the sun, irradiance is also measured by facing the solar power meter at same angle facing north to obtain the most accurate radiation data possible.

3.4 Comparison between the measured irradiance data and the data from NIWA database

Irradiance data was obtained hourly between the hours of 6:00 am and 8:00 pm from 10 December 2017 to 15 December 2017, using the solar power meter at the solar panel installation site. As this meter only measures solar irradiance and doesn't have features to measure temperature, an average temperature of 25°C was assumed. Solar data for the same consecutive days was also obtained from the NIWA database using a calculator called solarView. This calculator estimates the solar energy that can be collected by a solar panel at a given address. The program combines an image of the landscape with irradiance data from the nearest climate station [29]. The percentage variance between the two sources of data with three different weather conditions, including cloudy, sunny and rainy days is shown in Figure 3-10, Figure 3-11 and Figure 3-12.

Of the three different weather day comparisons, the cloudy day percentage variance was greatest. This is because a solar power meter measures the instantaneous solar radiation, while the NIWA instrument measures the instantaneous radiation every 3 seconds and then calculates the average over the hour. On a cloudy day, there are frequent changes in the solar radiation reaching the surface due to shading by the clouds. Therefore, readings showing large variance from the NIWA values were due to the cloud shading at the time of measurement using the solar power meter as shown in the Figure 3-10.

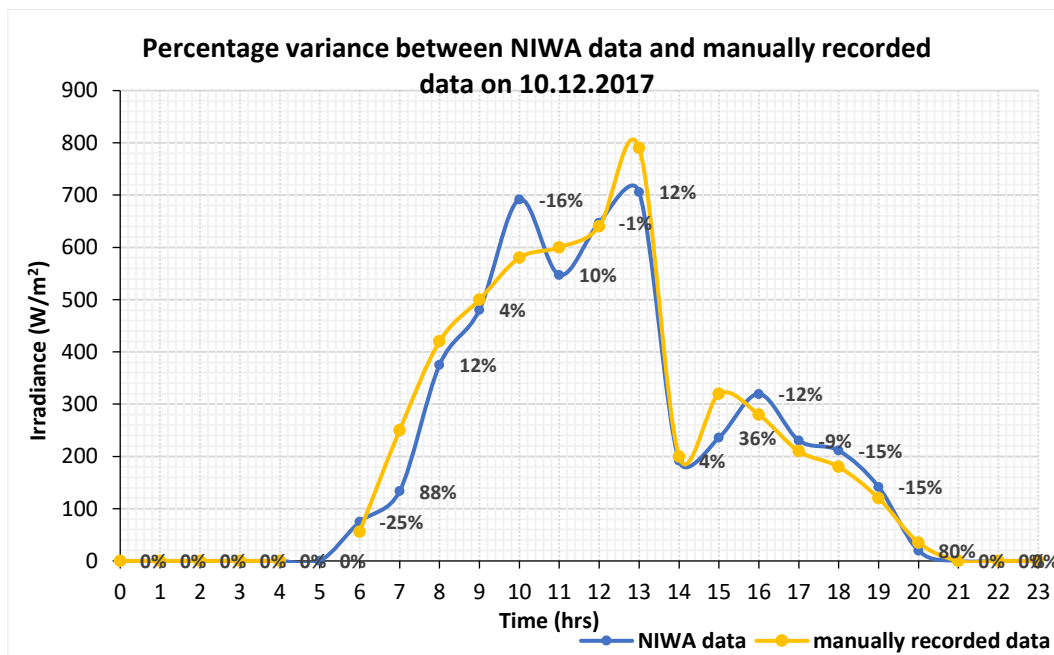


Figure 3-10: Percentage variance between NIWA solar radiation data and manually recorded data on 10.12.2017, in cloudy weather

During the sunny day, the solar radiation remained almost constant throughout the day as the sky was clear, with no clouds to cause shading of the solar panels. In this case, the measured data and the data from NIWA database follow an almost identical curve, as shown in Figure 3-11.

The manual measurements showed that whenever there is cloud shading at the time of measurement, the irradiance value drops drastically. The weather in Hamilton frequently changes, which affects irradiance values. This intermittent nature of solar power is the main challenge that solar power systems face. Therefore, this needs to be carefully studied during field data collection to achieve efficient installation and operation of the solar PV panels. Solar data analysis is also very important to get the maximum energy output from the solar array.

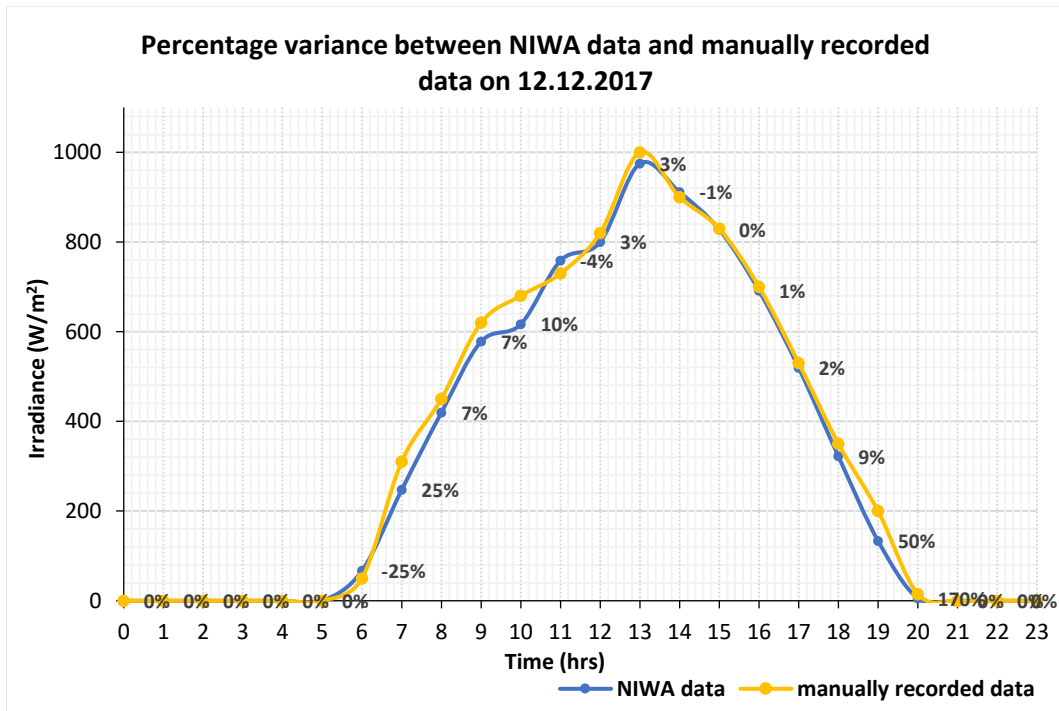


Figure 3-11: Percentage variance between NIWA solar radiation data and manually recorded data on 12.12.2017, in sunny weather

Similarly, on the rainy day, the percentage variance was also minimal as the solar radiation remained almost constant throughout the day. The irradiance values for the rainy day were low compared to the other days, as shown in Figure 3-12.

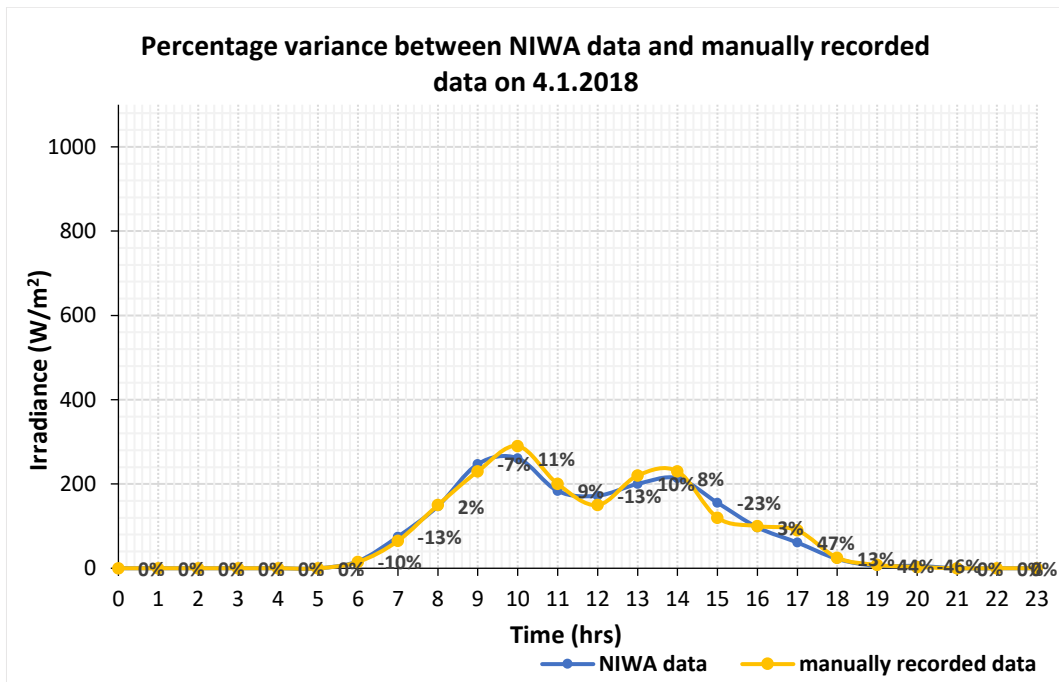


Figure 3-12: Percentage variance between NIWA solar radiation data and manually recorded data on 4.1.2018, in rainy weather

Since the solar power meter measures only the instantaneous irradiance value, it doesn't take account of changes in irradiance due to changes in the weather during the rest of the hour. In contrast, the NIWA data logger measures the total radiant energy for entire hour and the equivalent solar radiation in W/m^2 gives an accurate value for the solar radiation available for the period. The NIWA data acquisition incorporates the frequent changes in irradiance values due to frequent changes in the weather, which is very common in most places in New Zealand. Moreover, NIWA has been recording national climate data for almost 30 years in its database, using reliable and complex instruments. Therefore, NIWA's solar radiation data was used for the simulation and testing of the SCALED circuit.

3.5 Creating irradiance-temperature profiles in the PV simulator

The state-of-the-art Elgar PV simulator is a programmable digital power source designed to simulate the electrical behaviour of terrestrial PV arrays [24]. It has the capacity to easily create irradiance-temperature profiles by entering ramp and dwell-time data. It also allows the importation of third party applications or real-time data acquisition from actual solar panels. A sample of irradiance and temperature records of 1st January 2018 at the University of Waikato is presented in Table 3-1.

Table 3-1: Irradiance-temperature data on 1.1.2018 (source: NIWA)

Sl.no	Time (hr)	Irradiance (W/m2)	Temperature (°C)
1	0	0	10.4
2	1	0	9.1
3	2	0	8.7
4	3	0	9.2
5	4	0	8.8
6	5	52	10.7
7	6	233	13.3
8	7	439	15.6
9	8	639	17.9
10	9	736	19.1
11	10	878	20.3
12	11	1061	20.4
13	12	622	22.8
14	13	630	23.5
15	14	350	22.7
16	15	81	23.4
17	16	50	22
18	17	0	21
19	18	0	20.5

20	19	0	18.8
21	20	0	16.9
22	21	0	15.6
23	22	0	13.6
24	23	0	13.1

Figure 3-13 shows the sample irradiance-temperature profile for 1st January 2018 at the University of Waikato. Similar profiles can be created for various combinations of the data over different days with diverse climatic conditions.

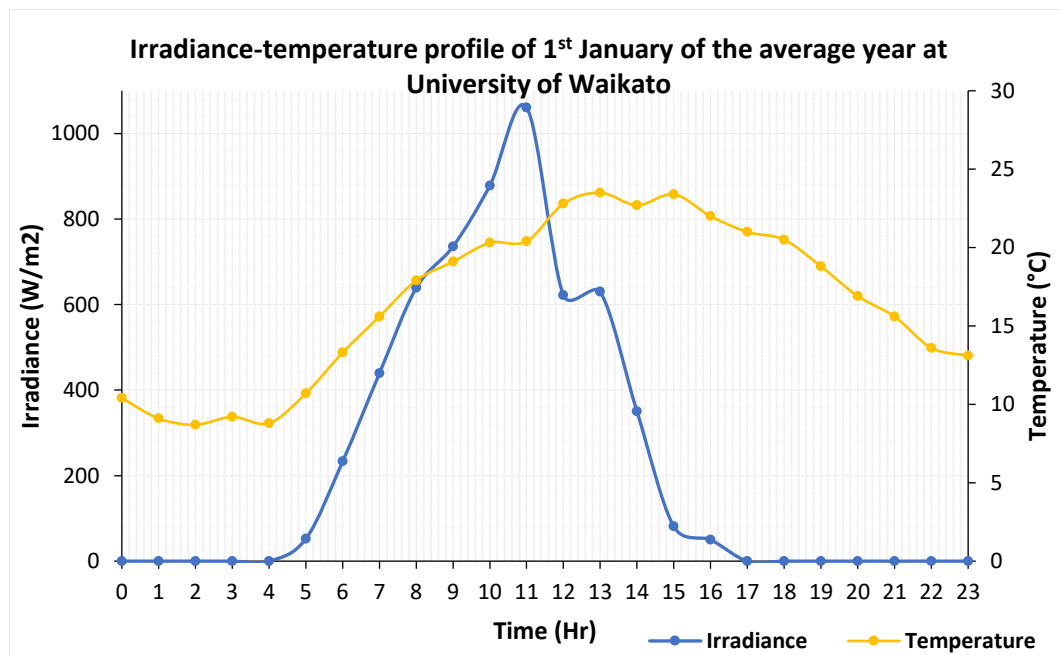


Figure 3-13: Sample irradiance-temperature profile on 1.1.2018

3.5.1 Modelling of irradiance-temperature profile in PV simulator

The Elgar PV simulator software has its own format for entering irradiance and temperature data to create a profile in the system. A lengthy profile can be entered as a table by breaking it down into a sequence of segments [24]. Each segment may ramp from one irradiance-temperature point to another, or stay at the specified level for a programmable interval. Figure 3-14 (a) shows the sample template where the irradiance and temperature data are entered manually with the ramp time and dwell time. An average temperature of 25°C is used as temperature profiling is not required.

As the irradiance is hourly data, the ramp time is 3600 seconds and dwell time is taken as 10 seconds, assuming that the irradiance value remains constant for at least

10 seconds at that segment. A repeat cycle is used when the irradiance value remains the same for many cycles so that it is not necessary to enter the same data in each segment.

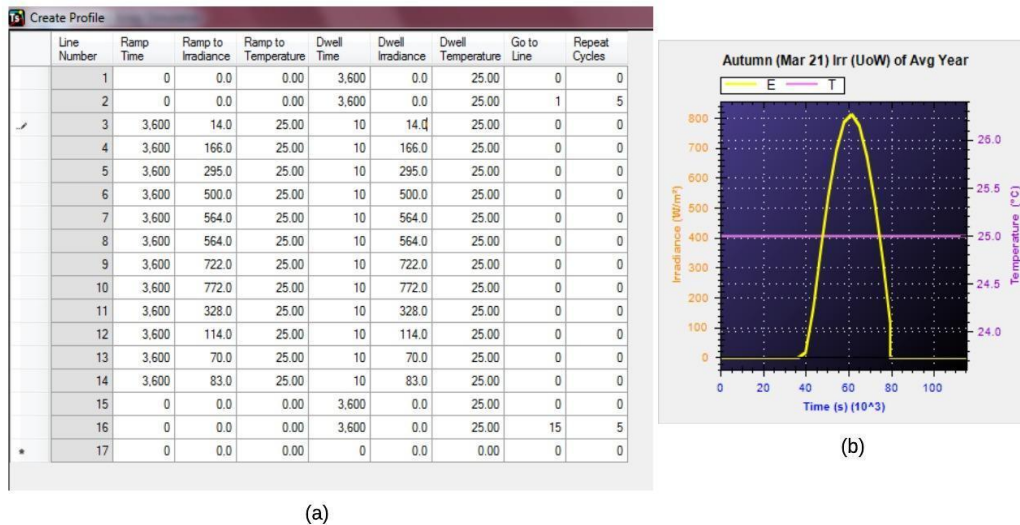


Figure 3-14: (a) Sample irradiance profile template of PV simulator (b) Sample irradiance curve created in PV simulator

After entering all the data in the ‘create’ template, the irradiance profile is created by clicking the Create button available at the bottom of the page. A sample irradiance curve is displayed in Figure 3-14 (b), which can then be selected to use in the simulation.

3.5.2 Creating an I-V curve in the PV simulator

The Elgar PV simulator also allows the easy creation of PV curves from manufacturer-supplied data. The I-V curve is created by entering certain specifications from the PV panel datasheet as shown in Figure 3-15 (a). The software also allows the direct import of data from solar module libraries. This can be done by installing the Solar Advisor Model (SAM), from which the desired solar panel can be selected to export all the available data to the PV simulator form.

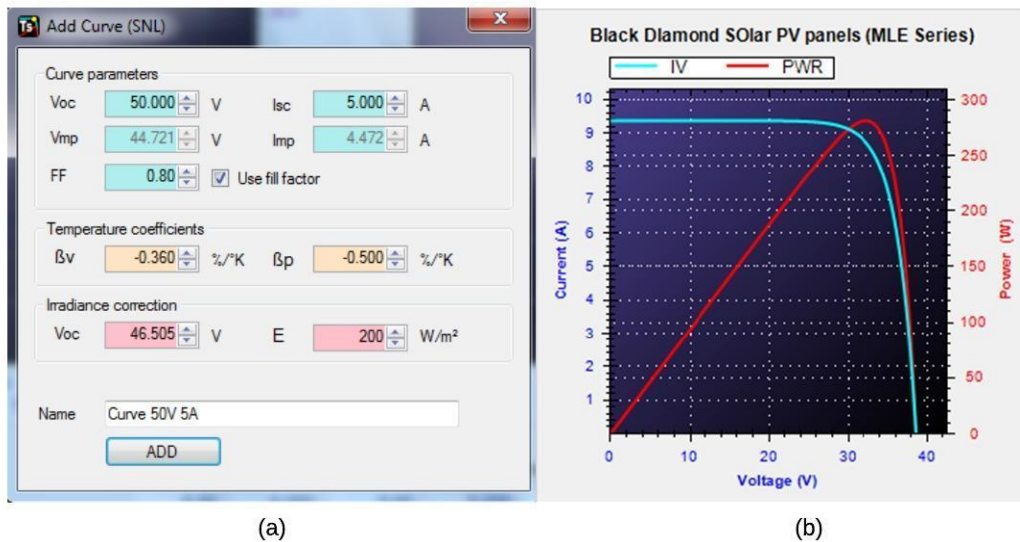
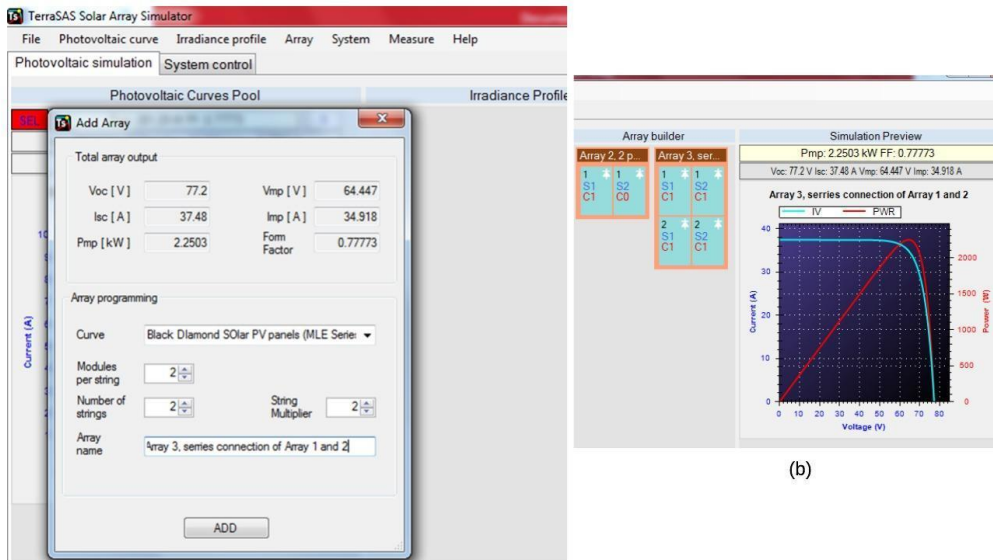


Figure 3-15: (a) Screenshot of the simulator showing entry of PV panel data to create an I-V curve (b) The I-V curve and power curve of a 280 W Mitsubishi MLE series PV module

Figure 3-15 (b) shows the I-V and the power curve of a Black Diamond solar PV panel (MLE series) manufactured by Mitsubishi Electric, which is the same panel that was installed for this project. The blue curve is the I-V curve and the power curve is in red. The I-V curve shows the operating characteristics of the PV panel from near constant current mode to constant voltage mode as the curve travels from 0 V to maximum voltage (V_{oc}).

3.5.3 PV array I-V curve

The PV simulator also has features allowing the creation of any number of solar array configurations. The total array output, including total V_{oc} , I_{sc} , V_{mp} and I_{mp} is calculated and entered in the respective fields in the 'add array' page as shown in Figure 3-16 (a). Then, by entering the number of strings, modules per string and string multiplier in the array programming section, a new array is created in the PV simulator system by clicking the 'add' button.



(a)

(b)

Figure 3-16: (a) PV Array programming for creating a PV array I-V curve (b) PV array I-V and power curve

The corresponding PV Array I-V curve and the power curve, consisting of two parallel strings with two modules per string, looks like the one in Figure 3-16 (b).

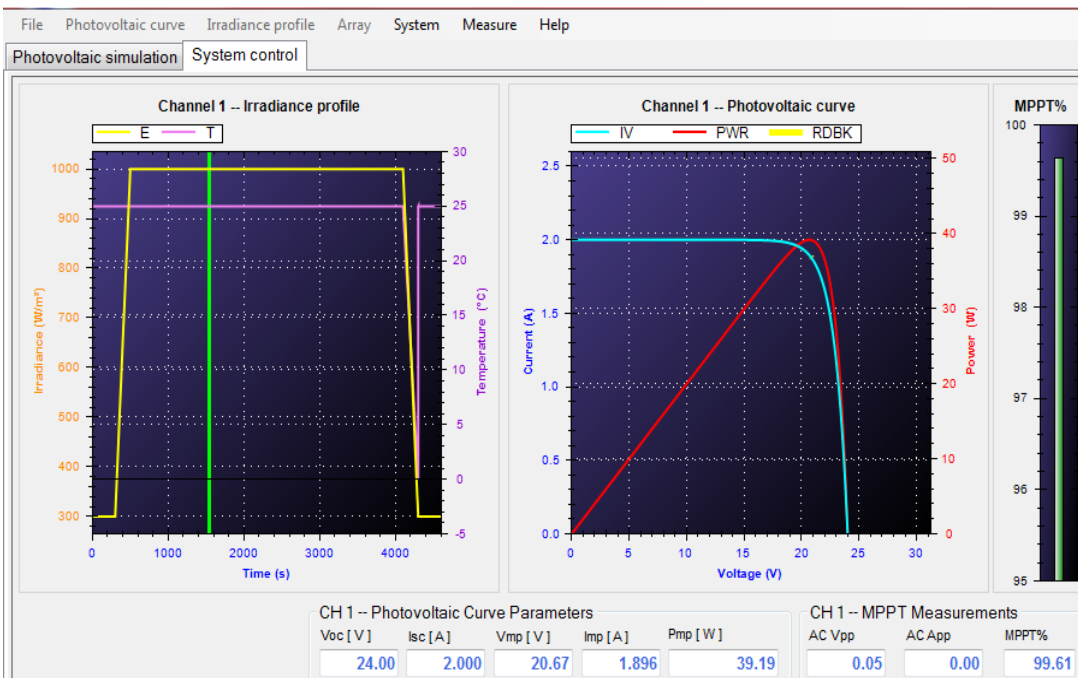


Figure 3-17: PV Simulator system control user interface

The I-V and irradiance-temperature curve can then be selected as desired for the simulation, as shown in Figure 3-17. It shows two tabs on the same page, the PV simulation and the system control, through which the simulation can be carried out. It also shows the value of MPPT in terms of percentage as displayed on the far-right side of Figure 3-17. As a result, the user exactly knows which region of the I-V curve the system is operating in, which is very important in terms of the operating characteristics of the PV panel.

3.6 NIWA SolarView tool

NIWA has developed an online tool called SolarView to calculate the solar energy that can be collected by a solar panel at a given address, given the panel direction and its inclination [29]. This gives basic information for people considering installing a solar power system. This program combines an image of the local landscape with the irradiance data from the nearest climate station, using more than ten years of sunlight hours data. It also considers the shading of solar power capturing devices by the landscape, such as distant hills and mountains, which can obstruct the radiant energy reaching the panel. Figure 3-18 shows an interactive screen through which we can enter the address at which the solar power system is to be installed.

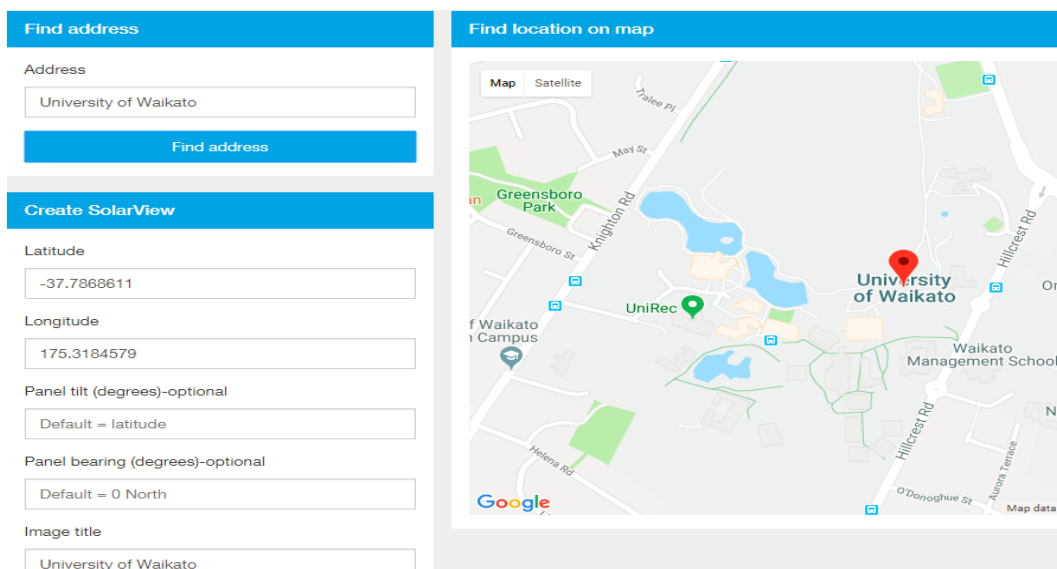


Figure 3-18: SolarView address selection screen

Based on the address, the tool calculates the panel orientation angles and the solar radiation data with a graphical view of the path of the sun during the days of the month for a year, as shown in Figure 3-19. The five curves are the path of the sun on 21st December (summer solstice), 21st June (winter solstice), 21st March (autumn equinox), 21st August and 21st October [29]. The number above the curve indicates the cumulative amount of solar energy that is received in 1 m² on that day and the number below the curve represents the time of the day, following the path of the sun from east to west.

The irradiance value represents the average amount of solar irradiance for a 30-day period centred on the given date. This tool provides only the basic information and guidance required to install a solar PV system. More accurate predictions of solar energy availability can also be obtained from NIWA as a commercial service. For this project, this SolarView tool guide was adequate to provide solar radiation details for the installation of the experimental solar array.

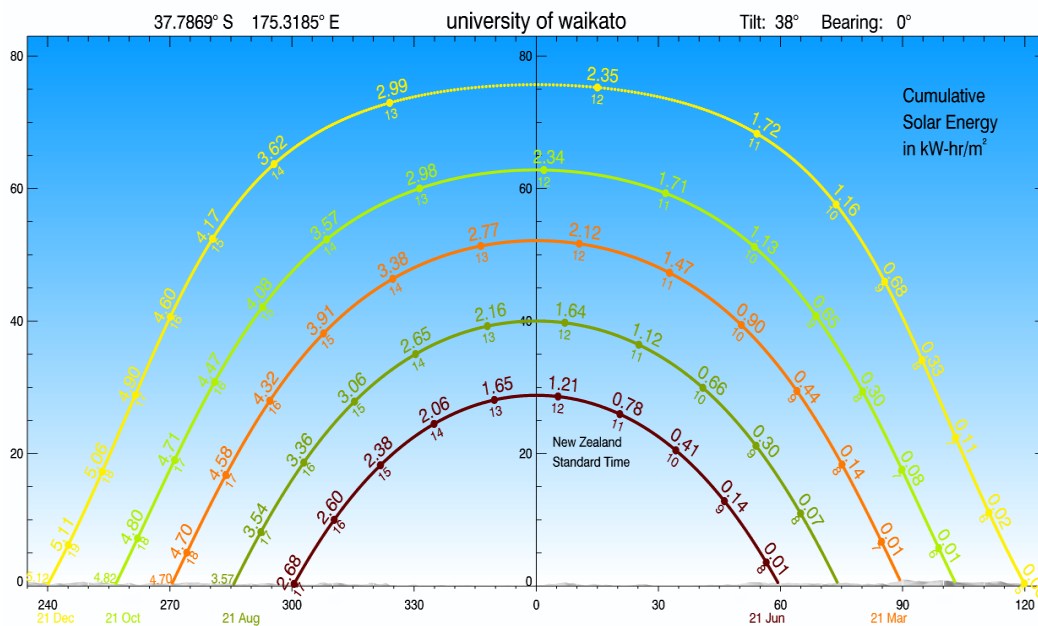


Figure 3-19: SolarView output showing the cumulative energy in kWh/m² showing the path of the sun

3.7 Installation of 1.12 kW solar array

Installation of the solar PV array was carried out on the rooftop of 'C' Block at the University of Waikato, based on the use of the SolarView tool as explained earlier. Managed by the Facilities Management Department of the university, both the installer and the research team were fully involved in the installation of the PV

module. Unlike a regular PV system, this system was installed without any other components such as an inverter, charge controller, or batteries. It just consisted of 4 Mitsubishi high performance monocrystalline PV-MLE series PV modules with a capacity of 280 watts each, 2 circuit breakers and 4 isolators as shown in configuration diagram in Figure 3-20.

The array consisted of 2 strings of solar array with 2 PV panels connected in parallel. Each string was connected to an isolator before the output cable was run down to the research lab, as shown in Figure 3-20. A total of four 6 mm² cables, two cables from each string, ran through the building ducts to the research lab where they were connected to two circuit breakers and then to another set of isolators. The output cable was then connected to the isolator and was available on the testing bench for testing of the SCALED circuit.

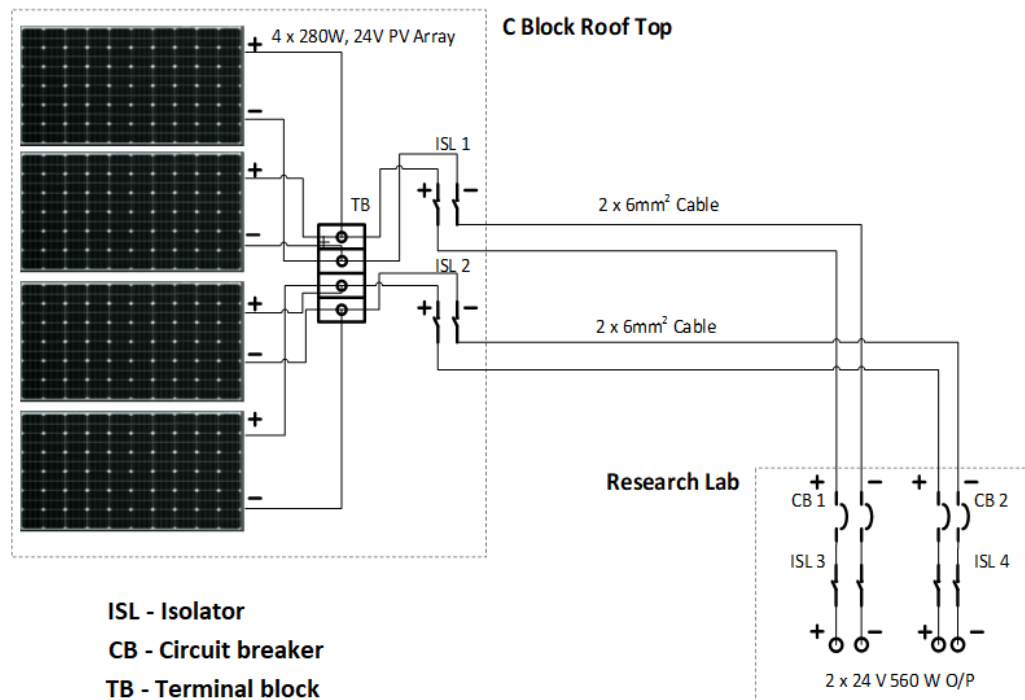


Figure 3-20: Solar panel configuration diagram

As per the requirements of the project, the output voltage had a reconfigurable terminal at the output side with voltage ranges of 24 V, 48 V and 96 V. The system was installed with two strings, each consisting of two panels in parallel producing two outputs with 24 V, 560 W each. To get an output of 96 V, all the PV panels were connected in series as shown in Figure 3-21 (a). To get an output of 48V two

strings were connected in series after the isolator in the research lab as shown in Figure 3-21 (b).

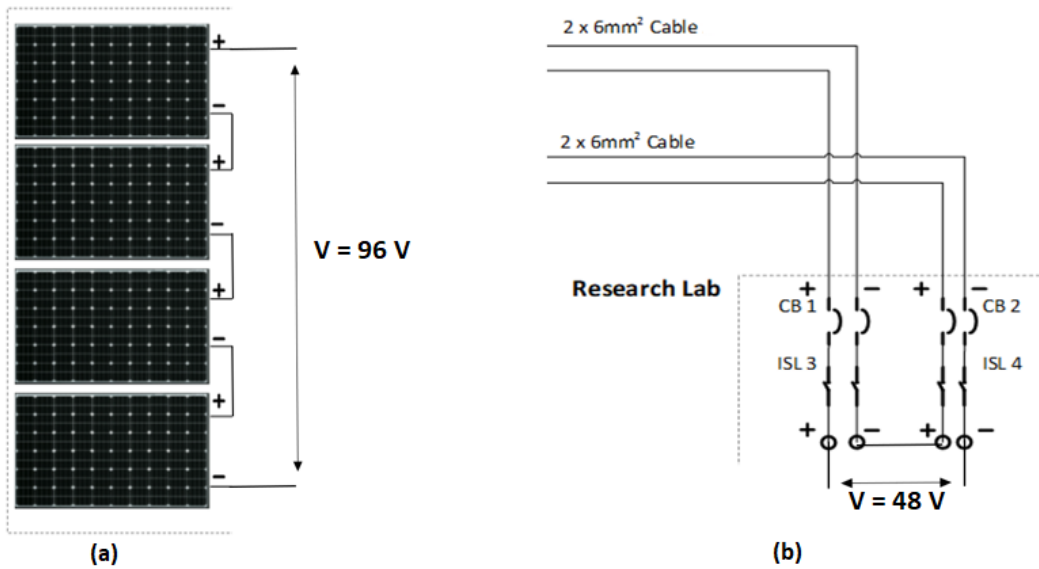


Figure 3-21: (a) PV panel configuration to get total output voltage of 96 V (b) Configuration at the output side to get total output voltage of 48 V

The 1.12 kW PV Array was installed on the flat roof with plenty of space for tapping solar power, as seen in Figure 3-22 (a). The angle of installation as determined using NIWA’s SolarView tool was achieved by mounting the structure to bring it to 38° facing north. This was done to receive the maximum solar energy from the sun as it travelled from east to west.



Figure 3-22: (a) 1.12 kW solar PV array installed at University of Waikato (b) Circuit breakers and isolators installed on the output side

Two parallel set of cables ran from each string to the research lab and were then connected to the circuit breaker and again to a set of isolators as shown in Figure 3-22 (b). This type of configuration provides the wide ranges of solar PV array output required for the testing of the SCALED application in a DC microgrid environment.

3.8 Energy storage for RE sources

DC microgrids, RE sources and ESDs have one common element: power and energy transfer occur in DC with increased overall efficiency [10]. RE sources such as the sun and wind are not continuous sources of energy; therefore, there is a need for devices to store energy in order to supply power to loads in the absence of the primary source.

Normally, RE sources such as PV modules supply energy to loads and simultaneously charge battery banks. During the night, when there is no solar power, the battery bank supplies power to the loads, thereby maintaining a continuous power supply. Rechargeable batteries are mostly used as ESDs for solar power systems. SCs also have their place in the solar PV system to stabilize momentary fluctuations in power output due to intermittent fluctuations in solar radiation caused by cloud cover or objects shading the PV panel for short periods. However, with recent improvements in the energy delivery ability of SCs, this project aims at using an SC bank to power a 12 V LED bank in a DC microgrid environment.

3.9 Charging SC bank directly from solar power

The time taken to charge a capacitor from a typical constant DC power supply depends on the time constant (τ), which is the product of capacitance (C) and the equivalent series resistance (R).

$$\tau = RC \tag{3-1}$$

The behavior of the SC while charging directly from solar power was interesting to observe. A fully discharged 50.4 V, 166 F SC was charged using the output of the first string of a solar array of 36.50 V_{oc}, 560 W on April 13, 2018 from 9.50 am to 10.25 am as shown in Figure 3-23. The weather during the experiment was partly cloudy with irregular sunshine. The charging current and the voltage were measured

every minute and simultaneously, the irradiance value was also measured on the roof top using a solar power meter.

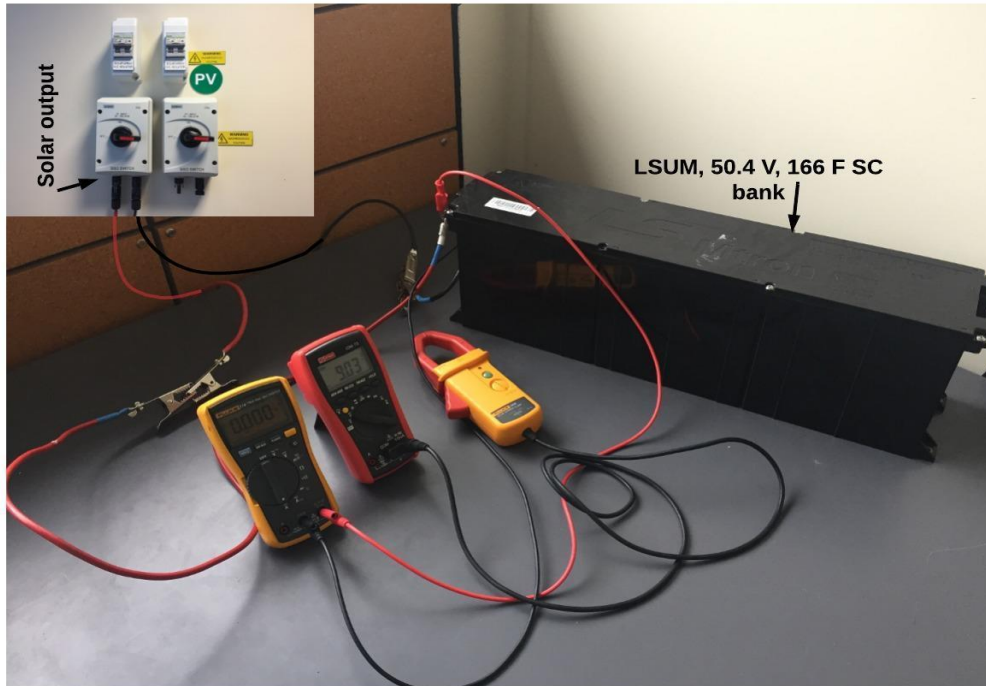


Figure 3-23: Charging of 50.4 V, 166 F SC bank directly from solar PV array output

The charging voltage, charging current and irradiance level versus time were plotted as shown in Figure 3-24. It took around 35 minutes to charge the SC bank to 36 V, which is approximately 75% of the total rated voltage of the SC bank. The SC bank cannot be charged beyond the maximum output voltage of the solar array, which is the V_{oc} of solar array output.

Table 3-2: Measurement data of charging current, charging voltage and irradiance level

Sl.no	Time (m)	Voltage (V)	Current (A)	Irradiance (W/m ²)
1	0	0.078	15.6	825
2	1	5.6	9.5	436
3	2	8.94	15.4	746
4	3	13.31	5.5	266
5	4	14.75	4.4	226
6	5	16.19	4.4	231
7	6	17.5	4.1	213
8	7	18.68	3.9	202
9	8	19.97	4.7	250
10	9	21.42	4.2	231
11	10	22.45	3.3	180

12	11	23.52	4.4	232
13	12	24.92	4.7	260
14	13	26.52	5.1	280
15	14	27.76	4.9	275
16	15	30.32	9	534
17	16	31.62	3.7	251
18	17	32.5	3.5	266
19	18	33.28	3	255
20	19	33.71	2.1	202
21	20	34.05	1.9	211
22	21	34.45	2.3	276
23	22	34.91	3.6	562
24	23	35.2	1	245
25	24	35.31	1	260
26	25	35.39	0.9	250
27	26	35.51	1.4	251
28	27	35.69	0.6	265
29	28	35.7	0.3	222
30	29	35.67	0.4	228
31	30	35.86	2.9	577
32	31	36.51	0.9	546
33	32	36.55	1.6	527
34	33	36.7	1.2	432
35	34	36.66	0.3	565

The graph clearly shows that the charging current curve follows the irradiance curve, establishing that the output current of the solar array is directly proportional to the level of solar irradiance. Also, it was observed that the rate of charging of the SC bank also depends on the charging current: the higher the irradiance, the shorter the charging time. The energy stored in the charged SC bank in the above experiment was around 30 Wh, which can power up to six 5 W LED lamps for an hour.

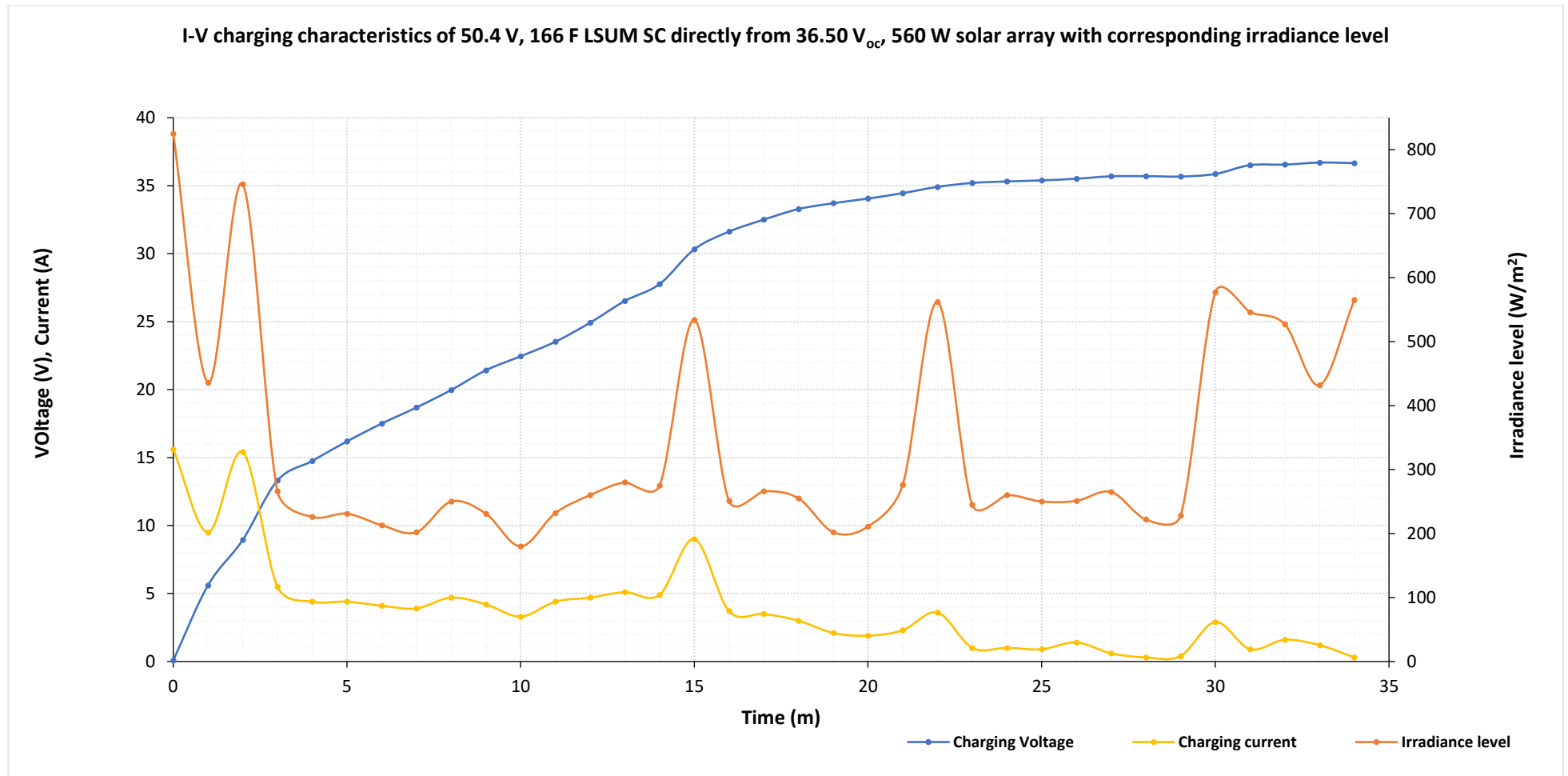


Figure 3-24: The charging voltage, charging current and corresponding irradiance level curves

Chapter 4
Energy Storage Devices &
Supercapacitors

4.1 General overview

Following The invention of the transistor in the late 1940s, electronic products and systems have become an essential part of the modern world, with interconnected global communication systems, intelligent white goods, electronic subsystem dominated automotives and a plethora of portable devices [3]. We have come to rely on a constant and steady electricity supply, which cannot be met using conventional energy sources alone. Therefore, we need devices that can store energy and use it any time, wherever and whenever required.

ESDs are the keystone of the future of sustainable energy systems [4]. They are very important for the continuous and consistent operation of any electrical and electronic system. An ESD is required to store energy and provide backup energy in the event of a failure in the main power supply. Such devices are extremely important in areas where power outages are common. Their role is even more important when they supply power to critical loads such as those in airports, semiconductor manufacturing industries, and computer server farms [3].

There are many different types of ESDs and it is a rapidly growing area of research, with many new technologies being developed to meet a variety of applications and requirements. The applications of ESDs range from smaller power and energy requirements such as wrist watches, which consume energy in microwatt-hours to milliwatt-hours, to larger energy requirements including uninterruptable power supplies in factories and working environments, which consume power at the level of 100 Watts to a few megawatts. This chapter provides descriptions of rechargeable batteries and supercapacitors and illustrates their fundamental differences.

4.1.1 Impact of the open circuit voltage and internal resistance of an energy source

A simple energy source with an energy storage capacity of E Wh is characterized by its open circuit voltage V_{oc} and its finite internal resistance r_{int} . Therefore, an ESD can be represented by a simplified equivalent circuit with a voltage source V and a lumped internal resistance r_{int} as shown in Figure 4-1 (a). We can have a load, in the form of a resistor depicted by R_L , connected to the device, which forms the closed circuit as shown in Figure 4-1 (b) [3].

Analyzing the circuit in Figure 4-1 using Ohm's law, the load current I_L is given by

$$I_L = \frac{V}{R_L + r_{int}} \quad (4-1)$$

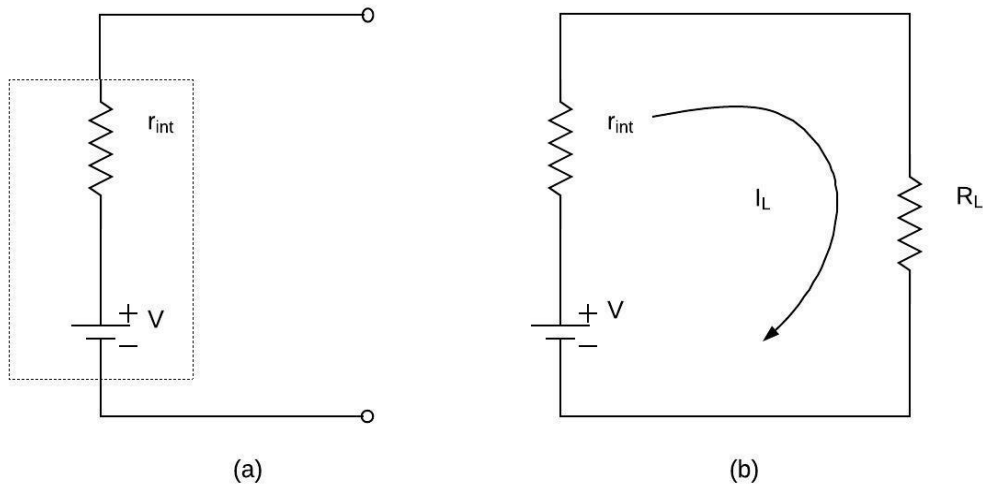


Figure 4-1: (a) ESD represented by a constant voltage source and fixed internal resistance, (b) Closed circuit formed by the external load R_L [3]

The voltage across the load is given by

$$V_L = \frac{VR_L}{R_L + r_{int}} \quad (4-2)$$

Which can be rewritten as

$$V_L = \frac{V}{1 + \frac{r_{int}}{R_L}} \quad (4-3)$$

Equation 4-3 shows that the voltage across the load R_L keeps dropping as the internal resistance r_{int} increases and keeps increasing as the source voltage increases. Therefore, a good energy source should have low internal resistance and a high open circuit voltage.

The power dissipated across the load is given by

$$\begin{aligned} P_L = V_L I_L &= \frac{V}{1 + \frac{r_{int}}{R_L}} \frac{V}{R_L + r_{int}} \\ &= \frac{V^2}{R_L} \left[\frac{1}{\left(1 + \frac{r_{int}}{R_L}\right)^2} \right] \end{aligned} \quad (4-4)$$

Equation 4-4 shows that the power deliverable at the load by an ideal source ($r_{\text{int}} = 0$) is given by

$$P_L = \frac{V^2}{R_L} \quad (4-5)$$

However, no power sources are ideal in practice. Therefore, Equation 4-4 shows that the power delivered is restricted by the internal resistance (r_{int}) of the power source. It can be seen that the internal resistance of a battery keeps on increasing with the discharge, as shown in Figure 2-3 in Chapter 2. Therefore, in rechargeable batteries, the power keeps on dropping due to the increase in internal resistance as the cell discharges. In contrast, SCs have very low and approximately constant internal resistance, in the order of milliohms, which allows them to drive large amounts of power into the load [3].

4.1.2 Maximum power transfer

In the simple circuit shown in Figure 4-1 (b), part of the power is dissipated in a series element across r_{int} , so the useful power delivered across the load is always less than the power deliverable by the energy source. The maximum power that can be transferred to the load can be obtained by differentiating Equation 4-4 with respect to R_L . We can show that the maximum possible load power occurs when $R_L = r_{\text{int}}$. Applying this in Equation 4-4, the maximum power P_{max} transferred is given by

$$P_{\text{max}} = \frac{V^2}{4R_L} \quad (4-6)$$

4.1.3 Different types of ESDs

Figure 4-2 gives a graphical representation of some of the common energy storage technologies. It compares available energy storage technologies in terms of capacity versus discharge time. Pumped storage and compressed air are among the highest capacities, with higher discharge times. Supercapacitors have relatively high capacity with very low discharge times and batteries fall in the middle with lower capacity than supercapacitors but higher discharge times. As ESDs come in different forms, Figure 4-2 also indicates short-term and longer-term applications depending on their discharge characteristics. Short-term ESDs are required in

applications needing backup energy for a short period of time, whereas long term ESDs are required in applications where backup energy is needed for a longer time.

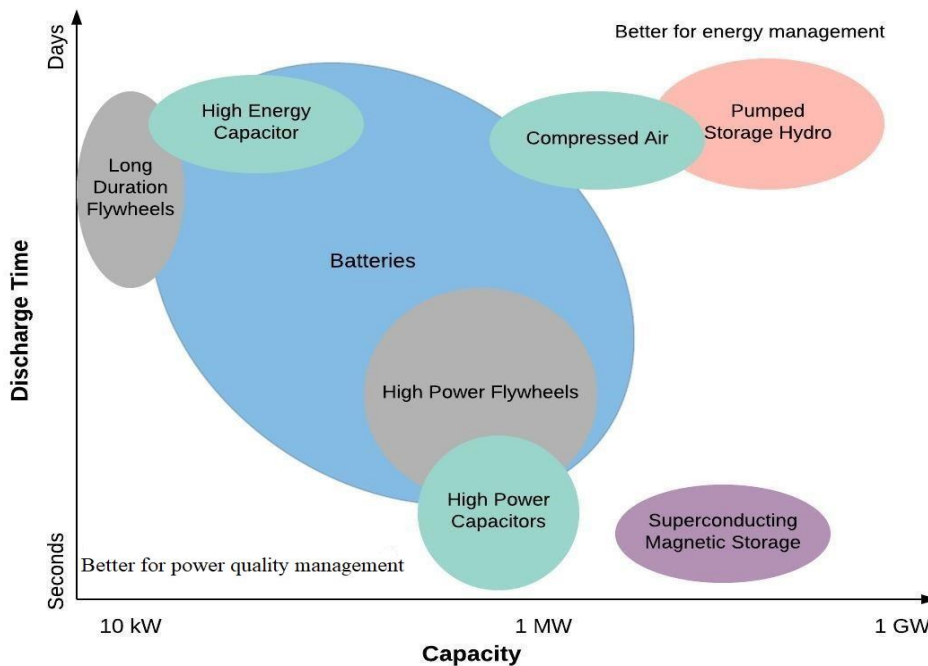


Figure 4-2: Energy storage technologies (source : EIA)

Some of the commonly used energy storage devices are as listed below, followed by brief descriptions of each:

1. Pumped storage
2. Fuel Cells
3. Flywheels
4. Compressed air
5. Batteries
6. SC banks

Pumped storage is the most common and efficient energy storage technology, using the gravitational potential energy of water. It pumps water to an elevated storage point when there is less demand for electricity and then uses it at times when there is high demand for electricity. It is very easy to commence generation, and such systems can come online whenever there is demand, with an efficiency of 70% to 80%.

A fuel cell is a galvanic cell in which the chemical energy of a fuel is converted directly into electrical energy by means of electrochemical processes [3]. There are many types of fuel cells, categorised by their power capabilities and applications. Hydrogen-based fuel cells make use of the reaction of hydrogen with oxygen to produce electricity through electrochemical processes. They do not emit any harmful gases as there is no combustion taking place.

Flywheels store energy from the kinetic energy of motion of a rotating mass and the rotational speed of the rotor. The kinetic energy stored in the rotor, E_k is given by

$$E_k = \frac{1}{2} J\omega^2 \quad (4-7)$$

Where J is the moment of inertia and ω is the angular velocity.

This type of system is highly efficient, but it poses dangers due to its very high-speed rotating parts.

Compressed air is a type of mechanical energy storage system, where energy is stored as compressed air for later use. Natural caverns are often used as air reservoirs to store large amounts of energy, from where energy extraction may finally occur in a gas turbine. The efficiency of compressed air energy storage system is relatively low, at less than 50%.

Batteries are one of the oldest and most widely used energy storage technologies, which store energy in the form of chemical energy. Batteries come in many different chemical compositions and forms. They basically work on electrochemical reactions, which produce free electrons that create an electric current. They are generally highly efficient and can store large amounts of energy. More details of rechargeable batteries are provided in later in this chapter.

SC banks are a relatively new and emerging technology in energy storage. They are very high capacitance capacitors with lower voltages. They are usually combined with battery packs to form a hybrid storage system to get the best performance from both. SCs are known for their high-power densities, with very high-power handling capacities for short periods. More details about SCs are provided later in this chapter.

4.1.4 Technical specifications of ESDs

ESDs are characterized by a set of general specifications, which allow us to quantitatively compare various families of devices [3]. These specifications are listed, with brief explanations, as follows:

1. Energy density

Energy density is the amount of energy stored per unit volume or unit mass. It is called gravimetric energy density when mass is used and volumetric energy density when space is used. The units of measurement are Watt-hours per litre or Watt-hours per kilogram

2. Power density

Power density is the amount of power delivered per unit volume or unit mass. It is called the volumetric power density when volume is used and gravimetric power density when mass is used. The units of measurement are Watts per litre and Watts per kilogram.

3. Cycle life

The cycle life of an ESD is the ability to withstand repetitive deep discharging and recharging as per the manufacturer's cyclic charging recommendations while still proving the minimum required capacity. It is measured in terms of numbers of cycles of discharging and recharging.

4. Cyclic energy density

Cyclic energy density is defined as the product of energy density and cycle life. This gives the energy density over the service life of the ESD, which provides more composite characteristics for comparison.

5. Self-discharge

Self-discharge is a measure of how long an ESD can retain its stored energy when left unused on a shelf. It is normally measured by monitoring the open circuit voltage over time.

6. Charge acceptance

Charge acceptance is the ratio of charge fed into the device (C_{charge}) to the charge that is delivered to the load (C_{load}). This depends on the temperature, charge/discharge rate, age and overall conditions of the ESD. It is measured in coulombs or Ampere-hours and is also called the coulomb-efficiency.

4.2 Rechargeable battery technology overview

Following the invention of the lead-acid battery by Gaston Planté in 1859, electrochemistry has progressed steadily over the last one and half centuries [3]. With recent advancements in the technology of portable devices, the demand for ESDs has increased drastically. Batteries are broadly classified into two types: primary (disposable) and secondary (rechargeable). Depending on the chemistries and the sizes, both types of batteries are further classified into many different categories.

The commonly available disposable batteries offer significantly greater energy density with lower rates of self-discharge. Some of the commonly available disposable batteries include: carbon-zinc, alkaline-MnO₂, lithium-MnO₂, lithium-sulphur dioxide, silver-oxide, and zinc-air. They are usually cheaper than rechargeable batteries. They are reasonably established in the battery market with ongoing attempts to further increase the energy density and reduce self-discharge rates to increase shelf life.

Mature rechargeable battery chemistries are: lead acid, nickel cadmium, nickel metal hydride, lithium-ion, lithium-polymer and lithium-iron phosphate [3]. The large and increasing demand from the electric vehicle (EV) market and portable devices has led many companies to invest huge sums of money into the research and development of new battery chemistries with higher energy densities, superior cycle life, better environmental friendliness and safer operation. Many rechargeable batteries are used in electronic systems, varying in size, weight, cycle life, cost and operating temperature range. Nickel-based chemistries were used to power most earlier consumer appliances. Now lithium ion batteries are more popular, with higher performance in terms of energy and power delivery capability. Lead acid batteries are the oldest and still most widely used rechargeable batteries, mostly in the automobile industry. The following sections explain the fundamentals of rechargeable batteries, especially lead acid, with some experimental findings.

4.2.1 Battery charging and discharging behavior

The charge acceptance of sealed lead-acid batteries in most situations is quite high, typically greater than 90% [3]. A 90% charge acceptance means that for every ampere-hour of charge introduced into the cell, the cell will be able to deliver 0.9

Ah to the load. Charging of a battery depends on many factors, including the cell temperature, charge rate, cell SOC, age of cell and the method of charging.

The discharge voltage of a sealed lead acid battery typically remains relatively constant almost throughout its discharge period. Figure 4-3 shows the typical discharge curve of a rechargeable battery, where the voltage remains almost constant, near to its nominal voltage, until about 80% of its discharge capacity is reached. As it approaches the end of its discharge capacity, it is characterized by a sharp decrease in voltage, which is called the knee of the discharge curve. This is mainly due to an increase in its internal resistance with the increase in percentage discharge.

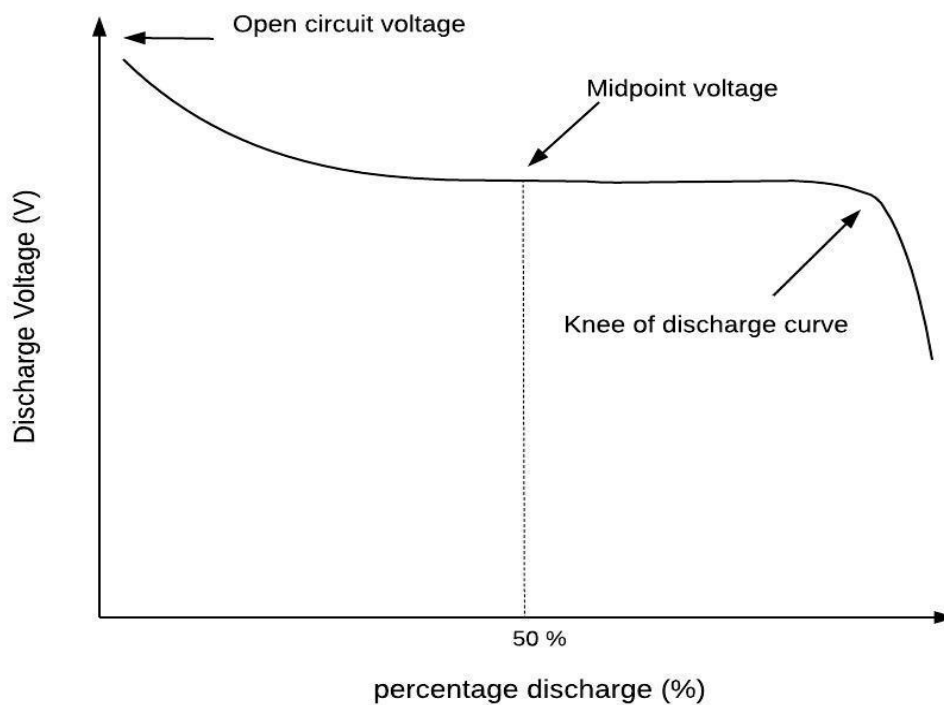


Figure 4-3: Typical discharge curve of a rechargeable batteries [3]

To demonstrate these charging and discharging characteristics, a fully discharged 12 V, 12 Ah sealed lead acid battery was charged using a bench power supply with constant current of 2 A. The lead acid battery was quite old, and the experiment was carried out at room temperature. The whole charging process took around two hours. The measured data are recorded in Table 4-1.

Table 4-1: 12 V, 12 Ah lead acid battery charging current and voltage measurement data

Sl.no	Time (m)	Charging Current (A)	Charging Voltage (V)
1	0	0	12.51
2	5	2.09	14.61
3	10	2.07	14.66
4	15	2.08	14.65
5	20	2.06	14.65
6	25	2.07	14.65
7	30	2.05	14.65
8	35	2.06	15.32
9	40	2.04	15.32
10	45	2.05	15.31
11	50	2.03	15.32
12	55	2.02	15.32
13	60	2.01	15.32
14	65	2.01	15.32
15	70	2	15.32
16	75	1.9	15.32
17	80	1.8	13.7
18	85	1.8	13.75

Figure 4-4 shows a graphical representation of the charging current and voltage. The voltage initially increased to around 15 V and then remained constant throughout the process until the final voltage stabilized at 13.7 V. The charging current was maintained constant at around 2 A throughout the charging period.

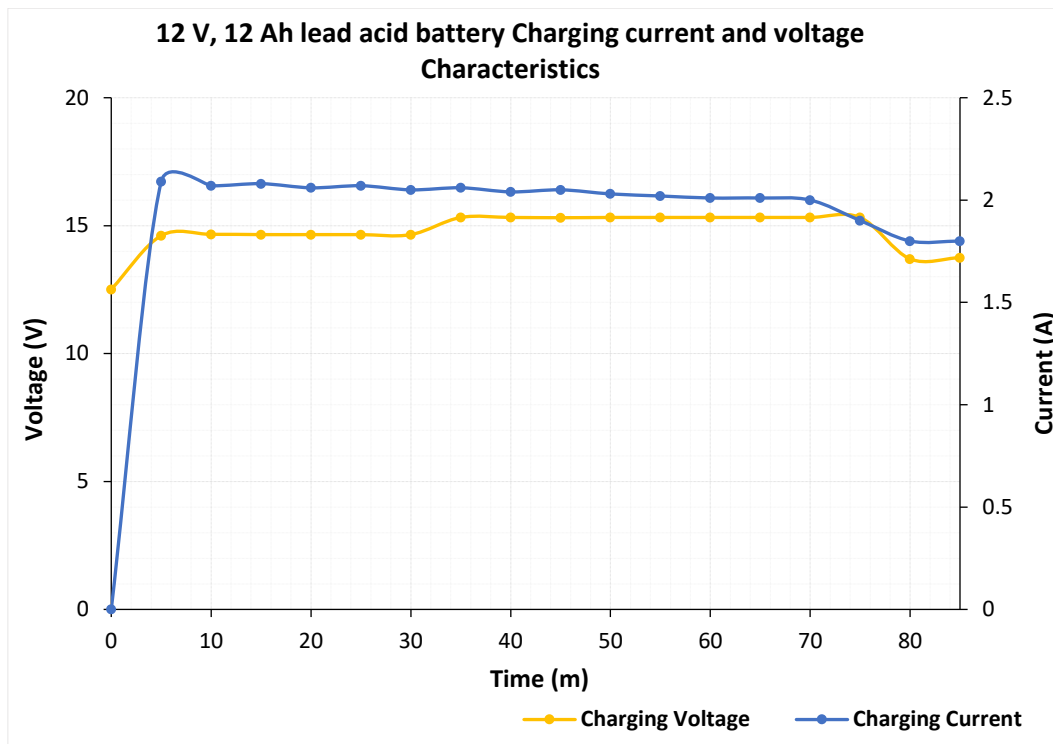


Figure 4-4: 12 V, 12 Ah lead acid Battery charging current and voltage characteristics

Discharging of a lead acid battery is possible at wide ranges of temperatures, but it largely depends on the amount of current drawn from it. The discharge voltage typically remains constant throughout most of the discharge period. The fully charged 12 V, 12 Ah battery was discharged in this experiment using a 20 W LED bank made up of four sets of 5 W LED lamps in parallel.

Table 4-2: 12 V, 12 Ah lead acid battery discharging current and voltage measurement data

Sl.no	Time (m)	Discharging Current (A)	Discharging Voltage (V)
1	0	0	13.27
2	5	1.85	12.55
3	10	1.83	12.51
4	15	1.83	12.47
5	20	1.83	12.43
6	25	1.84	12.39
7	30	1.84	12.37
8	35	1.84	12.35
9	40	1.85	12.31
10	45	1.86	12.27
11	50	1.87	12.24
12	55	1.87	12.22
13	60	1.87	12.2
14	65	1.88	12.18

15	70	1.88	12.15
16	75	1.89	12.12

The typical characteristic of a battery is that it can provide continuous energy for longer periods because of its higher energy density. Figure 4-5 represents the discharging voltage and current characteristics. There was little variation in battery voltage throughout the discharging process, and the discharge current remained approximately constant.

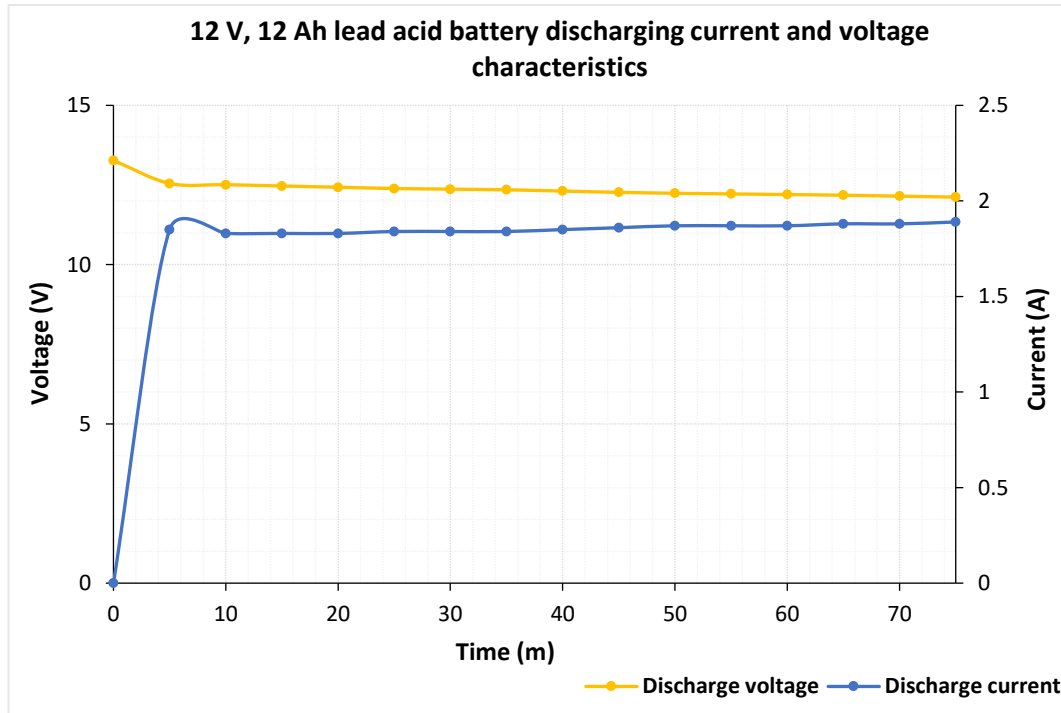


Figure 4-5: Discharging current and voltage characteristics of a lead acid battery using 20 W LED bank as load

The LED lamp characteristics show that they have a voltage range of constant brightness as shown in Figure 2-10 in Chapter 2. The LED bank in this case also draws a constant current as the battery can deliver a constant voltage, maintaining constant brightness. As this project focused on using SCs as an energy storage system, the discussion of SCs is mostly covered here.

4.3 Supercapacitor

The concept of a double layer capacitance was first developed by German physicist Hermann von Helmholtz [3]. A supercapacitor is based on the same principle as an electrostatic capacitor, with higher effective capacitance that is achieved by

increasing the area of the plate and reducing the distance between the electrodes. A capacitor stores electrical charge across its parallel plates when connected to a DC voltage and releases it when it is required by the circuit.

The capacitance of a parallel plate capacitor is given by the formula:

$$C = \epsilon \frac{A}{d} \quad (4-8)$$

Where C - capacitance

ϵ - permittivity of the dielectric material

A - Area of electrode

d – distance between the electrodes

An EDLC or SC consists of porous carbon electrodes with double layer capacitance where the charges are accumulated, forming an electric double layer. Figure 4-6 shows the difference in the construction of different types of capacitors. Though supercapacitors are limited by their operating voltage, with voltages confined to around 2.5 V to 2.7 V, a higher voltage with higher energy can be achieved by connecting them in series.

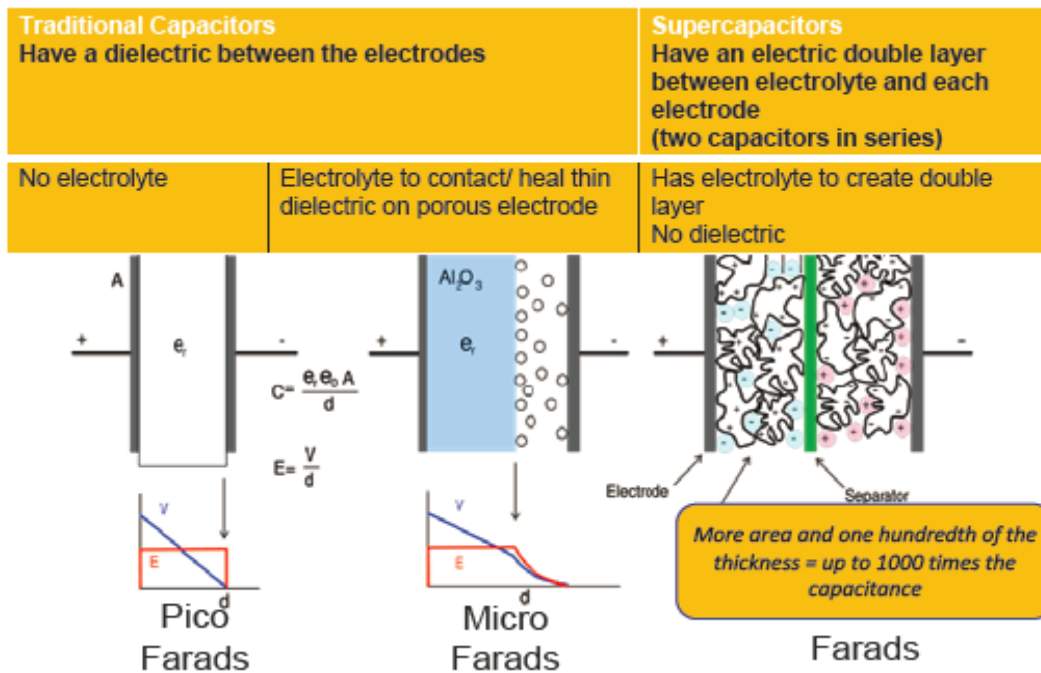


Figure 4-6: Constructional difference between traditional capacitors and supercapacitors [4]

Figure 4-6 shows the different types of capacitors in increasing order of capacitance from picofarads to farads. Higher capacitance is achieved by increasing the surface area of the electrodes and the distance between them.

4.3.1 Supercapacitor charging and discharging behavior

SCs' quick charge and discharge characteristics have numerous advantages and disadvantages. The short time to charge is convenient and the quick discharge enables the production of short bursts of power, which makes them applicable in specific fields; for example, as truck starters. The disadvantage is that they cannot feed the load for longer periods, which makes them unsuitable for applications requiring energy over longer time periods. Figure 4-7 (a) demonstrates the internal distribution of ions when the capacitor is charged. It quickly aligns to the opposite polarity ready to provide energy whenever a load is connected across it.

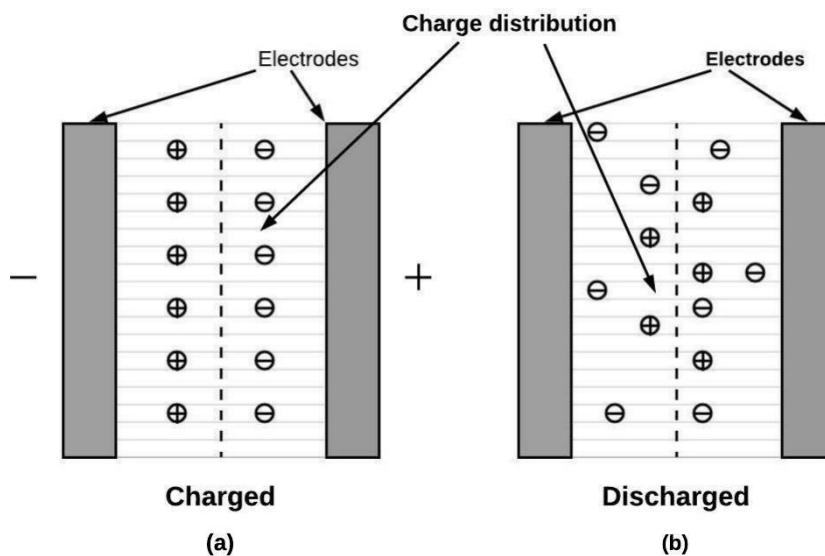


Figure 4-7: Distribution of ions in charged and discharged capacitor

In contrast, a discharged capacitor will have a random distribution of ions as shown in Figure 4-7 (b). The open circuit voltage in this state will be near to zero, showing that there is no more energy left to discharge. A typical discharge characteristic of SCs over the discharge period is shown in Figure 4-8. The voltage decreases at a steady rate over the period of discharge.

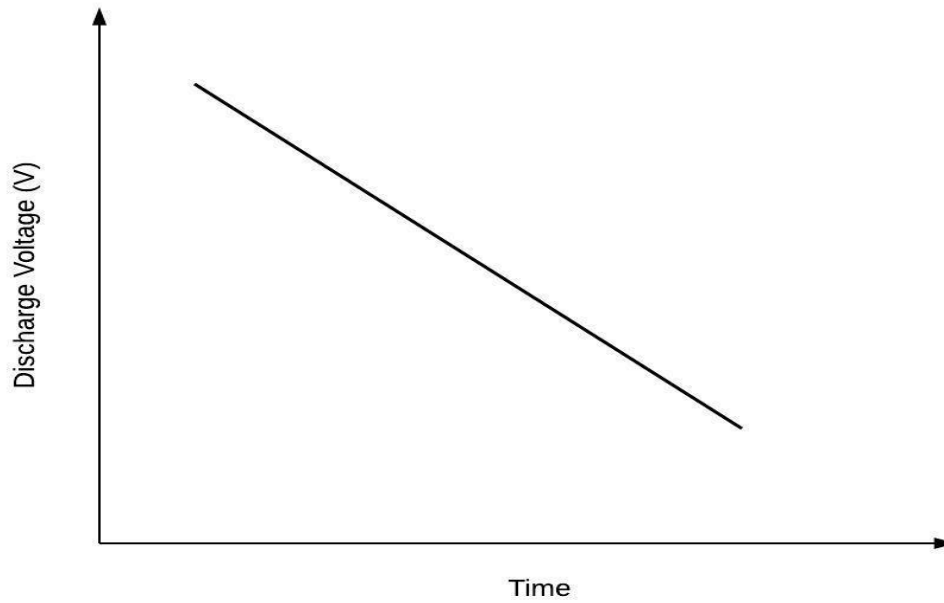


Figure 4-8: Typical discharge characteristics of SCs

A 43.2 V, 93.75 F SC bank was assembled using 16 SCs, each 2.7 V, 1500 F, as shown in Figure 4-9. The SC bank was charged using a bench power supply of 30 V with a constant current of 2 A.



Figure 4-9: SC bank assembled using 16 SCs, each of 2.7 V, 1500 F.

The charging current and voltage were measured every 5 minutes and results are shown in Table 4-3.

Table 4-3: SC charging current and voltage measurement data

Sl.no	Time (m)	Charging Current (A)	Charging Voltage (V)
1	0	0	1.04
2	5	2.09	8.05
3	10	2.08	14.19
4	15	2.08	19.31
5	20	2.08	23.5
6	25	2.08	27.1
7	30	2.07	30.48
8	36.5	0.41	31.41

The charging process took only around 30 minutes with a final terminal voltage of 30 V. The current and voltage were then plotted as shown in Figure 4-10. The voltage initially increased at a constant rate and then once it became almost equal to the source voltage, it remained steady until the end of the charging period. The charging current initially increased to around 2.09 A and remained almost constant throughout the charging process, and then towards the end, it reduced sharply to zero. A fully discharged capacitor, when connected to a DC power supply, acts as a short circuit drawing the maximum current. But as its terminal voltage increases over time, the charging current keeps on decreasing until the capacitor doesn't accept any more charge, which is when the capacitor voltage becomes equal to the source voltage.

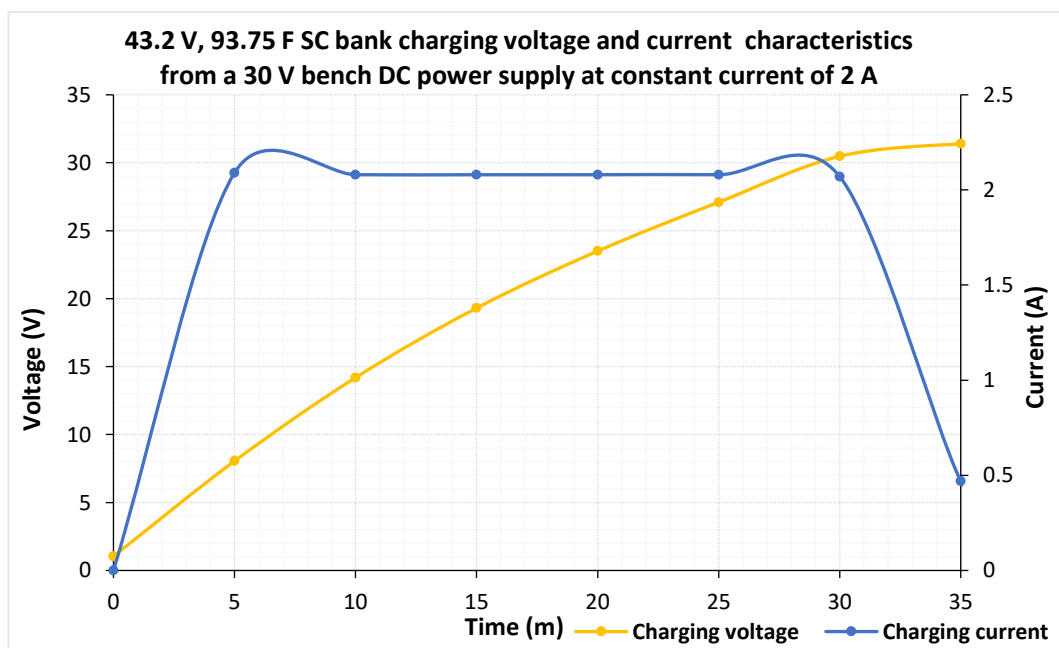


Figure 4-10: Supercapacitor charging voltage and current characteristics

To obtain the discharge characteristics, a 20 W LED bank was used as a load, like the one used for discharging the lead acid battery. As the SC discharged, the terminal voltage initially decreased slowly with an almost constant discharge current of 1.8 A.

Table 4-4: SC discharging current and voltage measurement data

Sl.no	Time (m)	Discharging Current (A)	Discharging Voltage (V)
1	0	0	31.18
2	5	1.16	28.04
3	10	1.28	24.78
4	15	1.45	21.03
5	20	1.34	17.3
6	25	1.84	12.9
7	30	4.97	3.7
8	32	0.1	1.21

Towards the end of the discharging process, the voltage decreased at a faster rate and the current increased at same rate, maintaining constant brightness.

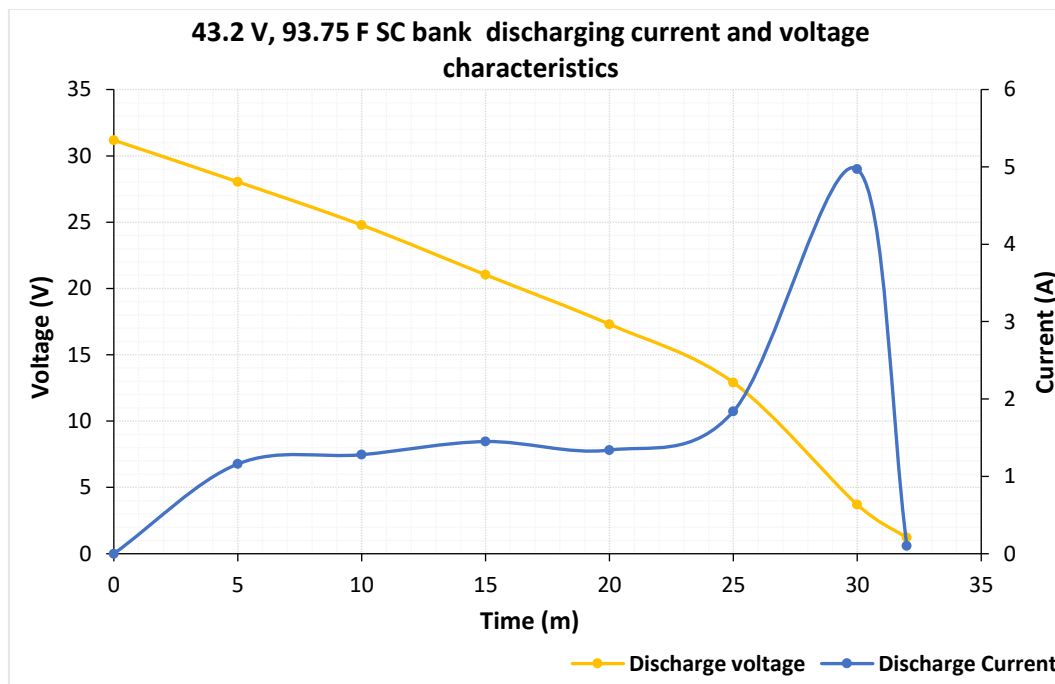


Figure 4-11: SC discharging voltage and current characteristics using 20 W LED bank as load

4.4 Hybrid capacitor

A newer family of SCs called hybrid capacitors was recently introduced to the market. Hybrid capacitors have relatively higher energy and density than the usual

SCs. There has subsequently been rapid development in the hybridization of batteries and capacitors. Many manufacturing companies have started manufacturing hybrid capacitors due to their advantages over other SCs. The SAMWHA ESD-SCAP is a promising energy storage device that is positioned between a conventional EDLC and a Li-ion battery [30]. Figure 4-12 shows a comparison of all types of capacitors and batteries in a simple table, including some important details such as energy density and power density.

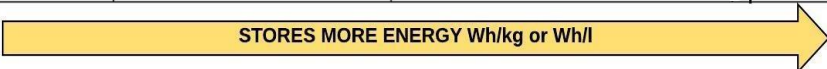
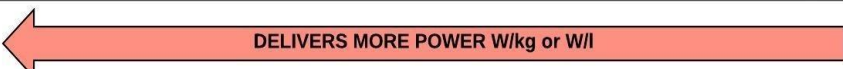
Traditional Capacitor	Supercapacitors/ Ultracapacitors	Hybrid supercapacitor	Batteries
	Symmetrical EDLC	Asymmetric EDLC	
		One SC electrode + one Battery electrode	
			
			

Figure 4-12: Different SCs and batteries in terms of energy and power density [4]

4.5 Battery capacitor

One of the most advanced supercapacitors from SAMWHA is called a battery capacitor, with a capacitance value as high as 70,000 F. It is a perfect combination of Li-ion battery and supercapacitor technology that makes it possible to simultaneously achieve high power density, high energy density, long cycle life and safety.

It has the following features [30]:

- It exhibits excellent input/output characteristics over a wide SOC range of 0 to 100%
- The capacity remains at 70% after 15,000 cycles
- The battery capacitor can accept large current input and output during charging and discharging. Thus, it provides rapid charging to 80% of capacity in 6 minutes at 10C

- There is no risk of fire or explosion because the lithium titanium oxide is applied as an anode material

SAMWHA’s battery capacitors find applications in solar power systems, emergency lighting, industrial machinery, the automotive industry, and uninterruptable power supplies.

4.6 Comparison between different types of SCs

Figure 4-13 compares the three different types of SCs: conventional SCs; hybrid capacitors; and battery capacitors in terms of their sizes and different parameters. All three types of capacitors have similar dimensions but in terms of stored energy, the advanced battery capacitor can store around 9 times the energy that can be stored in traditional SCs.



Figure 4-13: Three different types of SCs

The parameters of the above three capacitors are compared and tabulated as shown in Table 4-5. The comparison shows that there has been a considerable increase in the energy density and power density in SC technology over time.

Table 4-5: Comparison of three different types of SCs

Parameters	Supercapacitor	Hybrid capacitor	Battery capacitor
Manufacturer	LS Mtron Ltd.	Samwha Capacitor Co., Ltd.	Samwha Capacitor Co., Ltd.
Type / Part no.	LSUC	ESD SCAP CL	ESD SCAP CB
Rated voltage	2.7 V	2.8 V	2.7 V
Capacitance	3000 F	7500 F	40,000 F
Cycle life time	1,000,000 cycles	>50,000 cycles	>20,000 cycles
ESR (DC)	0.23 mΩ	0.8 mΩ	0.7 mΩ
Operating temperature	-40 – 65 °C	-20 – 40 °C	-20 – 50 °C
Maximum stored energy	3.04 Wh	5.488 Wh	26.27 Wh
weight	0.515 kg	0.560 kg	0.710 kg
Dimensions	Φ60 X L138mm	Φ60 X L138mm	Φ60 X L138mm

4.6.1 Comparison of discharge current and voltage characteristics of different types of SCs

Energy density and power density are the most important parameters of ESDs. SCs are high power density devices with relatively lower energy densities. However, with improvements in technology, recent hybrid capacitors have been designed to achieve higher energy densities with the combination of capacitors and batteries.

To study the discharge characteristics of all of the above three capacitors, the fully charged SC was connected across a resistive load such as the car head lamp as shown in Figure 4-14. To get an accurate discharge curve, a constant current discharge load is required, which draws a constant current. Because the resistance of the bulb is not purely resistive change with voltage and temperature, this gives only the approximate discharge characteristics.

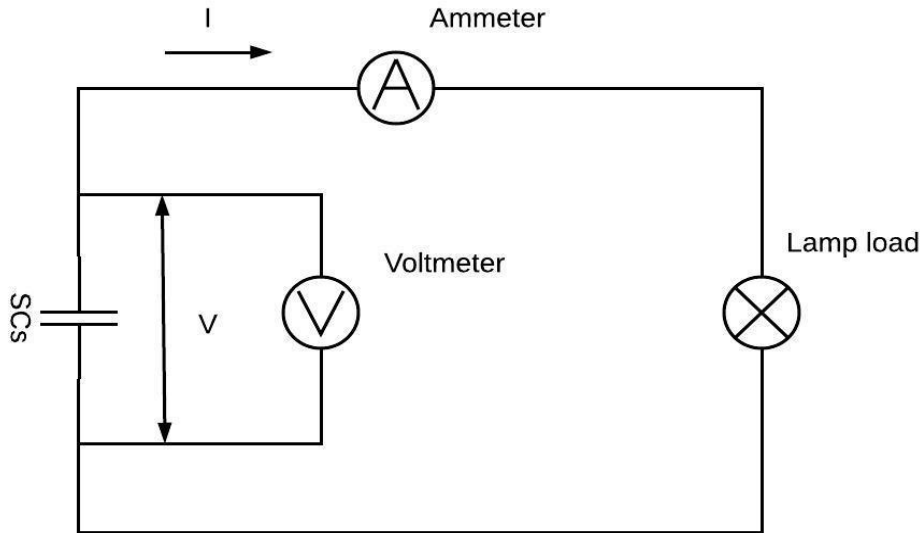


Figure 4-14: Experimental set up to obtain the discharge characteristics of different types of SCs

4.6.1.1 Discharge characteristics of SCs

Figure 4-15 shows the discharge characteristics for a 3000 F, 2.7 V, type LSUC SC. A 12 V, 21 W car head lamp was used as the load to discharge the SC. Both the voltage and the current decreased over the time of discharge as shown in Figure 4-15. It took around 3.5 hours to fully discharge the SC.

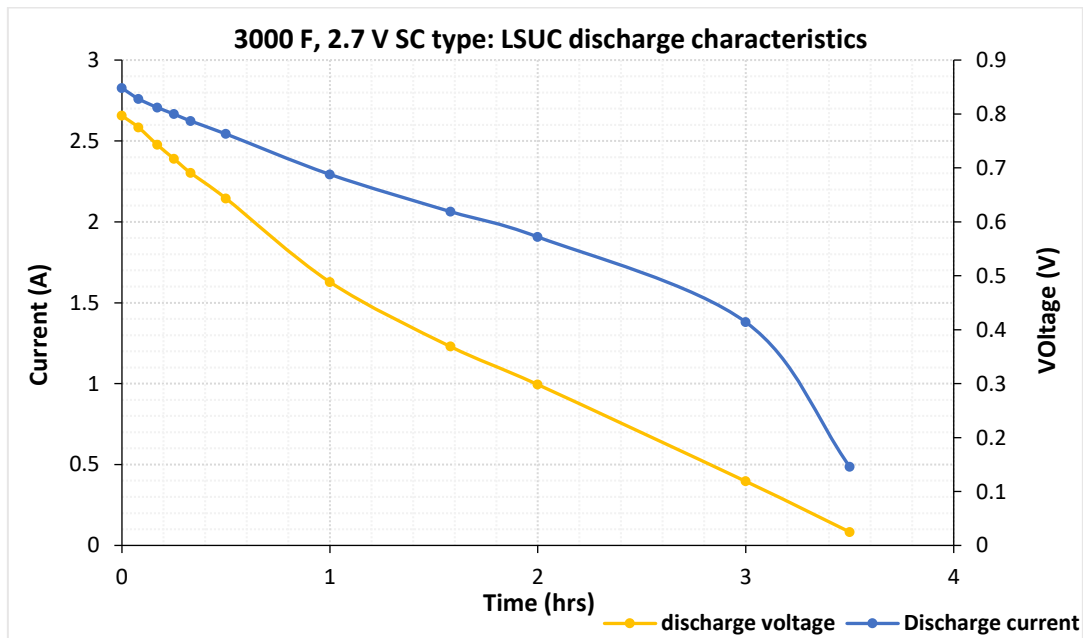


Figure 4-15: Discharge characteristics of 3000 F, 2.7 V, type: LSUC SC

4.6.1.2 Discharge characteristics of hybrid capacitor

The discharge characteristics of the 7500 F, 2.7 V, type: ESD CAP CL hybrid capacitor was quite different from the SC, as shown in Figure 4-16. The same 12 V, 21 W car head lamp was used as a load. This device maintains its terminal load voltage and current to around 80% of its maximum value for approximately 67% of the discharge period. At the end of discharging, both the current and the voltage decreased sharply. This device took around 4 hours to completely discharge.

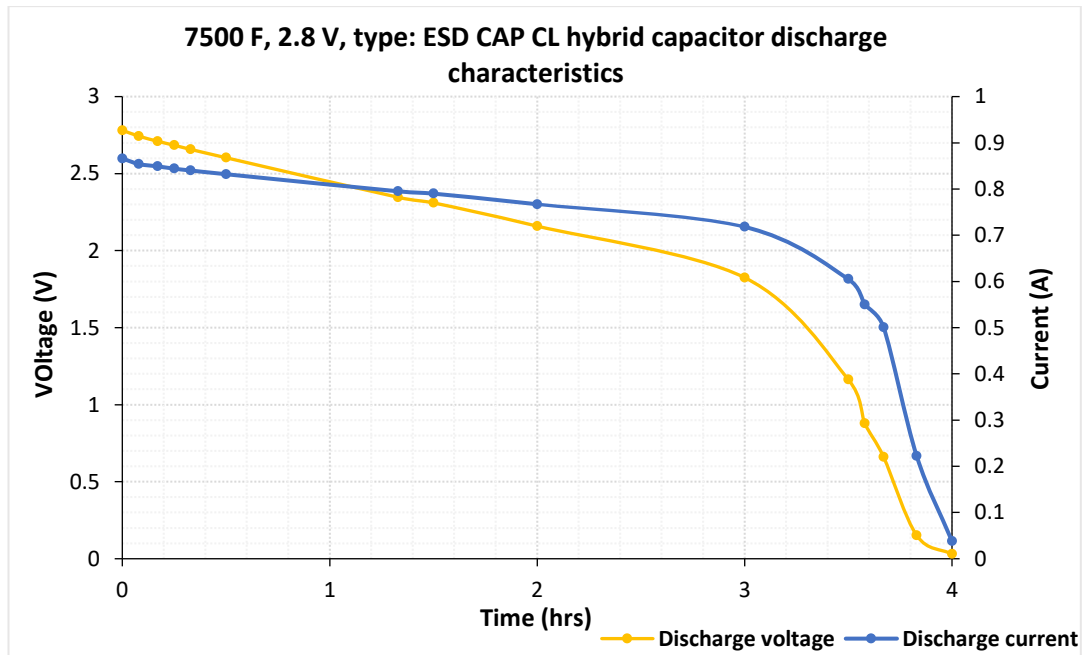


Figure 4-16: Discharge characteristics of 7500 F, 2.8 V, type: ESD CAP CL hybrid capacitor

4.6.1.3 Discharge characteristics of battery capacitor

The discharge curves of the battery capacitor almost resembled those of the battery, as shown in Figure 4-17. As this device delivers very high energy compared to the other two types of SCs, a 42 W, 12 V lamp was used to discharge this device. The curve shows that it maintained both its load current and the voltage almost constant for about 90% of the discharge time. In the final 10% of the discharge time, both current and voltage decreased sharply. It took around 11 hours to completely discharge the device.

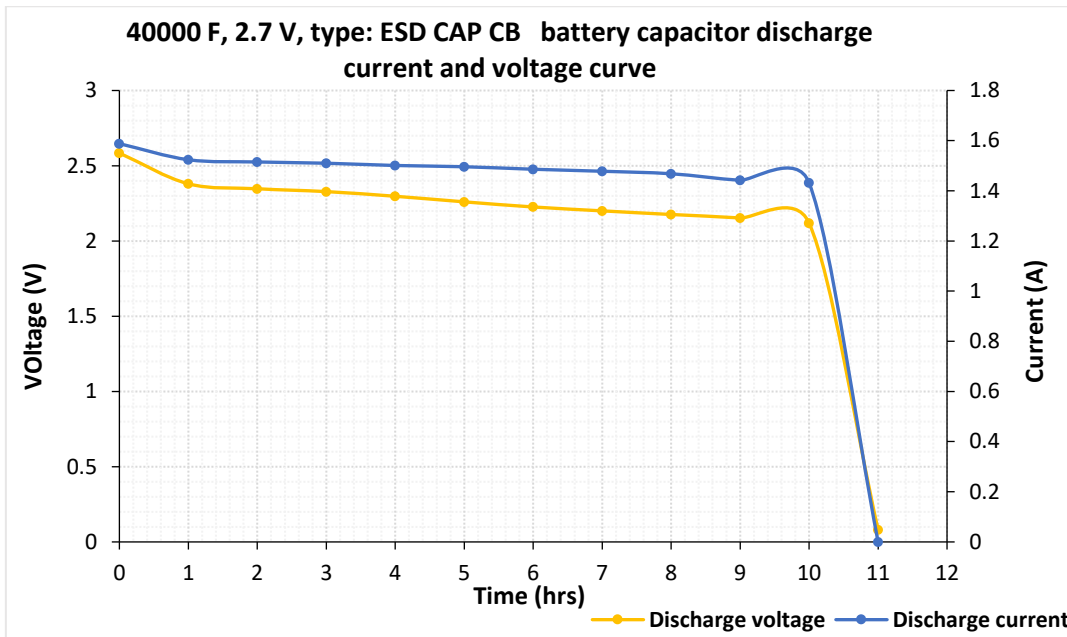


Figure 4-17: Discharge characteristics of 40000 F, 2.7 V, type: ESD CAP CB battery capacitor

To get the energy storage capability of all the above three types of SCs in a single graph, the hourly cumulative energy in Wh of each SC was calculated as shown in Table 4-6.

Table 4-6: Cumulative hourly discharge energy in Wh of all three types of SCs

Sl.no	Time (hrs)	SC voltage (V)	SC discharge energy (Wh)	Hybrid capacitor voltage (V)	Hybrid capacitor discharge energy (Wh)	Battery capacitor Current (A)	Battery capacitor Voltage (V)	Battery capacitor discharge energy (Wh)
1	0	2.656	0	2.781	0	1.588	2.584	0
2	1	1.628	1.120	2.448	1.983	1.524	2.38	3.627
3	2	0.994	1.689	2.159	3.639	1.515	2.347	7.183
4	3	0.396	1.853	1.825	4.949	1.51	2.328	10.698
5	4	0	0	0.03	4.950	1.501	2.297	14.146
6	5	0	0	0	0	1.496	2.26	17.527
7	6	0	0	0	0	1.486	2.226	20.835
8	7	0	0	0	0	1.478	2.2	24.086
9	8	0	0	0	0	1.468	2.176	27.281
10	9	0	0	0	0	1.442	2.153	30.385
11	10	0	0	0	0	1.432	2.119	33.420
12	11	0	0	0	0	0	0.081	33.420

The cumulative energy in Wh of each type of SC was then plotted against respective voltages in a single graph as shown in Figure 4-18. This graph clearly compares the energy storage capability in Wh of each type of SC. The energy storage capacity of

the recently introduced battery capacitor was found to be more than 10 times that of the conventional SCs.

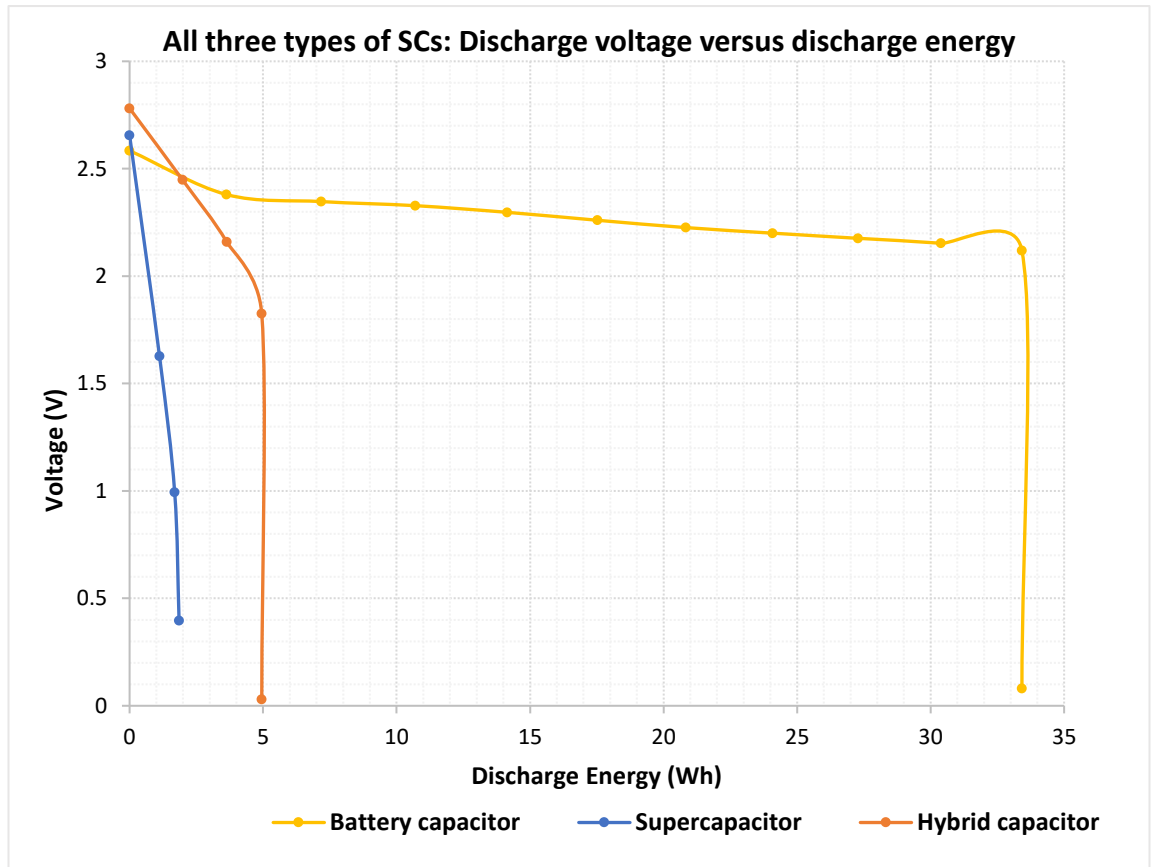


Figure 4-18: Graph showing discharge energy in Wh against voltage of all three types of SCs

4.6.2 Battery capacity versus SC capacity

Using the available parameters from the manufacturer’s datasheet, a comparison of the capacity of the battery and the SC was made in terms of Wh capability. The recently available battery capacitor of 40000 F was used to build an SC bank of nominal voltage 12 V to compare with the 12 V sealed lead acid battery as shown in Figure 4-19. The dimensions of the SC bank are approximate values only as it was assembled in-house in the University lab.



Parameters	Battery	SC bank
Manufacturer:	Century Batteries	Samwha capacitor
Model no:	YTX14-BS	ESD SCAP CB (40,000 F)
Overall Dimensions (mm):	Length: 150, Width: 87, Height: 145	~ Length: 150, Width: 120, Height: 138
Special Features:	AGM	Battery capacitor
Voltage:	12V	13.5
Ah:	12	12
Weight (kg):	4.59	3.55 (.710 X 5)

Figure 4-19: Comparison of the battery parameters and SC parameters

The estimated Wh capacity is given by the product of the nominal voltage of the battery and its Ah capacity:

$$\text{Wh capacity of Battery} = 12 \times 12 = 144 \text{ Wh} \quad (4-9)$$

An equivalent SC bank with the same nominal voltage can be built by connecting 5 battery capacitors (2.7 V, 40000 F) in series, with the equivalent energy calculation in Wh as follows.

The total equivalent capacitance is given by:

$$\text{Equivalent capacitance } (C_{eq}) = \frac{40000}{5} = 8000 \text{ F} \quad (4-10)$$

The energy stored in the SC bank is given by:

$$\begin{aligned} \frac{1}{2} CV^2 &= \frac{1}{2} \times 8000 \times 13.5^2 = 729000 \text{ j} = \frac{729000}{3600} \\ &= 202.5 \text{ Wh} \end{aligned} \quad (4-11)$$

This shows that an SC bank with the same nominal voltage and ampere-hour rating as the lead acid battery has a larger Wh capability than the battery. The energy delivery capability of this type of SC will increase further with ongoing rapid advancements in the technology.

Chapter 5

SCALED Circuit Concept Development and Initial Performance Test

5.1 Circuit concept development

A simple RC circuit, when connected to a constant DC power supply of voltage V_s with series resistance R , starts charging the capacitor C to its rated voltage as shown in Figure 5-1.

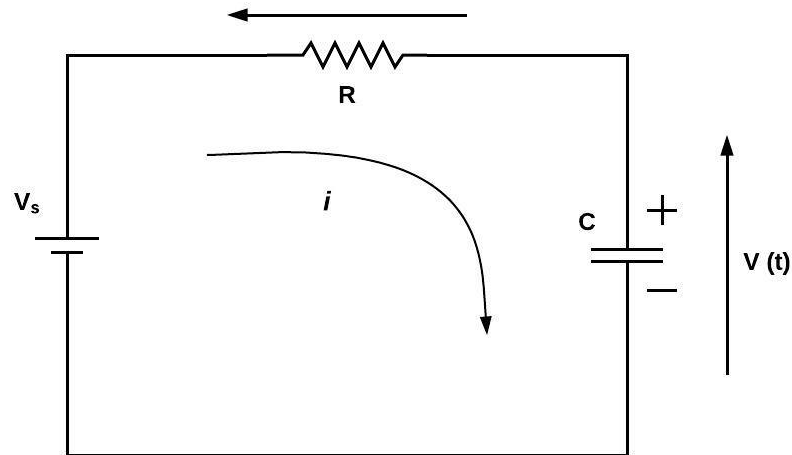


Figure 5-1: A basic RC circuit

When the capacitor is charged from 0 V to its rated voltage, the total energy E stored in the capacitor is given by Equation 5-1.

$$E = \frac{1}{2}CV_s^2 \quad (5-1)$$

This is only half of the total energy that is being supplied by the power supply. The other half of the energy is dissipated entirely across the loop resistance (R). If the same power supply is used to charge an electrochemical battery with nominal voltage (V) and total charge (Q), the energy stored in it is given by

$$E = QV \quad (5-2)$$

Equation 5-2 shows that an ideal battery can be charged with a theoretical efficiency of 100% whereas the charging efficiency of the capacitor is only 50%. However, if a pre-charged capacitor is used with some initial voltage, the losses across the loop resistance are reduced, increasing the overall efficiency of the charging. The

important thing to note here is that the 50% of energy dissipated across the loop resistance remains same irrespective of its ohmic resistance.

Figure 5-2 shows the charging voltage and current characteristics of an RC circuit. It takes around five-time constants (5τ) to fully charge the capacitor and it takes the same time for the current to decay down to zero. The time constant τ is the product of resistance (R) and capacitance (C). If the capacitor used is an SC, which has a large time constant, we can take advantage of this relationship between circuit efficiency and capacitor voltage to create a novel AC-DC converter with improved efficiency [11].

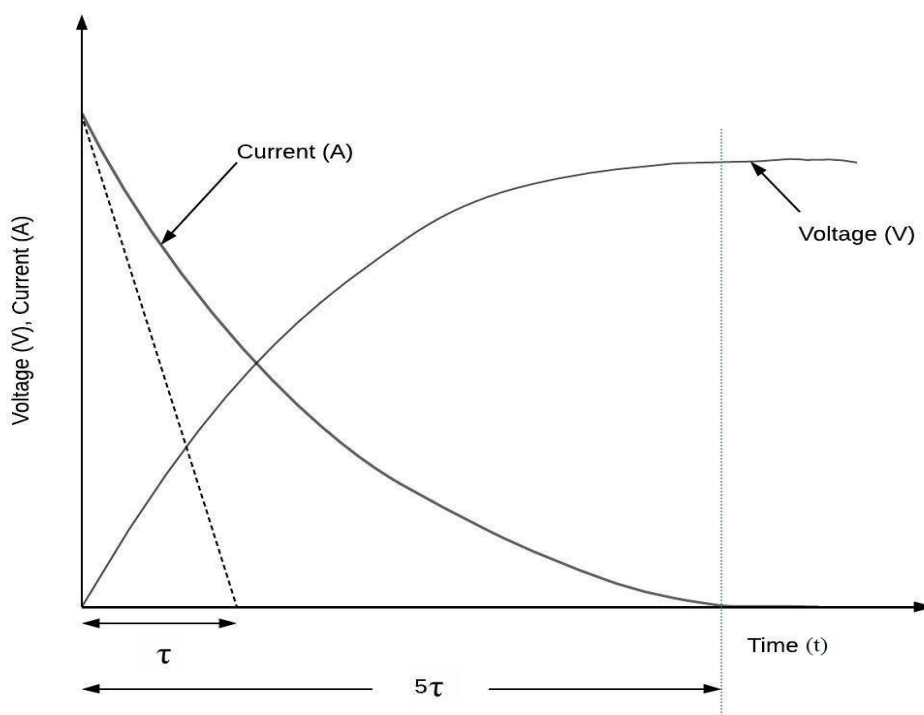


Figure 5-2: Capacitor voltage and loop current versus time [11]

If we further analyse the above circuit, the loop resistance R , also called the parasitic resistance R_p , is made up of three components: the internal resistance of the DC power supply r_s ; the total resistance of connecting components r_l ; and the equivalent series resistance of the capacitor r_c as shown in Figure 5-3 (a). An equivalent RC circuit with the series loop resistance broken down into these three components is shown in Figure 5-3 (b)

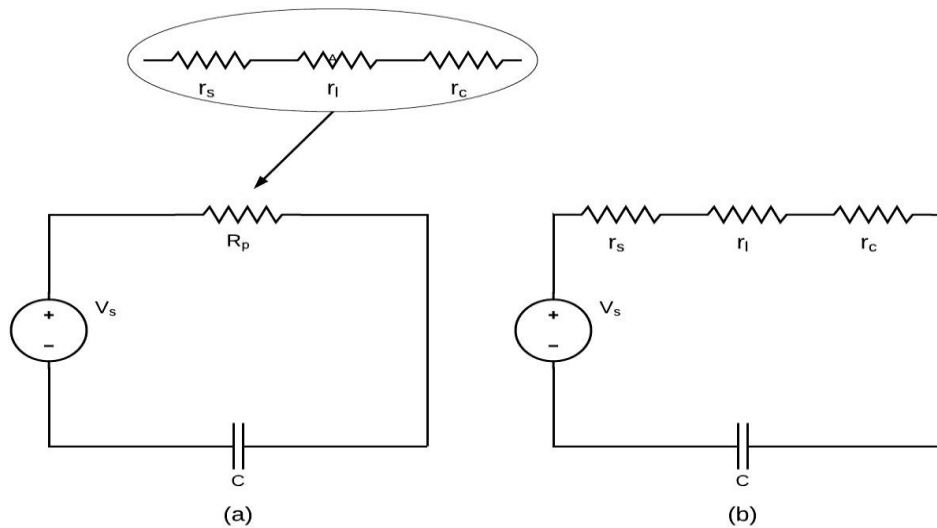


Figure 5-3: (a) Parasitic resistance R_p in a simple RC circuit (b) R_p Broken down into three parts consisting of source internal resistance r_s , loop resistance r_l and series resistance (ESR) of the capacitance r_c [11]

The analysis of the charging behaviour of the capacitor when charged from a non-zero charge state is detailed in the following sections.

5.2 Analysis of the charging behaviour of a capacitor

Figure 5-4 shows a typical capacitor charging circuit where R is the total loop resistance, V_s is the supply voltage and V_w is the final capacitor voltage. Here we consider the capacitor as a bank of SCs with large time constants and the charging source voltage is larger than the rated voltage of the SC bank [11].

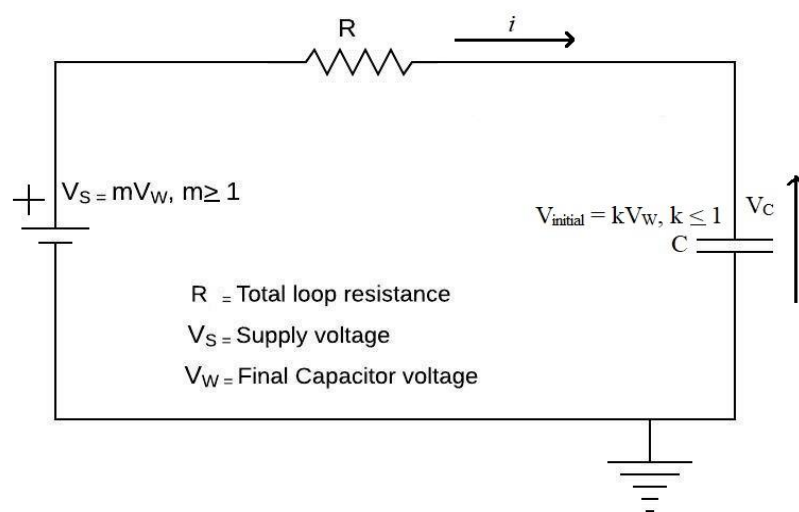


Figure 5-4: Capacitor charging circuit [11]

If we charge a fully discharged capacitor bank from 0 to V_W from a DC supply of mV_W , the capacitor voltage at time t is given by

$$v(t) = mV_W \left(1 - e^{-t/RC}\right) \quad (5-3)$$

where m is the power supply over-voltage factor which is ≥ 1 . The open circuit voltage of the power supply is m times the rated DC voltage of the capacitor.

Here we are considering the partial charging of the capacitor from voltage kV_W to V_W from times t_1 to t_2 respectively, where k is the initial voltage fraction, which is ≤ 1 . We are interested in analysis of the charging efficiency as a function of k and m in the partial charging between time t_1 and t_2 as shown by the bold curve in Figure 5-5.

The capacitor voltage at time t_1 with target voltage kV_W is given by

$$kV_W = mV_W \left(1 - e^{-t_1/RC}\right) \quad (5-4)$$

$$kV_W = mV_W - mV_W e^{-t_1/RC} \quad (5-5)$$

$$mV_W e^{-t_1/RC} = mV_W - kV_W \quad (5-6)$$

$$e^{-t_1/RC} = \frac{mV_W - kV_W}{mV_W} \quad (5-7)$$

$$e^{-t_1/RC} = \frac{m - k}{m} \quad (5-8)$$

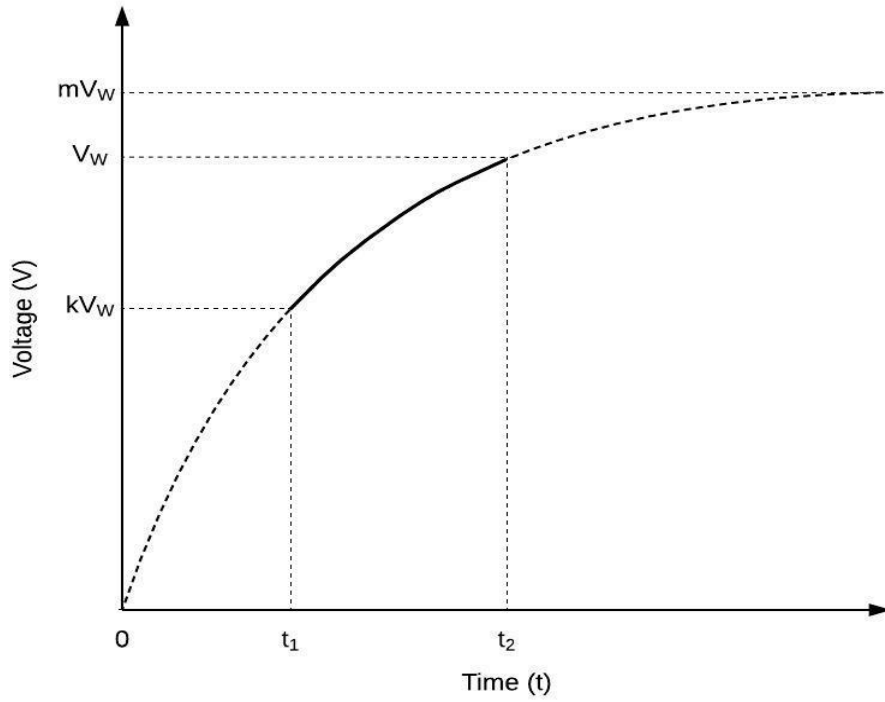


Figure 5-5: Partial capacitor charging curve (bold curve) from time t_1 to t_2 [11]

Similarly, the capacitor voltage at time t_2 with target voltage V_W is given by

$$V_W = mV_W \left(1 - e^{-t_2/RC} \right) \quad (5-9)$$

$$V_W = mV_W - mV_W e^{-t_2/RC} \quad (5-10)$$

$$mV_W e^{-t_2/RC} = mV_W - V_W \quad (5-11)$$

$$e^{-t_1/RC} = \frac{mV_W - V_W}{mV_W} \quad (5-12)$$

$$e^{-t_1/RC} = \frac{m - 1}{m} \quad (5-13)$$

The difference in energy stored (E_C) between charging times t_1 and t_2 is given by

$$E_C(t_1, t_2) = \frac{1}{2} CV_W^2 - \frac{1}{2} C(kV_W)^2 = \frac{1}{2} CV_W^2(1 - k^2) \quad (5-14)$$

The energy (E_R) dissipated in the resistor over the time interval t_1 to t_2 is given by the integral

$$E_R(t_1, t_2) = \int_{t_1}^{t_2} i^2 R dt \quad (5-15)$$

From the circuit in Figure 5-4, the loop current i is given by

$$i = \frac{V_s - V_C}{R} \quad (5-16)$$

$$i = \frac{mV_W - mV_W(1 - e^{-t/RC})}{R} \quad (5-17)$$

$$i = \frac{mV_W e^{-t/RC}}{R} \quad (5-18)$$

Using Equation 5-18 in Equation 5-15 and integrating it

$$E_R(t_1, t_2) = \int_{t_1}^{t_2} \left(\frac{mV_W e^{-t/RC}}{R} \right)^2 R dt = \frac{m^2 V_W^2}{R} \int_{t_1}^{t_2} e^{-2t/RC} dt \quad (5-19)$$

$$E_R(t_1, t_2) = \left(\frac{m^2 V_W^2}{R} \right) \left(-\frac{RC}{2} \right) \int_{t_1}^{t_2} e^{-2t/RC} dt \quad (5-20)$$

$$E_R(t_1, t_2) = \left(-\frac{m^2 V_W^2 C}{2} \right) \left[\left(e^{-t_2/RC} \right)^2 - \left(e^{-t_1/RC} \right)^2 \right] \quad (5-21)$$

Substituting the values of Equation 5-8 and Equation 5-13 in Equation 5-21

$$E_R(t_1, t_2) = \left(-\frac{m^2 V_W^2 C}{2} \right) \left[\left(\frac{m-1}{m} \right)^2 - \left(\frac{m-k}{m} \right)^2 \right] \quad (5-22)$$

$$= \left(-\frac{m^2 V_W^2 C}{2} \right) \left[\frac{m^2 + 1 - 2m - m^2 + 2mk - k^2}{m^2} \right] \quad (5-23)$$

$$E_R(t_1, t_2) = \frac{1}{2} CV_W^2 (k^2 - 2mk + 2m - 1) \quad (5-24)$$

The energy efficiency of the RC circuit is given by

$$\eta = \frac{E_C}{E_C + E_R} \quad (5-25)$$

Substituting the values of Equation 5-14 and Equation 5-24 in Equation 5-25

$$\eta = \frac{\frac{1}{2} CV_W^2 (1 - k^2)}{\frac{1}{2} CV_W^2 (1 - k^2) + \frac{1}{2} CV_W^2 (k^2 - 2mk + 2m - 1)} \quad (5-26)$$

$$\eta = \frac{(1 - k^2)}{(1 - k^2) + (k^2 - 2mk + 2m - 1)} = \frac{(1 - k^2)}{2m(1 - k)} \quad (5-27)$$

$$\eta = \frac{1 + k}{2m} \quad (5-28)$$

From the above efficiency equation, when $k = 0$ and $m=1$, the efficiency $\eta = \frac{1}{2}$ which is the normal result when the capacitor starts charging from its fully discharged state. But when $k > 0$ (the capacitor has some charge), and $m \geq 1$, there will definitely be an increase in efficiency.

5.3 Inserting a useful resistance in the RC loop

Inserting a useful resistance R_L in the circuit in Figure 5-3, the resulting circuit with its parasitic resistance R_p is shown in Figure 5-6 (a). A significant improvement in efficiency can be achieved by making the useful resistance absorb most of the energy dissipated in the loop resistance. The useful resistance could be a heater, a resistively loaded DC-DC converter, a loaded inverter or an LED lamp load. When an SC bank is charged, it results in a large time constant, and a switch can easily be used to avoid overcharging the capacitor, as shown in Figure 5-6 (b)

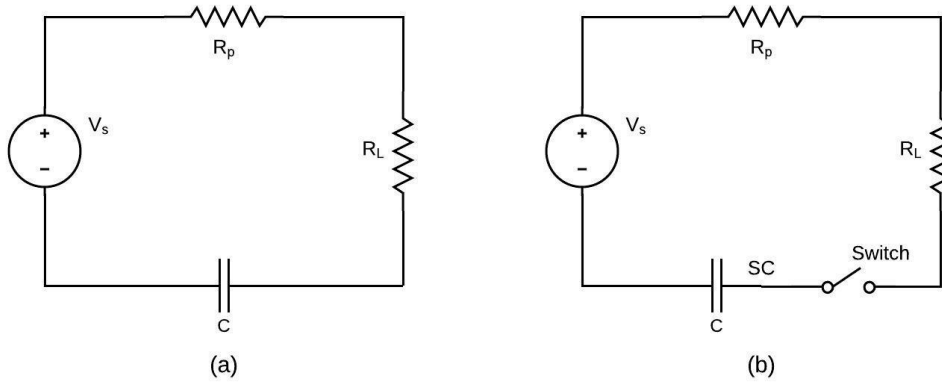


Figure 5-6: (a) Insertion of a useful resistive load in the capacitor charging loop to increase the charging efficiency. (b) An additional switch to prevent overcharging of the capacitor [11]

The energy efficiency η of the circuit can be redefined as

$$\eta = \frac{E_C + E_{R_L}}{E_C + E_{R_L} + E_{R_p}} \quad (5-29)$$

The improvement in the charging efficiency depends on the ratio of useful resistance to parasitic resistance ($R_L:R_p$). The larger the ratio, the more dissipation occurs in the useful resistance, thereby avoiding losses in parasitic resistances.

If we set the ratio of $R_L/R_p = P > 1$, we obtain a performance boost

$$\eta = \frac{1}{P + 1} \left(P + \frac{1 + k}{2m} \right) \quad (5-30)$$

For $R_L:R_p = 1:1$

$$\eta = \frac{1}{2} \left(\frac{1 + k}{4m} \right) \quad (5-31)$$

For $R_L:R_p = 9:1$

$$\eta = \frac{9}{10} \left(\frac{1 + k}{20m} \right) \quad (5-32)$$

These efficiencies at different ratios of $R_L:R_p$ are shown in Figure 5-7, which indicates that there is a significant increase in efficiency as the ratio of $R_L:R_p$ increases.

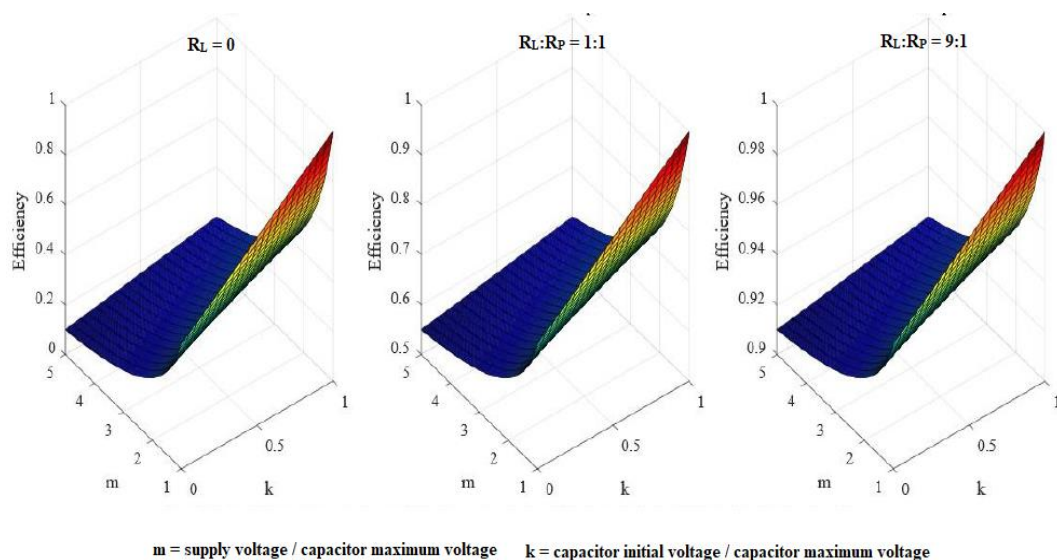


Figure 5-7: Overall efficiency of powering a useful load within a capacitor charging loop [11]

Analysis of the circuit in Figure 5-6 (b) shows that the efficiency of a capacitor charging circuit can vary over a wide range, where charging efficiency increases with the capacitor starting at a non-zero initial voltage [11]. This conceptual approach to increasing the charging efficiency of the RC circuit and more importantly to avoiding losses across the loop resistance is the point where our design for new circuit topology has emerged in the family of SC-assisted circuit topologies developed at the University of Waikato. Analysis of the charging behaviour of the capacitor when charged from non-zero charge is provided in following sections.

5.4 SCALED circuit topology configuration

Based on circumventing losses by adding a useful load such as an LED load in the capacitor charging loop as discussed, the project team, using a few components as shown in a simple block diagram in Figure 5-8 (a), designed the SCALED circuit prototype. The five major components used to design the initial circuit were:

1. PIC16F684 microcontroller
2. PVN012PBF Photo relays
3. OP491 Operational amplifier
4. Resistors and diodes
5. SC banks and LED banks

The design made use of a single SC bank and LED bank with two switches, which achieved the basic function of switching between the supply source (V_{ss}) and the ESD source (SC). To make this switching happen automatically, a PIC16F684 microcontroller was used as the main controller and an OP491 Operational amplifier as the feedback signal converter, as shown in Figure 5-8 (b). Some resistors and diodes were also used as voltage dividers and to block the reverse flow of feedback signals.

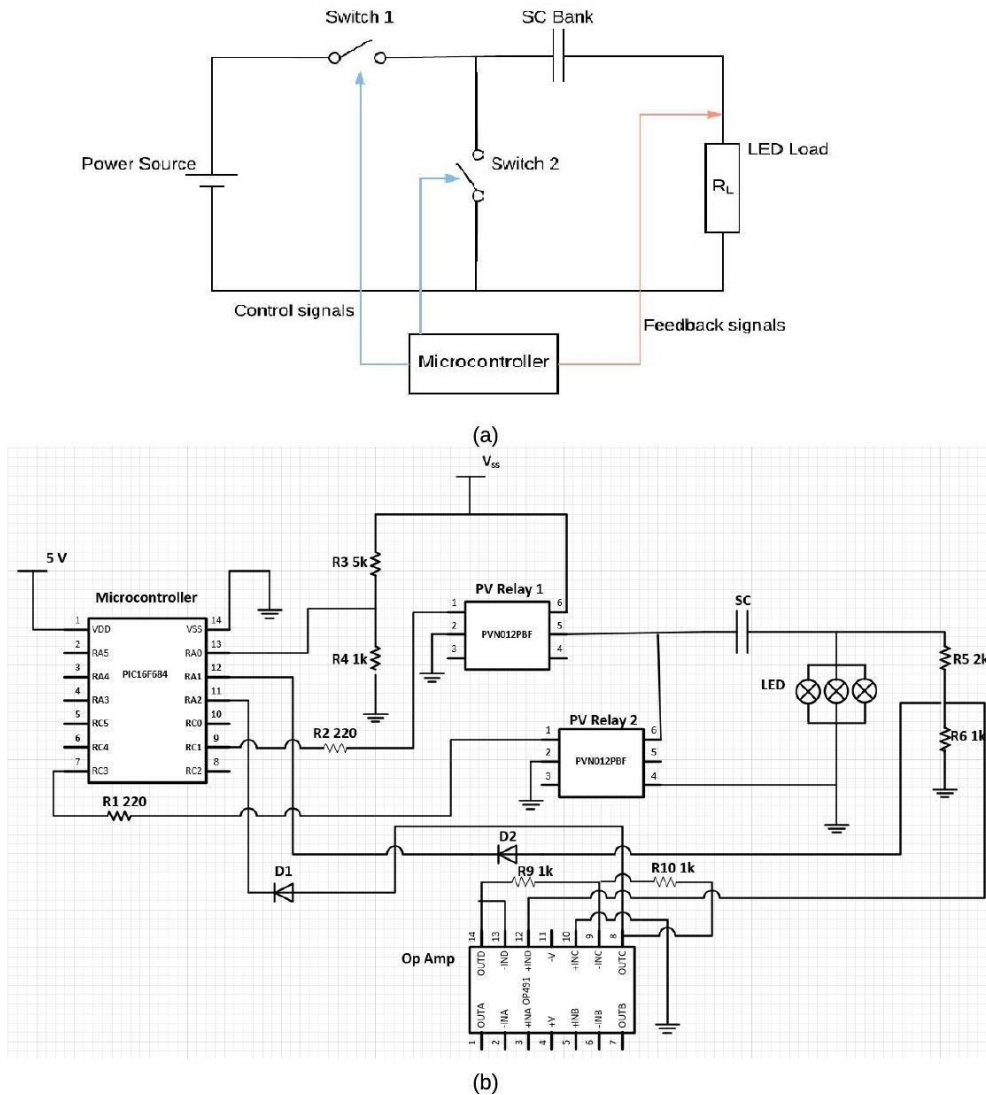


Figure 5-8: (a) Initial SCALED circuit block diagram. (b) First SCALED prototype circuit diagram

5.4.1 Basic circuit operation

Normally PV relay 1 switch is ON, supplying power to the load as well as charging the SC bank from the solar supply. The voltage across the LED load is continuously

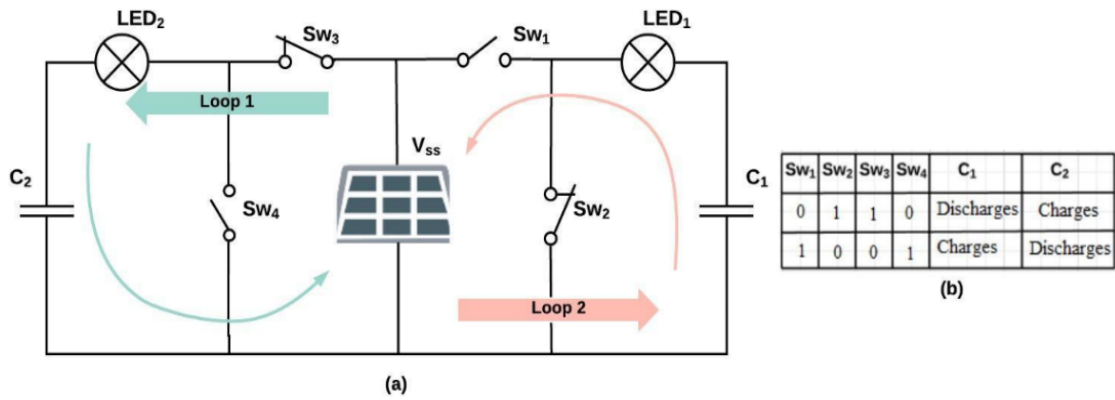
monitored via feedback from the resistive dividers R5 and R6. Once the voltage across the LED goes below the minimum constant brightness operating range of the LED, the PV relay 2 switch is automatically turned ON, changing over the power source to the SC banks. This cycle of changeover repeats depending on the feedback signal, which depends on the main supply source V_{ss} , thereby powering the LED within its constant brightness operating region.

The control circuit is programmed using PIC programming to ensure automatic operation of the circuits. The SC bank and the LED bank in the SCALED circuit with the source V_{ss} form a simple RC circuit as discussed earlier.

5.4.2 Solar LED technique

The technique to achieve continuous operation of the LED and SC combination from a renewable energy source like a solar power supply (V_{ss}) is shown in Figure 5-9 (a). The microcontroller sends signals as per the truth table in Figure 5-9 (b). This technique operates in two conditions using four switches.

1. When switch 1 (Sw_1) and switch 4 (Sw_4) are open and switch 2 (Sw_2) and switch 3 (Sw_3) are closed, capacitor bank C_1 discharges, powering LED₁ and the solar power charges capacitor C_2 , simultaneously powering LED₂
2. When switch 2 (Sw_2) and switch 3 (Sw_3) are open and switch 1 (Sw_1) and switch 4 (Sw_4) are closed, capacitor bank C_2 discharges, powering LED₂, and the solar power charges capacitor C_1 , simultaneously lighting LED₁



SW ₁	SW ₂	SW ₃	SW ₄	C ₁	C ₂
0	1	1	0	Discharges	Charges
1	0	0	1	Charges	Discharges

(b)

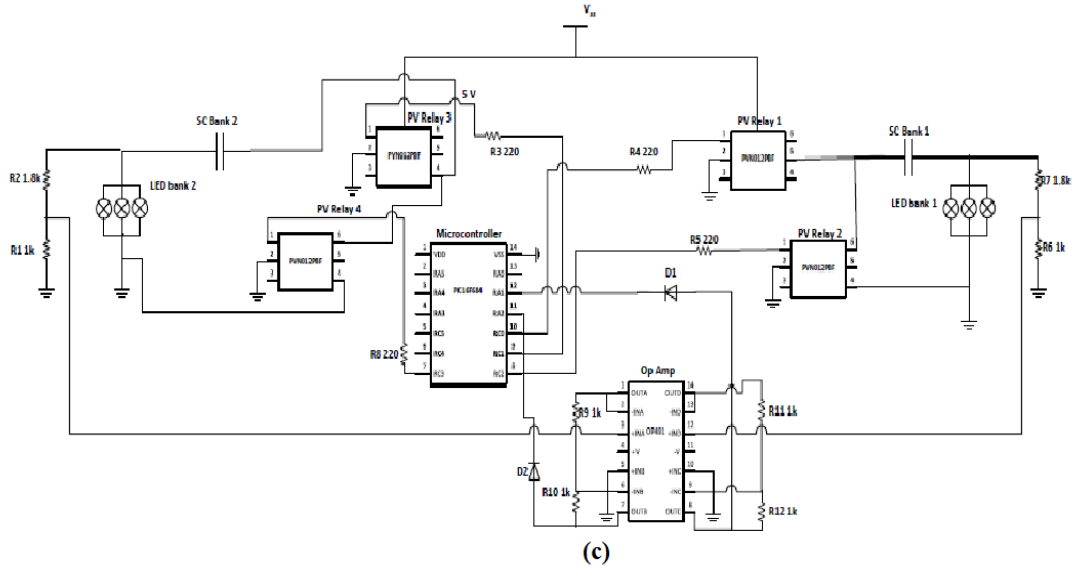


Figure 5-9: (a) Block diagram of SC and LED arrangement. (b) Truth table of control signals [31]. (c) Second version of SCALED circuit topology with two identical SC and LED banks

5.4.3 SCALED circuit with solar LED technique

Figure 5-9 (c) shows the second version of the circuit with two identical SC and LED banks. This extends the first circuit prototype, making it twice as effective, using the same supply source, as the earlier version. It operates so that the continuous simultaneous operation of both the LED banks is achieved from the same power supply source with timely assistance from the SC banks.

The PCB was designed using EAGLE PCB design software. Figure 5-10 shows a sample SCALED PCB board that was designed and assembled by the team at the University of Waikato electronics lab for the initial testing.

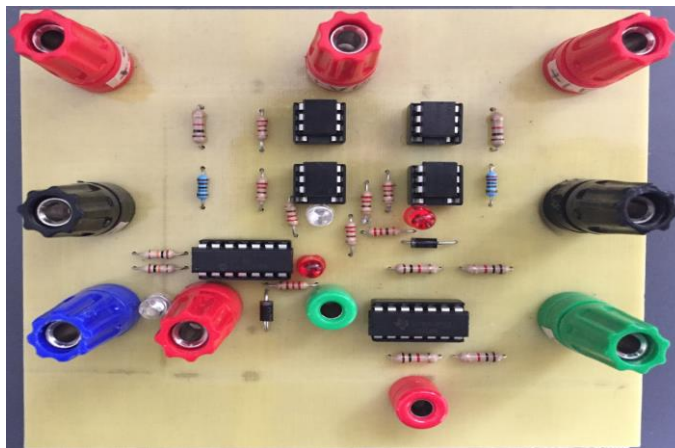


Figure 5-10: Preliminary version of PCB developed for initial testing

The PV relays first used as switches had a lower ampere capacity, which caused some problem with the switches burning out when connected to the solar output. To overcome this issue, higher ampere rating MOSFET switches were used.

5.4.4 Ultracapacitor module from LS Mtron

LS ultracapacitor modules from LS Mtron are new-generation energy storage devices with great power and reliability. They provide optimal solutions for high voltage and current requirements by connecting ultracapacitor cells in series [6]. The module used for this project was a 166 F, 50.4 V rated module as shown in Figure 5-11.



Specifications:

Part no: LSUM 050R4P0166F EA AB
 Rated voltage : 50.4 V
 Max. Current : 1900 A
 Resistance DC : 7.8 mΩ
 Short circuit current : 6.5 kA
 Cell balancing and overvoltage protection
 Specific Energy : 4.2 Wh/kg
 Stored energy : 58.6 Wh
 Operating temperature range: -40 ~ 65 °C
 Cycle life: 1,000,000 cycles

Figure 5-11: 166 F 50.4 V Ultracapacitor from LS Mtron with specifications [6]

The above-mentioned features make this module suitable for a wide variety of applications because of the high available energy and wider voltage range.

5.5 Initial circuit testing

The initial performance test of the circuit was carried out using a bench power supply as the source voltage V_{ss} , as shown in Figure 5-12. This was carried out to observe the performance of the circuit with a controlled current and voltage source before powering it using the solar output. The equipment and devices used are listed below.

1. 30 V, 2 A dual output bench power supply as main supply source
2. Dual output power supply to power the ICs
3. Two identical 166 F, 50 V SC banks
4. Two identical 10 W (2 x 5) LED banks
5. Multimeters as measuring devices

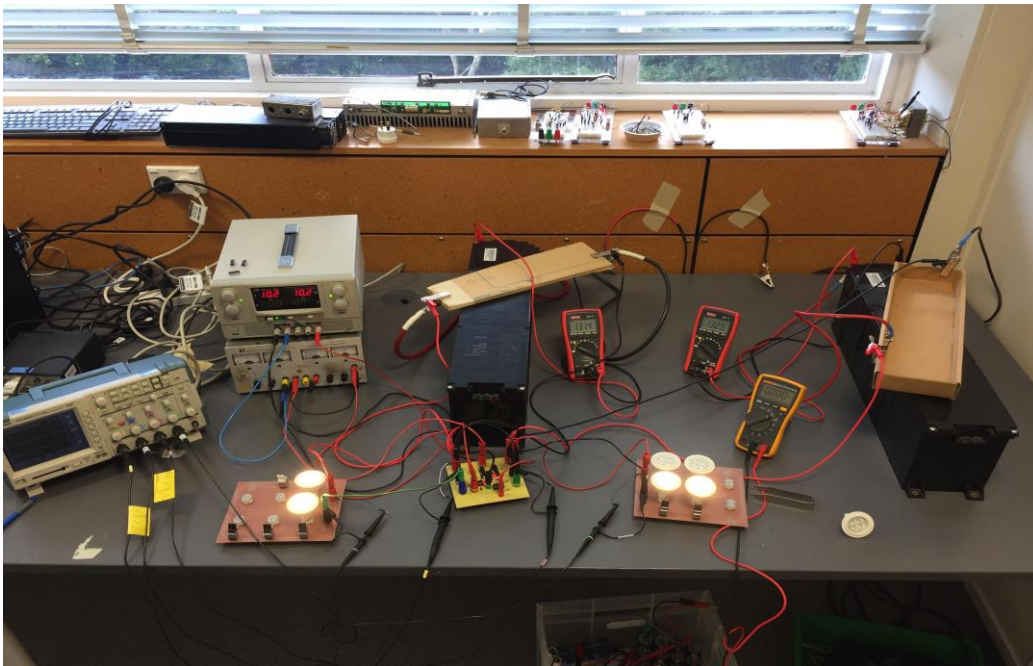


Figure 5-12: SCALED circuit testing set-up for initial testing

The initial performance evaluation was carried out by measuring the voltage across each LED and SC banks. Since the testing covered a long period of time and a high number of measurements needed to be recorded, we tried to arrange an automatic recording system. The four-channel oscilloscope that was commonly used for multiple measurements had a restriction in the time scale, which prevented the

whole cycle of switching being captured. Therefore, we manually recorded the data every minute to observe the performance of the circuit, as shown in Table 5-1.

Table 5-1: Measurement data of SC banks and LED banks voltages

Sl.no	Time (m)	BANK 1		BANK 2		Remarks
		SC Bank 1 Voltage (V)	LED Bank 1 Voltage (V)	SC Bank 2 Voltage (V)	LED Bank 2 Voltage (V)	
1	0	14.84	-14.62	10.22	0	
2	1	14.64	-14.57	10.34	18.65	
3	2	14.49	-14.41	10.52	18.5	
4	3	14.33	-14.24	10.71	18.32	
5	4	14.17	-14.08	10.9	18.15	
6	5	14.01	-13.93	11.09	17.97	
7	6	13.86	-13.77	11.28	17.79	
8	7	13.71	-13.62	11.46	17.61	
9	8	13.55	-13.47	11.65	17.42	
10	9	13.39	-13.31	11.84	17.23	
11	10	13.24	-13.16	12.04	17.03	
12	11	13	-13.09	12.23	16.84	
13	12	12.95	-12.84	12.43	16.65	
14	13	12.78	-12.69	12.63	16.45	
15	14	12.64	-12.54	12.82	16.26	
16	15	12.48	-12.38	13.02	16.07	
17	16	12.33	-12.23	13.21	15.87	
18	17	12.16	-12.06	13.41	15.67	
19	18	12.01	-11.9	13.61	15.48	
20	19	11.84	-11.74	13.81	15.28	
21	20	11.66	-11.57	14	15.08	
22	21	11.51	-11.4	14.2	14.89	
23	22	11.36	-11.23	14.4	14.69	
24	23	11.18	-11.06	14.6	14.49	1 st changeover
25	24	11.08	18.21	14.67	-14.48	
26	25	11.31	17.75	14.48	-14.35	
27	26	11.45	17.6	14.36	-14.25	
28	27	11.64	17.4	14.22	-14.11	
29	28	11.86	17.18	14.08	-13.97	
30	29	12.07	16.97	13.94	-13.83	
31	30	12.28	16.75	13.81	-13.7	
32	31	12.48	16.55	13.68	-13.56	
33	32	12.69	16.34	13.55	-13.43	
34	33	12.89	16.13	13.41	-13.3	
35	34	13.13	15.89	13.29	-13.18	
36	35	13.33	15.68	13.17	-13.05	
37	36	13.54	15.47	13.04	-12.95	
38	37	13.75	15.25	12.91	-12.79	
39	38	13.96	15.03	12.78	-12.67	

40	39	14.78	14.79	12.65	-12.54	2 nd changeover
41	40	14.33	-14.26	12.59	16.59	
42	41	14.18	-14.11	12.81	16.36	
43	42	14.04	-13.96	13.02	16.14	
44	43	13.89	-13.8	13.25	15.93	
45	44	13.74	-13.66	13.46	15.7	
46	45	13.59	-13.5	13.68	15.49	
47	46	13.44	-13.35	13.89	15.28	
48	47	13.29	-13.2	14.1	15.06	
49	48	13.14	-13.04	14.31	14.85	
50	49	13	-12.91	14.53	14.63	
51	50	12.85	-12.75	14.74	14.42	
52	51	12.7	-12.6	14.95	14.2	
53	52	12.55	-12.45	15.16	14	
54	53	12.4	-12.3	15.37	13.78	
55	54	12.24	-12.14	15.58	13.56	
56	55	12	-11.75	15.8	13.36	
57	56	11.69	-11.43	16	13.14	
58	57	11.37	-11.1	16.21	12.93	3 rd changeover
59	58	11.06	18.04	16.36	-16.17	

Measurements were taken for three changeover switches, which took about an hour. The graph in Figure 5-13 illustrates the performance of the test circuit. For better efficiency and performance of the circuit, the SC bank was pre-charged to 14 V.

The results of the initial test showed that the changeover switching was happening as expected. There was a smooth transition between the main source and the SC bank source, maintaining the operating voltage range of the LEDs with the expected brightness.

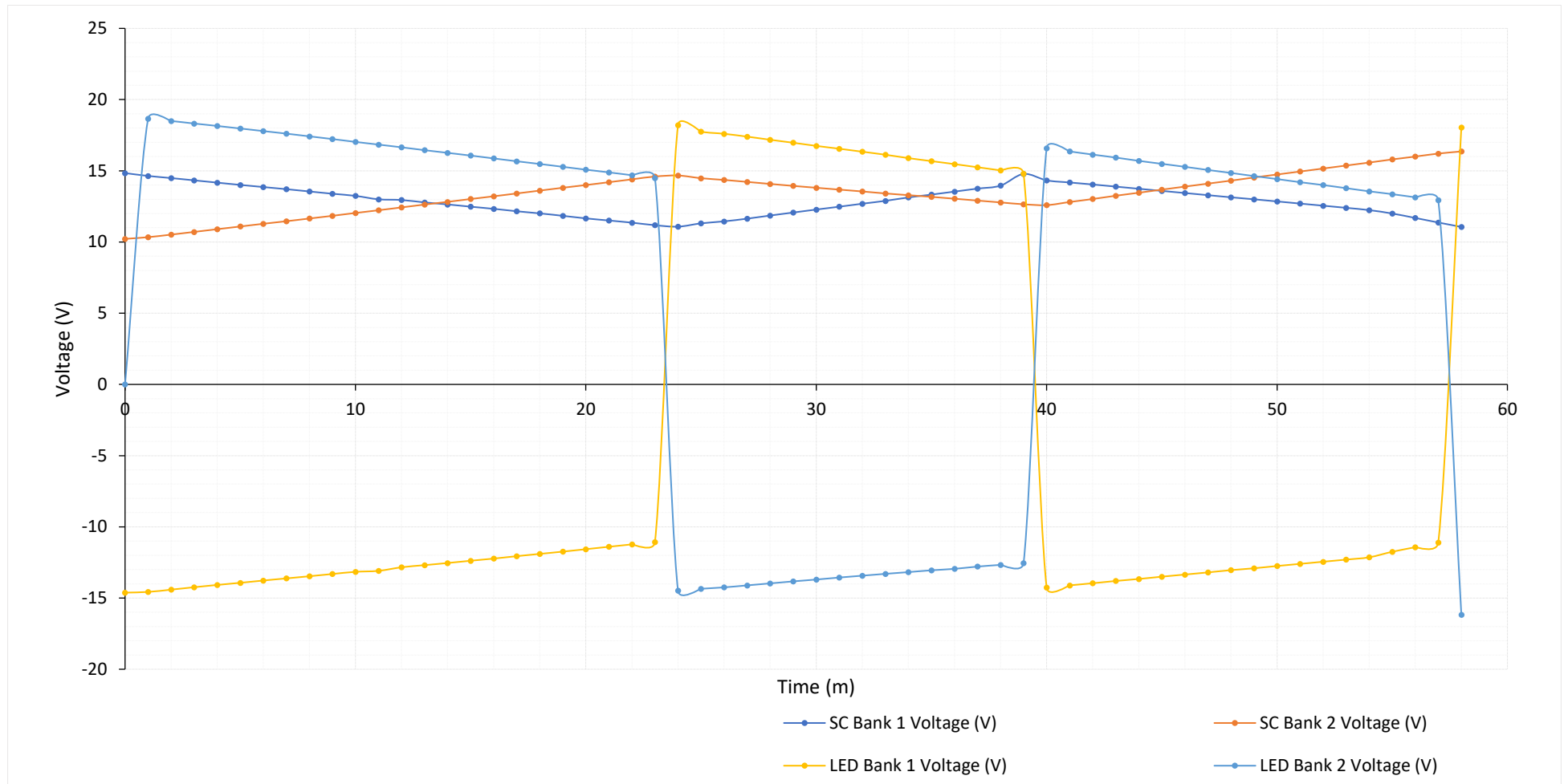


Figure 5-13: Preliminary testing result showing SC and LED banks voltage characteristics

5.6 Port of Auckland DC microgrid research project

The University of Waikato has a long and successful tradition of integrated research on environmental issues and plays a leading role in developing and researching technologies for a sustainable future. This provides unique perspectives on issues of importance to contemporary society, and answers to some of the key problems being faced by industries, governments and nations worldwide.

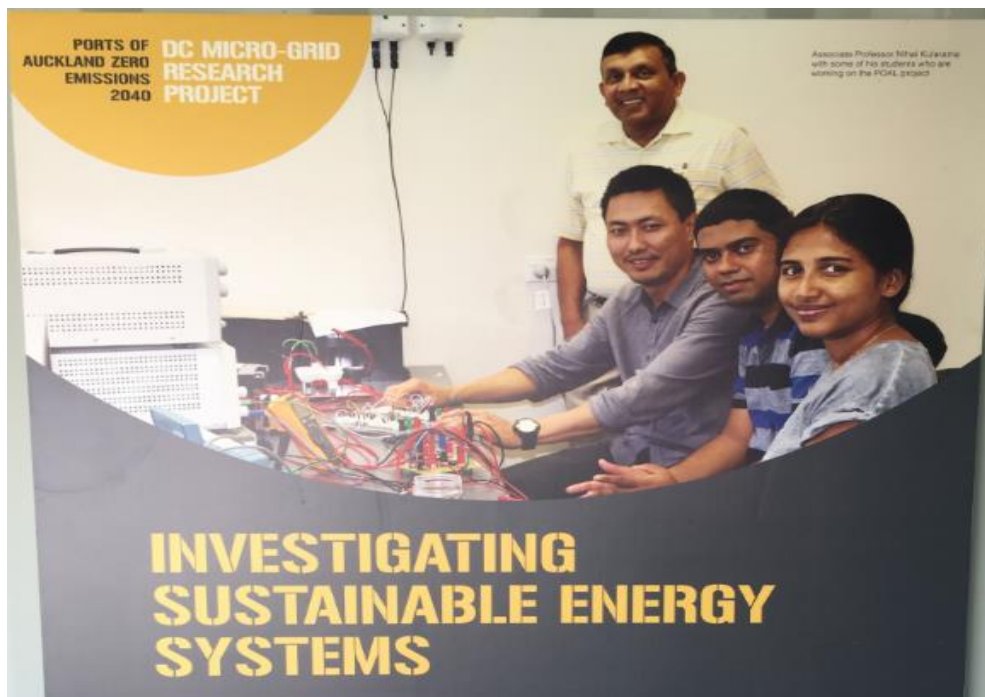


Figure 5-14: University of Waikato SCALED project team

Our project team has been working with Ports of Auckland Limited (POAL) on a pilot programme to establish a DC microgrid for the port and its freight hubs. This collaboration is part of POAL's long-term strategy to use more sustainable energy systems and to develop enduring partnerships, and to enable the port's 2040 zero emission roadmap [32].

This work for POAL was the result of an advisory role in an international IEEE committee in 2014 – 2015, investigating the advantages of DC in buildings. The team at the University of Waikato has been carrying out research in developing novel supercapacitor-assisted power converters and is now undertaking a new venture in developing a similar topology applicable in DC microgrids. POAL has seen the value of a DC microgrid, beginning with the installation of solar panels

and using DC for lighting at first, and then introducing it into air conditioning and white goods and finally, computers and information systems [32].



Figure 5-15: 40 ft container with DC microgrid research project prototype on display during 2018 annual POAL open day

With the initial SCALED circuit topology developed, the project team, in collaboration with POAL, built a prototype in a 40 ft container, which was displayed in the port's annual open day from 27–29 January 2018 at their premises in Auckland, as shown in Figure 5-15. The main intention of this is to continue using it as a public engagement tool to share information about the project and the port's wider sustainability perspectives. The research project was demonstrated to hundreds of enthusiasts and visitors during the open days.

Because POAL's research project fits extremely well with the United Nations' recommended sustainability targets, it was recently highlighted in the World Ports Sustainability Program (WPSP), run by the International Association of Ports and Harbours as shown in Figure 5-16.



Figure 5-16: POAL’s DC microgrid research project highlighted in world ports sustainability program [32]

The whole team believes that in the near future, we can set up a highly cost-effective DC microgrid initiative that can be practically implemented in mainstream electricity usage. This will have a huge impact on energy sustainability for POAL and other similar industries.

Chapter 6

Conclusion and Future Development

6.1 Conclusion

Developing sustainable energy systems to address global climate issues is a major challenge facing the world at present. Many bigger industries and companies are now seriously introducing climate initiatives to mitigate global warming and are looking for solutions for the production of sustainable energy. DC microgrid technology has huge potential to reduce the emission of harmful gases as it aims at using clean renewable energy and reducing the burning of fossil fuels. This project also aimed at lighting homes using solar energy assisted by SC technology. During this study, I learned that the exact behaviour of solar power needs to be understood and analysed, for which more reliable field data is required.

Most places in New Zealand receive in excess of 2000 hrs of sunshine annually, which means an average of around 5 sun hours daily. The Chatham Islands receives the lowest level of sunshine at 1437.3 hours, which is still more than that received by many places in Germany. Germany is the first major renewable energy economy in the world and with its government's target to achieve installed solar capacity of 66 GW by 2030, the future of solar energy is looking very promising. Although solar power generation in New Zealand started slowly, recent findings have shown that there is rapid growth in solar PV panel power generation. The installed capacity at the end of December 2016 was 47 MW, which represented a 52% increase over the year.

Using the reliable and accurate solar data from NIWA's climate database, solar irradiance data was carefully analysed and configured in a solar PV simulator designed to emulate the dynamic electrical behaviour of a terrestrial PV solar array. In addition, a 1 KW solar array was also installed, guided by NIWA's solar view tool. This ground work enabled the project team to set up a small DC microgrid environment to carry out the testing of the circuit topology.

The latest hybrid supercapacitor available on the market is a battery capacitor with very high-power density and energy density. This type of ESD fills the gap between batteries and supercapacitors, using the best features of both and making it useful for many applications. With rapid advances in SC technology, its application to address the issue of intermittent power fluctuations in renewable energy sources such as solar power may allow high reliability of operation in DC microgrid environments.

6.2 Future development

New Zealand is among the least developed countries in terms of harnessing solar energy. To take advantage of this natural source of plentiful, free energy, the government, research institutions and relevant industries should work together. The University of Waikato now has its own solar irradiance data library created in the PV simulator, which can be used at any time in the lab. The University will also soon have a fully-fledged Renewable Energy lab with all the necessary solar-based testing facilities including a PV simulator, solar PV array and other equipment. I perceive a sea of opportunity for developments of this type of project in future.

This early version of the project was aimed at powering low voltage residential LED lamps. Later, the team will investigate powering white goods with a suitable MPPT-type technique for SCs. In the long run, all electrical appliances operable from 230 V AC could be replaced by DC operating systems. To keep the research team at the University, there needs to be ongoing development of this project. As the project team has already started working with a range of industries, there is huge potential for the technology to be taken further in developing circuit topologies that can ultimately achieve the goal of combatting global climate change.

References

- [1] National Renewable Energy Laboratory. (2017). *Solar Energy Basics*. Retrieved January, 2018, from <https://www.nrel.gov/workingwithus/re-solar.html>.
- [2] MBIE (Ministry of Business, Innovation and Employment). (2017). *Energy in New Zealand 2017*. Retrieved January, 2018, from <http://www.mbie.govt.nz/info-services/sectors-industries/energy/energy-data-modelling/publications/energy-in-new-zealand>.
- [3] Kularatna, N. (2015). *Energy Storage Devices for Electronic Systems: Rechargeable Batteries and Supercapacitors*. London, U.K.: Elsevier.
- [4] Franco, G., & Kularatna, N. (2017). *Supercapacitors*. Presented at APEC 2017 - Applied Power Electronics Conference 2017, 27-29 March 2017, Tampa, FL.
- [5] Kularatna, N., Kankanamge, K., & Fernando, J. (2011). Supercapacitors enhance LDO efficiency - Part 2: Implementation. *Power Electronics Technology*, 37(5), 30-33.
- [6] LS Mtron. (2017). *LS Ultracapacitor: New-Generation Energy Storage Devices with Great Power and Great Reliability*. Retrieved January, 2018, from <https://cantecsystems.com/images/stories/virtuemart/pdf/LSUC-Family-Apr-2017.pdf>.
- [7] Fernando, J., Kularatna, N., Round, H., & Talele, S. (2014) Implementation of the supercapacitor-assisted surge absorber (SCASA) technique in a practical surge protector. In *IECON 2014 - 40th Annual Conference of the IEEE Industrial Electronics Society* (pp. 5191-5195). Dallas, TX: IEEE.
- [8] Gurusinge, N., Kularatna, N., Round, W. H., & Steyn-Ross, D. A. (2017). Energy-limited transient-mode fast supercapacitor charger topology. *IEEE Transactions on Power Electronics*, 32(2), 911–914.
- [9] Kularatna, N., Milani, K., & Round, W. H. (2015) Supercapacitor energy storage in solar application: A design approach to minimize a fundamental loss issue by partitioning the load and the storage device. In *24th International Symposium on Industrial Electronics (ISIE), 3-5 June 2015* (pp. 1308–1312). Buzios, Brazil: IEEE.
- [10] Fernando, J., & Kularatna, N. (2015) Supercapacitors for distributed energy storage in DC microgrids and loads. In *ICDCM 2015 - 1st International Conference on DC Microgrids, 7-10 June 2015* (pp. 339–342). Atlanta, GA: IEEE.
- [11] Ariyaratna, T., Jayananda, J., Kularatna, N., & Steyn-Ross, D. A. (2017) Potential of supercapacitors in noval power converters as semi-ideal lossless voltage droppers. In *IECON 2017 - 43rd Annual Conference of the IEEE Industrial Electronics Society, 29 Oct.-1 Nov. 2017* (pp. 1429-1434). Beijing, China: IEEE.

- [12] Khan, M. N. (2013). *Understanding LED Illumination*. Bosa Roca, MD: CRC Press.
- [13] Pereira, L. S., Pontes, Y., & da Costa, F. M. (2017). *Energy efficiency in the replacement of fluorescent lamps by LED: Application in a store*. Presented at 2017 Brazilian Power Electronics Conference (COBEP), 19–22 Nov. 2017.
- [14] Littelfuse. (2016). *LED Light-Emitting Diode (LED) Design Guide*. Retrieved January, 2018, from http://www.littelfuse.com/~media/electronics/design_guides/led_protectors/littelfuse_led_lighting_design_guide.pdf.pdf.
- [15] Diodes Incorporated. (2018). *CREE LED Solution Provider: LED Drivers*. Retrieved January, 2018, from <https://www.diodes.com/design/support/led-partners/cree/>.
- [16] National Institute of Water and Atmospheric Research (NIWA). (2016). *Overview of New Zealand's Climate*. Retrieved January, 2018, from <https://www.niwa.co.nz/education-and-training/schools/resources/climate/overview>.
- [17] Chappell, P. R. (2014). *The Climate and Weather of Waikato*. (2nd ed.). Wellington, New Zealand: NIWA.
- [18] Beaudet, A. (2015). *How do Solar Panels Work?* Retrieved January, 2018, from <https://www.altestore.com/blog/2015/10/how-do-solar-panels-work/>.
- [19] ODC Energy PVT. Ltd. (2018). Retrieved 12 December, 2017, from <http://www.odcenergy.com>.
- [20] Sinha, D., Bandhu Das, A., Dhak, D. K., & Sadhu, P. K. (2014) Equivalent circuit configuration for solar PV cell. In *ICONCE 2014 - 1st International Conference on Non Conventional Energy* (pp. 58-60). Kalyani, India: IEEE.
- [21] Sanyo. (2017). *Sanyo 200 spec sheet*. Retrieved 12 November, 2017, from <https://www.sanyo.com>.
- [22] Singh, G. K. (2013). Solar power generation by PV (photovoltaic) technology: A review. *Energy*, 53, 1-13.
- [23] AMETEK Programmable Power. (2017). *Standalone TerraSAS Photovoltaic Simulator*. Retrieved January, 2018, from http://www.programmablepower.com/custom-power-supply/ETS/downloads/AMETEK_ETS_Datasheet.pdf.
- [24] AMETEK Programmable Power. (2017). *ELGAR ETS600X Photovoltaic Simulator Operation and Maintenance Manual*. M551066-01 Rev D. 33p. http://www.programmablepower.com/custom-power-supply/ETS/downloads/ETS600X_Operation-Maintenance_Manual_M551066-01_RevD.pdf.

- [25] Kotra, S., Mishra, M. K., & Chaithanya, N. P. (2017). *Design and small signal analysis of DC microgrid with hybrid energy storage system*. Presented at Asia-Pacific Power and Energy Engineering Conference (APPEEC) 2017, 8-10 Nov. 2017.
- [26] Dragicevic, T., & Buticchi, G. (2017). *Power architectures, applications and control of DC distribution Systems and Microgrids*. Presented at ICDCM 2017 - 2nd International Conference on DC Microgrids, 27-29 June 2017, Nuremberg, Germany.
- [27] Ahmad, A., Anderson, T. T., & Lie, T. T. (2015). Hourly global solar irradiation forecasting for New Zealand. *Solar Energy*, 122, 1398-1408.
- [28] Sengupta, M., Habte, A., Kurtz, S., Dobos, A., Wilbert, S., Lorenz, E., Stoffel, T., Renné, D., Gueymard, C., Myers, D., Wilcox, S., Blanc, P., & Perez, R. (2015). *Best Practices Handbook for the Collection and Use of Solar Resource Data for Solar Energy Applications*. Technical Report NREL/TP-5D00-63112. National Renewable Energy Laboratory, Golden, CO. 255p. <https://www.nrel.gov/docs/fy15osti/63112.pdf>.
- [29] National Institute of Water and Atmospheric Research (NIWA). (n.d.). SolarView [Computer software]. <https://solarview.niwa.co.nz/>.
- [30] Samwha Capacitor. (2018). *ESD-SCAP*. www.samwha.com/electrics.
- [31] Froger, P., Kularatna, N., & Gurusinghe, N. (2015). *Supercapacitor assisted solar LED lighting*. Presented at Ei-CESI conference.
- [32] Dobson, G. (2018). *Solar-Powered Micro-Grid Research at Port*. Retrieved January, 2018, from <http://evtalk.co.nz/solar-powered-micro-grid-research-at-port/>.

Appendices

7.1 Mean daily global radiation in mega jules per square meter of different places of New Zealand (source: NIWA)

LOCATION	JAN	FEB	MAR	APR	MAY	JUN	JUL	AUG	SEP	OCT	NOV	DEC	YEAR
Kaitaia	21.7	19.4	16.4	11.6	8.5	7.0	7.7	10.1	13.5	16.9	19.9	22.1	14.5
Whangarei	21.4	18.2	15.5	11.1	8.2	7.0	7.4	10.1	13.6	17.0	19.6	20.4	14.1
Auckland	22.7	19.5	15.9	11.5	8.1	6.5	7.2	9.9	13.7	17.4	20.7	22.2	14.6
Tauranga	23.4	20.0	16.5	11.8	8.3	6.8	7.1	9.9	13.7	17.6	20.9	22.3	14.8
Hamilton	22.1	19.2	15.8	11.3	7.8	6.3	7.0	9.4	13.0	16.6	20.2	21.6	14.2
Rotorua	22.5	19.5	15.9	11.5	8.0	6.4	7.0	9.3	12.9	16.8	20.2	21.5	14.3
Gisborne	23.4	19.3	15.5	11.1	7.7	6.3	6.6	9.8	14.2	18.6	21.7	23.3	14.8
New Plymouth	23.9	21.1	16.8	11.5	7.8	6.1	7.0	9.7	13.2	17.2	21.5	22.2	14.8
Napier	22.9	19.4	15.8	11.2	7.9	6.4	6.8	9.9	14.0	18.5	21.7	22.8	14.8
Wanganui	23.7	20.4	16.1	10.9	7.3	5.7	6.5	9.1	12.9	17.0	21.3	22.6	14.4
Palmerston North	22.1	19.6	15.2	10.5	7.0	5.3	6.1	8.6	12.1	15.6	19.6	20.9	13.5
Masterton	22.4	18.8	15.1	10.0	7.0	5.4	5.8	8.7	12.8	16.9	21.0	22.1	13.8
Wellington	23.3	20.0	15.2	10.3	6.4	4.7	5.6	8.5	12.5	16.6	20.0	22.1	13.8
Nelson	23.4	20.4	16.1	11.5	7.7	5.7	6.4	9.0	13.3	16.9	20.9	22.7	14.5
Blenheim	23.7	20.1	17.0	11.5	7.8	5.8	6.6	9.8	13.7	18.7	22.1	23.2	15.0
Westport	21.7	19.2	14.8	9.6	6.4	4.7	5.8	8.2	11.6	15.6	20.0	20.4	13.2
Kaikoura	21.4	18.3	14.9	10.1	6.8	5.3	6.0	8.9	12.8	17.5	21.4	22.1	13.8
Hokitika	21.2	18.4	14.3	9.6	6.1	4.7	5.6	8.0	11.6	15.5	19.4	20.4	12.9
Christchurch	21.6	18.2	14.1	9.6	6.0	4.6	5.3	7.9	12.1	16.7	20.8	21.6	13.2
Mt Cook	22.2	19.8	14.7	10.1	5.6	4.2	5.2	7.8	11.2	16.6	21.6	21.4	13.4
Lake Tekapo	23.9	20.7	15.7	10.7	6.6	5.5	6.0	8.7	13.3	18.6	23.5	23.6	14.7
Timaru	20.3	17.0	13.7	9.7	6.0	5.1	5.8	8.3	12.4	16.6	19.7	20.6	12.9
Queenstown	23.5	20.8	15.6	10.3	6.1	4.8	5.8	8.5	12.9	18.3	22.0	24.0	14.4
Clyde	22.8	20.3	15.3	9.8	5.7	4.4	4.9	8.1	12.9	17.7	22.2	23.6	14.0
Manapouri	21.6	18.7	13.6	8.8	5.1	3.7	4.4	7.2	11.3	16.5	20.6	22.2	12.8

LOCATION	JAN	FEB	MAR	APR	MAY	JUN	JUL	AUG	SEP	OCT	NOV	DEC	YEAR
Dunedin	19.1	17.0	12.4	8.2	4.8	3.7	4.4	6.6	10.7	15.3	18.3	19.4	11.7
Invercargill	19.9	17.1	12.3	7.9	4.5	3.5	4.2	6.9	11.0	15.4	19.6	21.3	12.0
Chatham Islands	20.1	17.3	12.9	8.4	5.3	4.0	4.8	7.3	11.1	15.0	19.1	20.7	12.2
Antarctica,ScottBase	25.0	13.6	4.4	0.4	0.0	0.0	0.0	0.1	2.4	10.7	22.9	28.8	9.0

7.2 Mean Monthly total sunshine hours of various places of New Zealand (source: NIWA)

LOCATION	JAN	FEB	MAR	APR	MAY	JUN	JUL	AUG	SEP	OCT	NOV	DEC	YEAR
Kaitia	223.5	201.7	201.1	160.6	143.0	126.8	138.6	161.8	165.3	190.7	192.7	209.9	2115.7
Auckland	228.8	194.9	189.2	157.3	139.8	110.3	128.1	142.9	148.6	178.1	188.1	197.2	2003.1
Tauranga	261.5	217.3	214.0	183.9	165.3	135.4	151.0	173.4	174.1	212.7	224.2	232.7	2345.6
Hamilton	229.8	192.9	193.3	165.1	138.3	112.8	126.4	144.1	147.5	174.8	187.1	207.6	2019.6
Rotorua	242.9	205.9	199.7	170.5	145.1	119.1	130.7	152.1	155.1	190.8	200.1	215.8	2127.8
Gisborne	249.9	200.7	190.7	164.9	145.6	128.6	124.1	163.3	180.7	219.4	217.5	232.4	2217.7
Taupo	224.3	202.6	179.7	156.3	126.3	96.1	116.5	134.6	140.0	179.6	190.4	204.6	1950.9
New Plymouth	248.4	225.0	212.8	177.8	143.9	118.1	138.0	162.7	162.6	189.6	206.9	211.6	2197.2
Napier	249.3	202.6	201.7	172.4	155.6	130.7	134.7	166.8	181.2	213.9	216.2	233.7	2258.7
Wanganui	250.2	213.5	192.1	159.4	129.0	99.2	120.7	137.8	147.5	180.1	203.6	221.9	2055.0
Palmerston North	212.4	191.0	173.5	145.6	109.3	79.1	103.8	119.9	124.2	142.6	165.3	176.7	1743.5
Masterton	238.6	204.4	169.2	155.6	132.0	99.9	114.9	128.6	148.0	184.0	185.6	221.3	1982.2
Wellington	246.9	210.9	205.2	161.3	132.7	99.1	118.9	147.3	163.2	192.8	209.3	222.8	2110.3
Nelson	267.5	231.4	230.4	196.2	175.7	143.3	159.0	182.2	189.3	221.4	234.9	241.1	2472.4
Blenheim	262.2	223.7	230.8	193.7	172.7	151.6	157.1	183.9	189.5	226.7	234.7	248.8	2475.3
Westport	213.0	174.9	164.2	151.5	114.7	93.4	120.7	118.6	138.9	158.4	171.7	179.4	1799.3
Kaikoura	247.8	193.8	183.8	173.3	145.8	118.8	136.9	155.7	175.9	194.2	198.7	212.4	2137.1
Hokitika	219.5	187.4	177.3	146.7	119.1	98.7	126.1	136.7	141.0	167.8	184.0	189.4	1893.8
Christchurch	237.9	195.0	191.2	162.6	140.8	117.1	127.1	153.9	169.5	203.8	223.7	219.9	2142.5
Mt Cook	184.8	167.2	151.1	125.3	92.1	66.1	74.5	113.0	130.3	149.4	158.5	168.7	1580.9
Lake Tekapo	253.8	220.9	230.9	199.4	145.4	139.9	149.7	170.1	200.0	231.7	241.5	234.0	2417.4
Timaru	192.7	170.2	168.6	158.0	130.1	121.0	131.0	151.5	156.5	183.4	189.0	179.7	1931.9
Queenstown	230.3	207.3	187.0	145.4	87.8	71.8	88.3	120.0	153.6	197.7	216.6	223.5	1929.2
Alexandra	231.4	199.8	193.7	158.2	121.2	87.1	90.7	135.9	164.7	193.9	214.1	215.0	2005.8
Te Anau	184.2	178.5	152.9	125.3	84.8	64.9	66.0	115.6	138.4	178.6	192.3	180.1	1661.4

LOCATION	JAN	FEB	MAR	APR	MAY	JUN	JUL	AUG	SEP	OCT	NOV	DEC	YEAR
Dunedin	179.6	158.0	146.1	125.9	108.4	95.3	110.6	122.2	136.8	165.5	166.9	168.3	1683.7
Invercargill	185.9	167.2	142.6	117.2	87.5	78.7	97.9	123.0	139.8	173.0	181.3	188.2	1682.2
Chatham Islands	191.3	145.5	124.2	106.3	81.2	61.8	74.4	101.0	109.1	129.7	148.9	164.0	1437.3

7.3 Solar irradiance data measured at the University of Waikato using solar power meter from 10/12/2017 to 15/12/2017

Irradiance data Recorded on 10.12.2017, in partly cloudy weather

Sl. no	Date	Time (hr)	Irradiance (W/m ²)	Avg. Temperature (°C)	Remarks
1	10/12/2017	6:00	56	25	
2	10/12/2017	7:00	250	25	
3	10/12/2017	8:00	420	25	
4	10/12/2017	9:00	500	25	
5	10/12/2017	10:00	580	25	
6	10/12/2017	11:00	600	25	
7	10/12/2017	12:00	640	25	
8	10/12/2017	13:00	790	25	
9	10/12/2017	14:00	200	25	Cloudy
10	10/12/2017	15:00	320	25	
11	10/12/2017	16:00	280	25	
12	10/12/2017	17:00	210	25	
13	10/12/2017	18:00	180	25	
14	10/12/2017	19:00	120	25	
15	10/12/2017	20:00	35	25	

Irradiance data Recorded on 11.12.2017, in partly cloudy slight rain

Sl. no	Date	Time (hr)	Irradiance (W/m ²)	Avg. Temperature (°C)	Remarks
1	11/12/2017	6:00	45	25	
2	11/12/2017	7:00	280	25	
3	11/12/2017	8:00	440	25	
4	11/12/2017	9:00	510	25	
5	11/12/2017	10:00	500	25	
6	11/12/2017	11:00	390	25	
7	11/12/2017	12:00	800	25	
8	11/12/2017	13:00	520	25	
9	11/12/2017	14:00	610	25	
10	11/12/2017	15:00	700	25	
11	11/12/2017	16:00	350	25	
12	11/12/2017	17:00	460	25	

13	11/12/2017	18:00	400	25	
14	11/12/2017	19:00	200	25	
15	11/12/2017	20:00	45	25	

Irradiance data Recorded on 12.12.2017, in sunny weather

Sl. no	Date	Time (hr)	Irradiance (W/m ²)	Avg. Temperature (°C)	Remarks
1	12/12/2017	6:00	50	25	
2	12/12/2017	7:00	310	25	
3	12/12/2017	8:00	450	25	
4	12/12/2017	9:00	620	25	
5	12/12/2017	10:00	680	25	
6	12/12/2017	11:00	730	25	
7	12/12/2017	12:00	820	25	
8	12/12/2017	13:00	1000	25	
9	12/12/2017	14:00	900	25	
10	12/12/2017	15:00	830	25	
11	12/12/2017	16:00	700	25	
12	12/12/2017	17:00	530	25	
13	12/12/2017	18:00	350	25	
14	12/12/2017	19:00	200	25	
15	12/12/2017	20:00	15	25	

Irradiance data Recorded on 13.12.2017, in mostly sunny weather

Sl. no	Date	Time (hr)	Irradiance (W/m ²)	Avg. Temperature (°C)	Remarks
1	13/12/2017	6:00	60	25	
2	13/12/2017	7:00	310	25	
3	13/12/2017	8:00	460	25	
4	13/12/2017	9:00	530	25	
5	13/12/2017	10:00	200	25	Light cloud
6	13/12/2017	11:00	720	25	
7	13/12/2017	12:00	740	25	

8	13/12/2017	13:00	980	25	
9	13/12/2017	14:00	810	25	
10	13/12/2017	15:00	690	25	
11	13/12/2017	16:00	620	25	
12	13/12/2017	17:00	540	25	
13	13/12/2017	18:00	360	25	
14	13/12/2017	19:00	130	25	
15	13/12/2017	20:00	10	25	

Irradiance data Recorded on 14.12.2017, in mostly cloudy weather

Sl. no	Date	Time (hr)	Irradiance (W/m ²)	Avg. Temperature (°C)	Remarks
1	14/12/2017	6:00	30	25	
2	14/12/2017	7:00	200	25	
3	14/12/2017	8:00	360	25	
4	14/12/2017	9:00	400	25	
5	14/12/2017	10:00	500	25	
6	14/12/2017	11:00	200	25	Heavy cloud
7	14/12/2017	12:00	800	25	
8	14/12/2017	13:00	920	25	
9	14/12/2017	14:00	650	25	
10	14/12/2017	15:00	570	25	
11	14/12/2017	16:00	800	25	
12	14/12/2017	17:00	440	25	
13	14/12/2017	18:00	200	25	
14	14/12/2017	19:00	150	25	
15	14/12/2017	20:00	30	25	

Irradiance data Recorded on 15.12.2017, in mostly cloudy weather

Sl. no	Date	Time (hr)	Irradiance (W/m ²)	Avg. Temperature (°C)	Remarks
1	15/12/2017	6:00	40	25	
2	15/12/2017	7:00	260	25	
3	15/12/2017	8:00	480	25	
4	15/12/2017	9:00	620	25	
5	15/12/2017	10:00	810	25	
6	15/12/2017	11:00	860	25	
7	15/12/2017	12:00	980	25	
8	15/12/2017	13:00	400	25	Light cloud
9	15/12/2017	14:00	780	25	
10	15/12/2017	15:00	750	25	
11	15/12/2017	16:00	690	25	
12	15/12/2017	17:00	440	25	
13	15/12/2017	18:00	320	25	
14	15/12/2017	19:00	200	25	
15	15/12/2017	20:00	25	25	

7.4 Solar Irradiance data measured using solar power meter on 4/1/2018 (rainy day)

Irradiance data Recorded on 04.01.2018, in rainy weather

Sl. no	Date	Time	Irradiance (W/m ²)	Avg. Temperature (°C)	Remarks
1	4/1/2018	6:00	15	25	
2	4/1/2018	7:00	65	25	
3	4/1/2018	8:00	150	25	
4	4/1/2018	9:00	230	25	
5	4/1/2018	10:00	290	25	
6	4/1/2018	11:00	200	25	

7	4/1/2018	12:00	150	25	Rain throughout the day
8	4/1/2018	13:00	220	25	
9	4/1/2018	14:00	230	25	
10	4/1/2018	15:00	120	25	
11	4/1/2018	16:00	100	25	
12	4/1/2018	17:00	90	25	
13	4/1/2018	18:00	25	25	
14	4/1/2018	19:00	8	25	
15	4/1/2018	20:00	3	25	

7.5 Daily global solar radiation from 10/12/2017 to 15/12/2017 (source: NIWA)

Station information:

Name	Agent Number	Network Number	Latitude (dec.deg)	Longitude (dec.deg)	Height (m)	Position Precision	Observing Authority
Hamilton, Ruakura 2 Ews	26117	C75734	-37.77567	175.30506	45	H	NIWA/AGRE SEARCH

Note: Position precision types are: "W" = based on whole minutes, "T" = estimated to tenth minute,

"G" = derived from gridref, "E" = error cases derived from gridref,

"H" = based on GPS readings (NZGD49), "D" = by definition i.e. grid points. [For more info](#)

[Back to Database Query Form](#)

Station	Date (NZST)	Time (NZST)	Amount (MJ/m2)	Amount (W/m2)	Period (Hrs)	Type	Freq	Orig
Hamilton, Ruakura 2 Ews	10/12/2017	22:59	18.02	208.57	24	G	D	D
Hamilton, Ruakura 2 Ews	11/12/2017	22:59	21.72	251.39	24	G	D	D
Hamilton, Ruakura 2 Ews	12/12/2017	22:59	28.34	328.01	24	G	D	D
Hamilton, Ruakura 2 Ews	13/12/2017	22:59	25.79	298.50	24	G	D	D
Hamilton, Ruakura 2 Ews	14/12/2017	22:59	28.22	326.62	24	G	D	D
Hamilton, Ruakura 2 Ews	15/12/2017	22:59	27.53	318.63	24	G	D	D

Radiation:Hourly Global

Station	Date (NZST)	Time (NZST)	Amount (MJ/m2)	Amount (W/m2)	Period (Hrs)	Type	Freq	Orig
Hamilton, Ruakura 2 Ews	10/12/2017	0:00	0	0.00	1	G	H	H
Hamilton, Ruakura 2 Ews	10/12/2017	1:00	0	0.00	1	G	H	H

Hamilton, Ruakura 2 Ews	10/12/2017	2:00	0	0.00	1	G	H	H
Hamilton, Ruakura 2 Ews	10/12/2017	3:00	0	0.00	1	G	H	H
Hamilton, Ruakura 2 Ews	10/12/2017	4:00	0	0.00	1	G	H	H
Hamilton, Ruakura 2 Ews	10/12/2017	5:00	0	0.00	1	G	H	H
Hamilton, Ruakura 2 Ews	10/12/2017	6:00	0.27	75.00	1	G	H	H
Hamilton, Ruakura 2 Ews	10/12/2017	7:00	0.48	133.33	1	G	H	H
Hamilton, Ruakura 2 Ews	10/12/2017	8:00	1.35	375.00	1	G	H	H
Hamilton, Ruakura 2 Ews	10/12/2017	9:00	1.73	480.56	1	G	H	H
Hamilton, Ruakura 2 Ews	10/12/2017	10:00	2.49	691.67	1	G	H	H
Hamilton, Ruakura 2 Ews	10/12/2017	11:00	1.97	547.22	1	G	H	H
Hamilton, Ruakura 2 Ews	10/12/2017	12:00	2.33	647.22	1	G	H	H
Hamilton, Ruakura 2 Ews	10/12/2017	13:00	2.54	705.56	1	G	H	H
Hamilton, Ruakura 2 Ews	10/12/2017	14:00	0.69	191.67	1	G	H	H
Hamilton, Ruakura 2 Ews	10/12/2017	15:00	0.85	236.11	1	G	H	H
Hamilton, Ruakura 2 Ews	10/12/2017	16:00	1.15	319.44	1	G	H	H
Hamilton, Ruakura 2 Ews	10/12/2017	17:00	0.83	230.56	1	G	H	H
Hamilton, Ruakura 2 Ews	10/12/2017	18:00	0.76	211.11	1	G	H	H
Hamilton, Ruakura 2 Ews	10/12/2017	19:00	0.51	141.67	1	G	H	H
Hamilton, Ruakura 2 Ews	10/12/2017	20:00	0.07	19.44	1	G	H	H
Hamilton, Ruakura 2 Ews	10/12/2017	21:00	0	0.00	1	G	H	H
Hamilton, Ruakura 2 Ews	10/12/2017	22:00	0	0.00	1	G	H	H
Hamilton, Ruakura 2 Ews	10/12/2017	23:00	0	0.00	1	G	H	H
Hamilton, Ruakura 2 Ews	11/12/2017	0:00	0	0.00	1	G	H	H
Hamilton, Ruakura 2 Ews	11/12/2017	1:00	0	0.00	1	G	H	H
Hamilton, Ruakura 2 Ews	11/12/2017	2:00	0	0.00	1	G	H	H
Hamilton, Ruakura 2 Ews	11/12/2017	3:00	0	0.00	1	G	H	H
Hamilton, Ruakura 2 Ews	11/12/2017	4:00	0	0.00	1	G	H	H
Hamilton, Ruakura 2 Ews	11/12/2017	5:00	0	0.00	1	G	H	H
Hamilton, Ruakura 2 Ews	11/12/2017	6:00	0.24	66.67	1	G	H	H
Hamilton, Ruakura 2 Ews	11/12/2017	7:00	0.88	244.44	1	G	H	H
Hamilton, Ruakura 2 Ews	11/12/2017	8:00	1.61	447.22	1	G	H	H
Hamilton, Ruakura 2 Ews	11/12/2017	9:00	2.26	627.78	1	G	H	H
Hamilton, Ruakura 2 Ews	11/12/2017	10:00	1.74	483.33	1	G	H	H
Hamilton, Ruakura 2 Ews	11/12/2017	11:00	1.33	369.44	1	G	H	H
Hamilton, Ruakura 2 Ews	11/12/2017	12:00	2.74	761.11	1	G	H	H
Hamilton, Ruakura 2 Ews	11/12/2017	13:00	1.67	463.89	1	G	H	H
Hamilton, Ruakura 2 Ews	11/12/2017	14:00	2.07	575.00	1	G	H	H
Hamilton, Ruakura 2 Ews	11/12/2017	15:00	2.51	697.22	1	G	H	H

Hamilton, Ruakura 2 Ews	11/12/2017	16:00	1.39	386.11	1	G	H	H
Hamilton, Ruakura 2 Ews	11/12/2017	17:00	1.5	416.67	1	G	H	H
Hamilton, Ruakura 2 Ews	11/12/2017	18:00	1.21	336.11	1	G	H	H
Hamilton, Ruakura 2 Ews	11/12/2017	19:00	0.53	147.22	1	G	H	H
Hamilton, Ruakura 2 Ews	11/12/2017	20:00	0.05	13.89	1	G	H	H
Hamilton, Ruakura 2 Ews	11/12/2017	21:00	0	0.00	1	G	H	H
Hamilton, Ruakura 2 Ews	11/12/2017	22:00	0	0.00	1	G	H	H
Hamilton, Ruakura 2 Ews	11/12/2017	23:00	0	0.00	1	G	H	H
Hamilton, Ruakura 2 Ews	12/12/2017	0:00	0	0.00	1	G	H	H
Hamilton, Ruakura 2 Ews	12/12/2017	1:00	0	0.00	1	G	H	H
Hamilton, Ruakura 2 Ews	12/12/2017	2:00	0	0.00	1	G	H	H
Hamilton, Ruakura 2 Ews	12/12/2017	3:00	0	0.00	1	G	H	H
Hamilton, Ruakura 2 Ews	12/12/2017	4:00	0	0.00	1	G	H	H
Hamilton, Ruakura 2 Ews	12/12/2017	5:00	0	0.00	1	G	H	H
Hamilton, Ruakura 2 Ews	12/12/2017	6:00	0.24	66.67	1	G	H	H
Hamilton, Ruakura 2 Ews	12/12/2017	7:00	0.89	247.22	1	G	H	H
Hamilton, Ruakura 2 Ews	12/12/2017	8:00	1.51	419.44	1	G	H	H
Hamilton, Ruakura 2 Ews	12/12/2017	9:00	2.08	577.78	1	G	H	H
Hamilton, Ruakura 2 Ews	12/12/2017	10:00	2.22	616.67	1	G	H	H
Hamilton, Ruakura 2 Ews	12/12/2017	11:00	2.73	758.33	1	G	H	H
Hamilton, Ruakura 2 Ews	12/12/2017	12:00	2.88	800.00	1	G	H	H
Hamilton, Ruakura 2 Ews	12/12/2017	13:00	3.51	975.00	1	G	H	H
Hamilton, Ruakura 2 Ews	12/12/2017	14:00	3.28	911.11	1	G	H	H
Hamilton, Ruakura 2 Ews	12/12/2017	15:00	2.98	827.78	1	G	H	H
Hamilton, Ruakura 2 Ews	12/12/2017	16:00	2.49	691.67	1	G	H	H
Hamilton, Ruakura 2 Ews	12/12/2017	17:00	1.87	519.44	1	G	H	H
Hamilton, Ruakura 2 Ews	12/12/2017	18:00	1.16	322.22	1	G	H	H
Hamilton, Ruakura 2 Ews	12/12/2017	19:00	0.48	133.33	1	G	H	H
Hamilton, Ruakura 2 Ews	12/12/2017	20:00	0.02	5.56	1	G	H	H
Hamilton, Ruakura 2 Ews	12/12/2017	21:00	0	0.00	1	G	H	H
Hamilton, Ruakura 2 Ews	12/12/2017	22:00	0	0.00	1	G	H	H
Hamilton, Ruakura 2 Ews	12/12/2017	23:00	0	0.00	1	G	H	H
Hamilton, Ruakura 2 Ews	13/12/2017	0:00	0	0.00	1	G	H	H
Hamilton, Ruakura 2 Ews	13/12/2017	1:00	0	0.00	1	G	H	H
Hamilton, Ruakura 2 Ews	13/12/2017	2:00	0	0.00	1	G	H	H
Hamilton, Ruakura 2 Ews	13/12/2017	3:00	0	0.00	1	G	H	H
Hamilton, Ruakura 2 Ews	13/12/2017	4:00	0	0.00	1	G	H	H
Hamilton, Ruakura 2 Ews	13/12/2017	5:00	0	0.00	1	G	H	H

Hamilton, Ruakura 2 Ews	13/12/2017	6:00	0.26	72.22	1	G	H	H
Hamilton, Ruakura 2 Ews	13/12/2017	7:00	0.89	247.22	1	G	H	H
Hamilton, Ruakura 2 Ews	13/12/2017	8:00	1.49	413.89	1	G	H	H
Hamilton, Ruakura 2 Ews	13/12/2017	9:00	1.84	511.11	1	G	H	H
Hamilton, Ruakura 2 Ews	13/12/2017	10:00	1.79	497.22	1	G	H	H
Hamilton, Ruakura 2 Ews	13/12/2017	11:00	2.45	680.56	1	G	H	H
Hamilton, Ruakura 2 Ews	13/12/2017	12:00	2.51	697.22	1	G	H	H
Hamilton, Ruakura 2 Ews	13/12/2017	13:00	3.6	1000.00	1	G	H	H
Hamilton, Ruakura 2 Ews	13/12/2017	14:00	2.82	783.33	1	G	H	H
Hamilton, Ruakura 2 Ews	13/12/2017	15:00	2.41	669.44	1	G	H	H
Hamilton, Ruakura 2 Ews	13/12/2017	16:00	2.29	636.11	1	G	H	H
Hamilton, Ruakura 2 Ews	13/12/2017	17:00	1.88	522.22	1	G	H	H
Hamilton, Ruakura 2 Ews	13/12/2017	18:00	1.17	325.00	1	G	H	H
Hamilton, Ruakura 2 Ews	13/12/2017	19:00	0.36	100.00	1	G	H	H
Hamilton, Ruakura 2 Ews	13/12/2017	20:00	0.03	8.33	1	G	H	H
Hamilton, Ruakura 2 Ews	13/12/2017	21:00	0	0.00	1	G	H	H
Hamilton, Ruakura 2 Ews	13/12/2017	22:00	0	0.00	1	G	H	H
Hamilton, Ruakura 2 Ews	13/12/2017	23:00	0	0.00	1	G	H	H
Hamilton, Ruakura 2 Ews	14/12/2017	0:00	0	0.00	1	G	H	H
Hamilton, Ruakura 2 Ews	14/12/2017	1:00	0	0.00	1	G	H	H
Hamilton, Ruakura 2 Ews	14/12/2017	2:00	0	0.00	1	G	H	H
Hamilton, Ruakura 2 Ews	14/12/2017	3:00	0	0.00	1	G	H	H
Hamilton, Ruakura 2 Ews	14/12/2017	4:00	0	0.00	1	G	H	H
Hamilton, Ruakura 2 Ews	14/12/2017	5:00	0	0.00	1	G	H	H
Hamilton, Ruakura 2 Ews	14/12/2017	6:00	0.23	63.89	1	G	H	H
Hamilton, Ruakura 2 Ews	14/12/2017	7:00	0.64	177.78	1	G	H	H
Hamilton, Ruakura 2 Ews	14/12/2017	8:00	1.59	441.67	1	G	H	H
Hamilton, Ruakura 2 Ews	14/12/2017	9:00	2.22	616.67	1	G	H	H
Hamilton, Ruakura 2 Ews	14/12/2017	10:00	2.46	683.33	1	G	H	H
Hamilton, Ruakura 2 Ews	14/12/2017	11:00	3.01	836.11	1	G	H	H
Hamilton, Ruakura 2 Ews	14/12/2017	12:00	2.83	786.11	1	G	H	H
Hamilton, Ruakura 2 Ews	14/12/2017	13:00	2.9	805.56	1	G	H	H
Hamilton, Ruakura 2 Ews	14/12/2017	14:00	3.05	847.22	1	G	H	H
Hamilton, Ruakura 2 Ews	14/12/2017	15:00	2.82	783.33	1	G	H	H
Hamilton, Ruakura 2 Ews	14/12/2017	16:00	2.71	752.78	1	G	H	H
Hamilton, Ruakura 2 Ews	14/12/2017	17:00	1.97	547.22	1	G	H	H
Hamilton, Ruakura 2 Ews	14/12/2017	18:00	1.21	336.11	1	G	H	H
Hamilton, Ruakura 2 Ews	14/12/2017	19:00	0.53	147.22	1	G	H	H

Hamilton, Ruakura 2 Ews	14/12/2017	20:00	0.04	11.11	1	G	H	H
Hamilton, Ruakura 2 Ews	14/12/2017	21:00	0	0.00	1	G	H	H
Hamilton, Ruakura 2 Ews	14/12/2017	22:00	0	0.00	1	G	H	H
Hamilton, Ruakura 2 Ews	14/12/2017	23:00	0	0.00	1	G	H	H
Hamilton, Ruakura 2 Ews	15/12/2017	0:00	0	0.00	1	G	H	H
Hamilton, Ruakura 2 Ews	15/12/2017	1:00	0	0.00	1	G	H	H
Hamilton, Ruakura 2 Ews	15/12/2017	2:00	0	0.00	1	G	H	H
Hamilton, Ruakura 2 Ews	15/12/2017	3:00	0	0.00	1	G	H	H
Hamilton, Ruakura 2 Ews	15/12/2017	4:00	0	0.00	1	G	H	H
Hamilton, Ruakura 2 Ews	15/12/2017	5:00	0	0.00	1	G	H	H
Hamilton, Ruakura 2 Ews	15/12/2017	6:00	0.21	58.33	1	G	H	H
Hamilton, Ruakura 2 Ews	15/12/2017	7:00	0.82	227.78	1	G	H	H
Hamilton, Ruakura 2 Ews	15/12/2017	8:00	1.6	444.44	1	G	H	H
Hamilton, Ruakura 2 Ews	15/12/2017	9:00	2.29	636.11	1	G	H	H
Hamilton, Ruakura 2 Ews	15/12/2017	10:00	2.82	783.33	1	G	H	H
Hamilton, Ruakura 2 Ews	15/12/2017	11:00	3	833.33	1	G	H	H
Hamilton, Ruakura 2 Ews	15/12/2017	12:00	3.49	969.44	1	G	H	H
Hamilton, Ruakura 2 Ews	15/12/2017	13:00	1.97	547.22	1	G	H	H
Hamilton, Ruakura 2 Ews	15/12/2017	14:00	2.76	766.67	1	G	H	H
Hamilton, Ruakura 2 Ews	15/12/2017	15:00	2.82	783.33	1	G	H	H
Hamilton, Ruakura 2 Ews	15/12/2017	16:00	2.35	652.78	1	G	H	H
Hamilton, Ruakura 2 Ews	15/12/2017	17:00	1.72	477.78	1	G	H	H
Hamilton, Ruakura 2 Ews	15/12/2017	18:00	1.09	302.78	1	G	H	H
Hamilton, Ruakura 2 Ews	15/12/2017	19:00	0.56	155.56	1	G	H	H
Hamilton, Ruakura 2 Ews	15/12/2017	20:00	0.04	11.11	1	G	H	H
Hamilton, Ruakura 2 Ews	15/12/2017	21:00	0	0.00	1	G	H	H
Hamilton, Ruakura 2 Ews	15/12/2017	22:00	0	0.00	1	G	H	H
Hamilton, Ruakura 2 Ews	15/12/2017	23:00	0	0.00	1	G	H	H

7.6 Rainy day solar irradiance data on 4/1/2018 (source: NIWA)

Radiation: Hourly Global

Station	Date (NZST)	Time (NZST)	Amount (MJ/m ²)	Amount (W/m ²)	Period (Hrs)	Type	Freq	Orig
Hamilton, Ruakura 2 Ews	4/1/2018	0:00	0	0.00	1	G	H	H
Hamilton, Ruakura 2 Ews	4/1/2018	1:00	0	0.00	1	G	H	H
Hamilton, Ruakura 2 Ews	4/1/2018	2:00	0	0.00	1	G	H	H
Hamilton, Ruakura 2 Ews	4/1/2018	3:00	0	0.00	1	G	H	H

Hamilton, Ruakura 2 Ews	4/1/2018	4:00	0	0.00	1	G	H	H
Hamilton, Ruakura 2 Ews	4/1/2018	5:00	0	0.00	1	G	H	H
Hamilton, Ruakura 2 Ews	4/1/2018	6:00	0.06	16.67	1	G	H	H
Hamilton, Ruakura 2 Ews	4/1/2018	7:00	0.27	75.00	1	G	H	H
Hamilton, Ruakura 2 Ews	4/1/2018	8:00	0.53	147.22	1	G	H	H
Hamilton, Ruakura 2 Ews	4/1/2018	9:00	0.89	247.22	1	G	H	H
Hamilton, Ruakura 2 Ews	4/1/2018	10:00	0.94	261.11	1	G	H	H
Hamilton, Ruakura 2 Ews	4/1/2018	11:00	0.66	183.33	1	G	H	H
Hamilton, Ruakura 2 Ews	4/1/2018	12:00	0.62	172.22	1	G	H	H
Hamilton, Ruakura 2 Ews	4/1/2018	13:00	0.72	200.00	1	G	H	H
Hamilton, Ruakura 2 Ews	4/1/2018	14:00	0.77	213.89	1	G	H	H
Hamilton, Ruakura 2 Ews	4/1/2018	15:00	0.56	155.56	1	G	H	H
Hamilton, Ruakura 2 Ews	4/1/2018	16:00	0.35	97.22	1	G	H	H
Hamilton, Ruakura 2 Ews	4/1/2018	17:00	0.22	61.11	1	G	H	H
Hamilton, Ruakura 2 Ews	4/1/2018	18:00	0.08	22.22	1	G	H	H
Hamilton, Ruakura 2 Ews	4/1/2018	19:00	0.02	5.56	1	G	H	H
Hamilton, Ruakura 2 Ews	4/1/2018	20:00	0	0.00	1	G	H	H
Hamilton, Ruakura 2 Ews	4/1/2018	21:00	0	0.00	1	G	H	H
Hamilton, Ruakura 2 Ews	4/1/2018	22:00	0	0.00	1	G	H	H
Hamilton, Ruakura 2 Ews	4/1/2018	23:00	0	0.00	1	G	H	H

7.7 University of Waikato hourly irradiance data of an average year

(source: NIWA)

NIWA Solar View Calculations

Query date: 24-Sep17

Description	university of waikato	
Latitude	-37.79	
Longitude	175.32	
Panel Tilt	38	
Bearing	0	
Ground Albedo	0.1	
Climate Station	26117	Hamilton
Years of Data	12	

Month & hour	Elevation	Azimuth	Hourly W/m2	Cumulative kWh/m2
Jan 0:00	-32.2	180	0	0
Jan 1:00	-30.5	163.6	0	0
Jan 2:00	-25.7	148.6	0	0
Jan 3:00	-18.4	135.5	0	0
Jan 4:00	-9.3	124.4	0	0
Jan 5:00	1	114.8	11	0.01
Jan 6:00	12.1	106	54	0.06
Jan 7:00	23.7	97.6	197	0.26
Jan 8:00	35.5	88.7	359	0.62
Jan 9:00	47.3	78.3	504	1.12
Jan 10:00	58.5	64	615	1.74
Jan 11:00	67.9	40.3	695	2.43
Jan 12:00	72.1	0	712	3.15
Jan 13:00	67.9	-40.3	702	3.85
Jan 14:00	58.5	-63.9	635	4.48
Jan 15:00	47.2	-78.2	527	5.01
Jan 16:00	35.5	-88.6	366	5.38
Jan 17:00	23.6	-97.5	194	5.57
Jan 18:00	12	-105.9	50	5.62
Jan 19:00	0.9	-114.7	12	5.63
Jan 20:00	-9.4	-124.3	0	5.63
Jan 21:00	-18.5	-135.4	0	5.63

Month & hour	Elevation	Azimuth	Hourly W/m2	Cumulative kWh/m2
Jan 22:00	-25.8	-148.5	0	5.63
Jan 23:00	-30.7	-163.5	0	5.63
Feb 0:00	-41.4	-179.2	0	0
Feb 1:00	-39.6	161.5	0	0
Feb 2:00	-34.2	144.3	0	0
Feb 3:00	-26.2	130	0	0
Feb 4:00	-16.4	118.2	0	0
Feb 5:00	-5.5	108.1	1	0
Feb 6:00	6	98.9	28	0.03
Feb 7:00	17.8	89.8	158	0.19
Feb 8:00	29.6	80.1	319	0.51
Feb 9:00	41	68.6	478	0.98
Feb 10:00	51.4	53.3	585	1.57
Feb 11:00	59.4	31.3	647	2.22
Feb 12:00	62.8	1.3	673	2.89
Feb 13:00	59.9	-29.1	638	3.53
Feb 14:00	52.1	-51.8	588	4.12
Feb 15:00	41.9	-67.4	475	4.59
Feb 16:00	30.5	-79.2	334	4.92
Feb 17:00	18.7	-88.9	174	5.1
Feb 18:00	6.9	-98	33	5.13
Feb 19:00	-4.7	-107.1	2	5.13
Feb 20:00	-15.7	-117.2	0	5.13
Feb 21:00	-25.6	-128.8	0	5.13
Feb 22:00	-33.9	-142.9	0	5.13
Feb 23:00	-39.6	-159.9	0	5.13
Mar 0:00	-52.2	178.5	0	0
Mar 1:00	-49.5	155	0	0
Mar 2:00	-42.7	135.6	0	0
Mar 3:00	-33.4	120.6	0	0
Mar 4:00	-22.6	108.7	0	0
Mar 5:00	-11.1	98.6	0	0
Mar 6:00	0.7	89.3	12	0.01
Mar 7:00	12.5	80	129	0.14

Month & hour	Elevation	Azimuth	Hourly W/m2	Cumulative kWh/m2
Mar 8:00	23.9	69.7	298	0.44
Mar 9:00	34.5	57.5	460	0.9
Mar 10:00	43.6	42	574	1.47
Mar 11:00	49.9	22.1	644	2.12
Mar 12:00	52	-1.6	653	2.77
Mar 13:00	49.3	-25	607	3.38
Mar 14:00	42.5	-44.3	532	3.91
Mar 15:00	33.1	-59.2	408	4.32
Mar 16:00	22.4	-71	264	4.58
Mar 17:00	10.9	-81.1	115	4.7
Mar 18:00	-1	-90.4	10	4.7
Mar 19:00	-12.8	-99.7	0	4.7
Mar 20:00	-24.2	-109.9	0	4.7
Mar 21:00	-34.9	-122.1	0	4.7
Mar 22:00	-44	-137.6	0	4.7
Mar 23:00	-50.4	-157.7	0	4.7
Apr 0:00	-63.7	173.2	0	0
Apr 1:00	-59.3	143.5	0	0
Apr 2:00	-50.6	122.6	0	0
Apr 3:00	-39.9	108.3	0	0
Apr 4:00	-28.3	97.2	0	0
Apr 5:00	-16.5	87.8	0	0
Apr 6:00	-4.8	78.8	2	0
Apr 7:00	6.6	69.5	80	0.08
Apr 8:00	17.3	59.2	234	0.32
Apr 9:00	26.8	47.1	383	0.7
Apr 10:00	34.4	32.4	497	1.2
Apr 11:00	39.2	15.1	567	1.76
Apr 12:00	40.3	-4	559	2.32
Apr 13:00	37.6	-22.6	500	2.82
Apr 14:00	31.5	-38.8	432	3.25
Apr 15:00	23	-52.3	311	3.56
Apr 16:00	12.9	-63.6	174	3.74
Apr 17:00	1.9	-73.4	32	3.77

Month & hour	Elevation	Azimuth	Hourly W/m2	Cumulative kWh/m2
Apr 18:00	-9.7	-82.4	0	3.77
Apr 19:00	-21.5	-91.4	0	3.77
Apr 20:00	-33.3	-101.3	0	3.77
Apr 21:00	-44.6	-113.4	0	3.77
Apr 22:00	-54.8	-130	0	3.77
Apr 23:00	-62.1	-154.5	0	3.77
May 0:00	-72	168.8	0	0
May 1:00	-66	132.3	0	0
May 2:00	-55.9	111.7	0	0
May 3:00	-44.5	98.7	0	0
May 4:00	-32.7	88.9	0	0
May 5:00	-20.9	80.2	0	0
May 6:00	-9.4	71.8	0	0
May 7:00	1.5	62.9	28	0.03
May 8:00	11.6	52.9	183	0.21
May 9:00	20.3	41.4	312	0.52
May 10:00	27	27.9	415	0.94
May 11:00	31.1	12.4	461	1.4
May 12:00	32	-4.1	480	1.88
May 13:00	29.4	-20.2	438	2.32
May 14:00	24	-34.7	378	2.7
May 15:00	16.2	-47.2	257	2.95
May 16:00	6.8	-57.9	108	3.06
May 17:00	-3.8	-67.2	2	3.06
May 18:00	-15	-75.8	0	3.06
May 19:00	-26.7	-84.3	0	3.06
May 20:00	-38.5	-93.3	0	3.06
May 21:00	-50.2	-104.3	0	3.06
May 22:00	-61.2	-120.1	0	3.06
May 23:00	-69.9	-147.5	0	3.06
Jun 0:00	-75.5	171.1	0	0
Jun 1:00	-69.3	129	0	0
Jun 2:00	-58.9	108	0	0
Jun 3:00	-47.3	95.6	0	0

Month & hour	Elevation	Azimuth	Hourly W/m2	Cumulative kWh/m2
Jun 4:00	-35.4	86.2	0	0
Jun 5:00	-23.7	77.9	0	0
Jun 6:00	-12.3	69.8	0	0
Jun 7:00	-1.5	61.1	5	0.01
Jun 8:00	8.3	51.5	137	0.14
Jun 9:00	16.9	40.5	268	0.41
Jun 10:00	23.5	27.6	371	0.78
Jun 11:00	27.6	13.1	433	1.21
Jun 12:00	28.7	-2.5	435	1.65
Jun 13:00	26.6	-17.9	411	2.06
Jun 14:00	21.6	-31.9	319	2.38
Jun 15:00	14.3	-44.2	220	2.6
Jun 16:00	5.3	-54.7	85	2.68
Jun 17:00	-4.9	-64	2	2.68
Jun 18:00	-15.9	-72.4	0	2.68
Jun 19:00	-27.4	-80.5	0	2.68
Jun 20:00	-39.2	-89	0	2.68
Jun 21:00	-51	-99.1	0	2.68
Jun 22:00	-62.4	-113.3	0	2.68
Jun 23:00	-72	-139.4	0	2.68
Jul 0:00	-72.8	176.2	0	0
Jul 1:00	-67.8	136.2	0	0
Jul 2:00	-58	113.7	0	0
Jul 3:00	-46.7	100	0	0
Jul 4:00	-34.9	89.9	0	0
Jul 5:00	-23	81.2	0	0
Jul 6:00	-11.5	72.8	0	0
Jul 7:00	-0.5	64.1	10	0.01
Jul 8:00	9.7	54.4	143	0.15
Jul 9:00	18.6	43.2	283	0.44
Jul 10:00	25.7	30.1	390	0.83
Jul 11:00	30.3	15	441	1.27
Jul 12:00	31.7	-1.3	447	1.71
Jul 13:00	29.8	-17.5	435	2.15

Month & hour	Elevation	Azimuth	Hourly W/m2	Cumulative kWh/m2
Jul 14:00	24.8	-32.3	351	2.5
Jul 15:00	17.4	-45.1	254	2.75
Jul 16:00	8.2	-56.1	119	2.87
Jul 17:00	-2.1	-65.6	5	2.88
Jul 18:00	-13.3	-74.3	0	2.88
Jul 19:00	-24.9	-82.7	0	2.88
Jul 20:00	-36.7	-91.5	0	2.88
Jul 21:00	-48.4	-102.1	0	2.88
Jul 22:00	-59.6	-116.7	0	2.88
Jul 23:00	-68.9	-141.6	0	2.88
Aug 0:00	-64.5	175.5	0	0
Aug 1:00	-60.4	144.8	0	0
Aug 2:00	-51.8	123.3	0	0
Aug 3:00	-41.1	108.6	0	0
Aug 4:00	-29.5	97.5	0	0
Aug 5:00	-17.7	88	0	0
Aug 6:00	-5.9	79.1	1	0
Aug 7:00	5.5	69.9	72	0.07
Aug 8:00	16.2	59.7	224	0.3
Aug 9:00	25.8	47.8	366	0.66
Aug 10:00	33.6	33.4	460	1.12
Aug 11:00	38.6	16.3	520	1.64
Aug 12:00	40	-2.6	517	2.16
Aug 13:00	37.6	-21.2	486	2.65
Aug 14:00	31.8	-37.6	417	3.06
Aug 15:00	23.5	-51.2	301	3.36
Aug 16:00	13.6	-62.6	171	3.54
Aug 17:00	2.6	-72.5	33	3.57
Aug 18:00	-8.9	-81.6	0	3.57
Aug 19:00	-20.7	-90.6	0	3.57
Aug 20:00	-32.5	-100.4	0	3.57
Aug 21:00	-43.9	-112.3	0	3.57
Aug 22:00	-54.1	-128.5	0	3.57
Aug 23:00	-61.7	-152.4	0	3.57

Month & hour	Elevation	Azimuth	Hourly W/m2	Cumulative kWh/m2
Sep 0:00	-52.9	172.6	0	0
Sep 1:00	-49	149.5	0	0
Sep 2:00	-41.4	131	0	0
Sep 3:00	-31.5	116.9	0	0
Sep 4:00	-20.5	105.6	0	0
Sep 5:00	-8.8	95.8	0	0
Sep 6:00	3	86.6	24	0.02
Sep 7:00	14.8	77.1	142	0.17
Sep 8:00	26	66.5	290	0.46
Sep 9:00	36.3	53.7	423	0.88
Sep 10:00	44.8	37.4	522	1.4
Sep 11:00	50.3	16.6	569	1.97
Sep 12:00	51.3	-7.2	571	2.54
Sep 13:00	47.5	-29.6	540	3.08
Sep 14:00	40.1	-47.8	450	3.53
Sep 15:00	30.4	-61.8	333	3.86
Sep 16:00	19.4	-73.2	202	4.07
Sep 17:00	7.9	-83	65	4.13
Sep 18:00	-4	-92.3	2	4.13
Sep 19:00	-15.7	-101.8	0	4.13
Sep 20:00	-27	-112.4	0	4.13
Sep 21:00	-37.4	-125.2	0	4.13
Sep 22:00	-46	-141.7	0	4.13
Sep 23:00	-51.6	-163	0	4.13
Oct 0:00	-41.3	171.3	0	0
Oct 1:00	-37.7	152.8	0	0
Oct 2:00	-30.8	136.9	0	0
Oct 3:00	-21.8	123.9	0	0
Oct 4:00	-11.3	113	0	0
Oct 5:00	-0.1	103.4	8	0.01
Oct 6:00	11.7	94.4	75	0.08
Oct 7:00	23.5	85.2	212	0.3
Oct 8:00	35.2	74.8	359	0.65
Oct 9:00	46.2	61.9	480	1.13

Month & hour	Elevation	Azimuth	Hourly W/m2	Cumulative kWh/m2
Oct 10:00	55.7	43.8	575	1.71
Oct 11:00	61.8	17.7	627	2.34
Oct 12:00	62.2	-14.1	641	2.98
Oct 13:00	56.7	-41.2	595	3.57
Oct 14:00	47.5	-60.2	513	4.08
Oct 15:00	36.6	-73.6	387	4.47
Oct 16:00	25	-84.2	240	4.71
Oct 17:00	13.1	-93.5	92	4.8
Oct 18:00	1.4	-102.5	14	4.82
Oct 19:00	-9.9	-112	0	4.82
Oct 20:00	-20.4	-122.8	0	4.82
Oct 21:00	-29.6	-135.5	0	4.82
Oct 22:00	-36.7	-150.9	0	4.82
Oct 23:00	-40.8	-169.1	0	4.82
Nov 0:00	-32.1	172.9	0	0
Nov 1:00	-29	156.9	0	0
Nov 2:00	-23	142.7	0	0
Nov 3:00	-14.9	130.5	0	0
Nov 4:00	-5.2	120.1	1	0
Nov 5:00	5.5	110.9	24	0.02
Nov 6:00	16.9	102.3	102	0.13
Nov 7:00	28.6	93.8	251	0.38
Nov 8:00	40.5	84.5	396	0.77
Nov 9:00	52.1	72.8	499	1.27
Nov 10:00	62.8	55.5	595	1.87
Nov 11:00	70.6	25.2	647	2.52
Nov 12:00	71.3	-18.9	659	3.17
Nov 13:00	64.3	-52	608	3.78
Nov 14:00	53.8	-70.7	535	4.32
Nov 15:00	42.3	-83	419	4.74
Nov 16:00	30.5	-92.6	280	5.02
Nov 17:00	18.7	-101.1	124	5.14
Nov 18:00	7.3	-109.6	32	5.17
Nov 19:00	-3.5	-118.7	3	5.17

Month & hour	Elevation	Azimuth	Hourly W/m2	Cumulative kWh/m2
Nov 20:00	-13.4	-128.9	0	5.17
Nov 21:00	-21.8	-140.8	0	5.17
Nov 22:00	-28.1	-154.7	0	5.17
Nov 23:00	-31.7	-170.4	0	5.17
Dec 0:00	-28.7	176.5	0	0
Dec 1:00	-26.4	161.2	0	0
Dec 2:00	-21.2	147.2	0	0
Dec 3:00	-13.8	135.1	0	0
Dec 4:00	-4.7	124.6	1	0
Dec 5:00	5.6	115.5	23	0.02
Dec 6:00	16.6	107.1	82	0.11
Dec 7:00	28.2	99	220	0.33
Dec 8:00	40	90.4	358	0.68
Dec 9:00	51.8	80.2	478	1.16
Dec 10:00	63.1	65.5	562	1.72
Dec 11:00	72.5	38.2	628	2.35
Dec 12:00	75.4	-12.2	640	2.99
Dec 13:00	68.8	-52.8	628	3.62
Dec 14:00	58.2	-72.9	548	4.17
Dec 15:00	46.6	-85	435	4.6
Dec 16:00	34.7	-94.3	302	4.9
Dec 17:00	23	-102.6	160	5.06
Dec 18:00	11.7	-110.7	49	5.11
Dec 19:00	0.9	-119.4	11	5.12
Dec 20:00	-8.9	-129.1	0	5.12
Dec 21:00	-17.3	-140.2	0	5.12
Dec 22:00	-23.8	-153.2	0	5.12
Dec 23:00	-27.8	-167.8	0	5.12

7.8 University of Waikato hourly irradiance data of an average season of an average year (source: NIWA)

NIWA Solar View Calculations

Query date: 24-Sep17

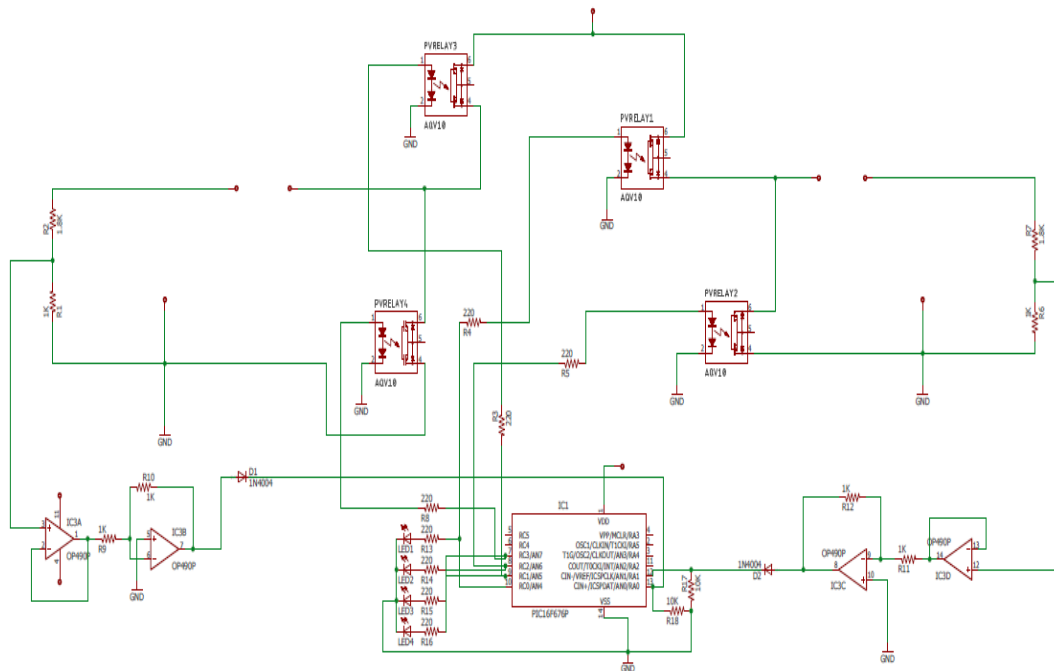
Description university of waikato
 Latitude -37.79
 Longitude 175.32
 Panel Tilt 38
 Bearing 0
 Ground Albedo 0.1
 Climate Station 26117 Hamilton
 Years of Data 12

Months & hour	Elevation	Azimuth	Hourly W/m2
Spring			
Sep, Oct, Nov 0:00	-52.9	172.6	0.00
Sep, Oct, Nov 1:00	-49	149.5	0.00
Sep, Oct, Nov 2:00	-41.4	131	0.00
Sep, Oct, Nov 3:00	-31.5	116.9	0.00
Sep, Oct, Nov 4:00	-20.5	105.6	0.33
Sep, Oct, Nov 5:00	-8.8	95.8	10.00
Sep, Oct, Nov 6:00	3	86.6	63.33
Sep, Oct, Nov 7:00	14.8	77.1	194.00
Sep, Oct, Nov 8:00	26	66.5	335.00
Sep, Oct, Nov 9:00	36.3	53.7	447.67
Sep, Oct, Nov 10:00	44.8	37.4	540.33
Sep, Oct, Nov 11:00	50.3	16.6	588.33
Sep, Oct, Nov 12:00	51.3	-7.2	599.00
Sep, Oct, Nov 13:00	47.5	-29.6	557.33
Sep, Oct, Nov 14:00	40.1	-47.8	479.67
Sep, Oct, Nov 15:00	30.4	-61.8	366.67
Sep, Oct, Nov 16:00	19.4	-73.2	232.67
Sep, Oct, Nov 17:00	7.9	-83	89.67
Sep, Oct, Nov 18:00	-4	-92.3	14.67
Sep, Oct, Nov 19:00	-15.7	-101.8	0.67
Sep, Oct, Nov 20:00	-27	-112.4	0.00
Sep, Oct, Nov 21:00	-37.4	-125.2	0.00
Sep, Oct, Nov 22:00	-46	-141.7	0.00
Sep, Oct, Nov 23:00	-51.6	-163	0.00
Summer			
Dec, Jan, Feb 0:00	-28.7	176.5	0.00
Dec, Jan, Feb 1:00	-26.4	161.2	0.00
Dec, Jan, Feb 2:00	-21.2	147.2	0.00
Dec, Jan, Feb 3:00	-13.8	135.1	0.00
Dec, Jan, Feb 4:00	-4.7	124.6	0.33

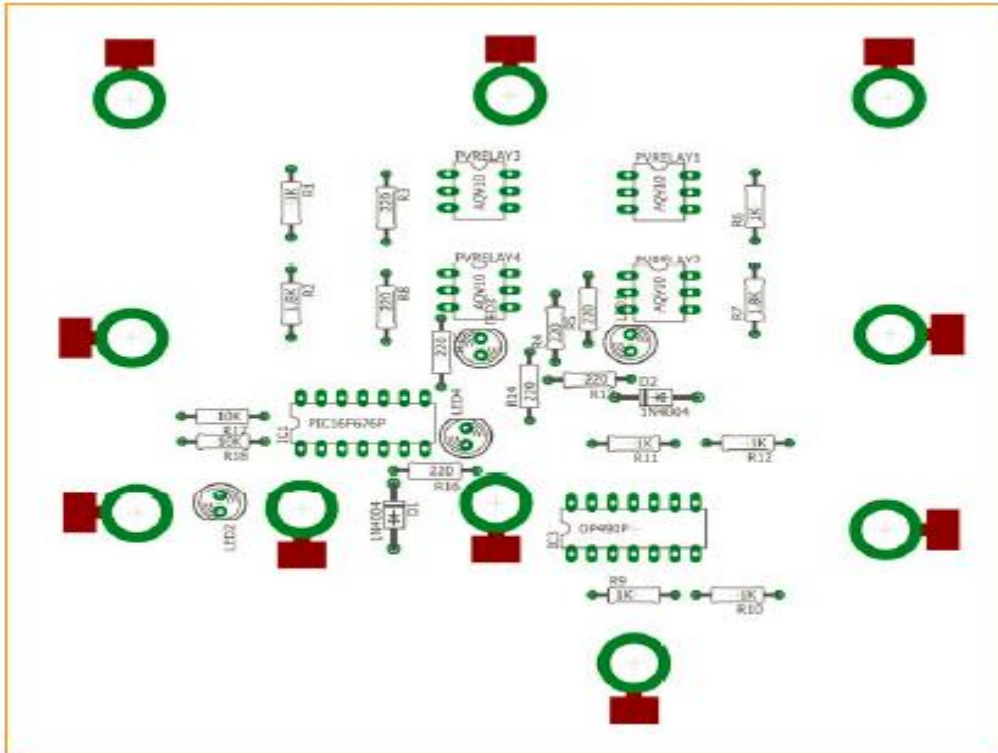
Dec, Jan, Feb 5:00	5.6	115.5	10.67
Dec, Jan, Feb 6:00	16.6	107.1	50.00
Dec, Jan, Feb 7:00	28.2	99	183.33
Dec, Jan, Feb 8:00	40	90.4	333.33
Dec, Jan, Feb 9:00	51.8	80.2	469.00
Dec, Jan, Feb 10:00	63.1	65.5	565.33
Dec, Jan, Feb 11:00	72.5	38.2	628.00
Dec, Jan, Feb 12:00	75.4	-12.2	645.67
Dec, Jan, Feb 13:00	68.8	-52.8	630.33
Dec, Jan, Feb 14:00	58.2	-72.9	567.33
Dec, Jan, Feb 15:00	46.6	-85	464.00
Dec, Jan, Feb 16:00	34.7	-94.3	323.00
Dec, Jan, Feb 17:00	23	-102.6	169.33
Dec, Jan, Feb 18:00	11.7	-110.7	40.33
Dec, Jan, Feb 19:00	0.9	-119.4	8.00
Dec, Jan, Feb 20:00	-8.9	-129.1	0.00
Dec, Jan, Feb 21:00	-17.3	-140.2	0.00
Dec, Jan, Feb 22:00	-23.8	-153.2	0.00
Dec, Jan, Feb 23:00	-27.8	-167.8	0.00
Autumn			
Mar, Apr, May 0:00	-52.2	178.5	0.00
Mar, Apr, May 1:00	-49.5	155	0.00
Mar, Apr, May 2:00	-42.7	135.6	0.00
Mar, Apr, May 3:00	-33.4	120.6	0.00
Mar, Apr, May 4:00	-22.6	108.7	0.00
Mar, Apr, May 5:00	-11.1	98.6	0.00
Mar, Apr, May 6:00	0.7	89.3	4.33
Mar, Apr, May 7:00	12.5	80	77.00
Mar, Apr, May 8:00	23.9	69.7	233.00
Mar, Apr, May 9:00	34.5	57.5	375.33
Mar, Apr, May 10:00	43.6	42	481.00
Mar, Apr, May 11:00	49.9	22.1	538.00
Mar, Apr, May 12:00	52	-1.6	546.00
Mar, Apr, May 13:00	49.3	-25	498.00
Mar, Apr, May 14:00	42.5	-44.3	433.67
Mar, Apr, May 15:00	33.1	-59.2	315.00
Mar, Apr, May 16:00	22.4	-71	177.67
Mar, Apr, May 17:00	10.9	-81.1	48.67
Mar, Apr, May 18:00	-1	-90.4	3.00
Mar, Apr, May 19:00	-12.8	-99.7	0.00
Mar, Apr, May 20:00	-24.2	-109.9	0.00
Mar, Apr, May 21:00	-34.9	-122.1	0.00
Mar, Apr, May 22:00	-44	-137.6	0.00
Mar, Apr, May 23:00	-50.4	-157.7	0.00
Winter			
Jun, Jly, Aug 0:00	-75.5	171.1	0.00

Jun, Jly, Aug 1:00	-69.3	129	0.00
Jun, Jly, Aug 2:00	-58.9	108	0.00
Jun, Jly, Aug 3:00	-47.3	95.6	0.00
Jun, Jly, Aug 4:00	-35.4	86.2	0.00
Jun, Jly, Aug 5:00	-23.7	77.9	0.00
Jun, Jly, Aug 6:00	-12.3	69.8	0.33
Jun, Jly, Aug 7:00	-1.5	61.1	28.00
Jun, Jly, Aug 8:00	8.3	51.5	163.33
Jun, Jly, Aug 9:00	16.9	40.5	298.00
Jun, Jly, Aug 10:00	23.5	27.6	395.33
Jun, Jly, Aug 11:00	27.6	13.1	450.00
Jun, Jly, Aug 12:00	28.7	-2.5	450.33
Jun, Jly, Aug 13:00	26.6	-17.9	428.67
Jun, Jly, Aug 14:00	21.6	-31.9	351.00
Jun, Jly, Aug 15:00	14.3	-44.2	250.67
Jun, Jly, Aug 16:00	5.3	-54.7	121.67
Jun, Jly, Aug 17:00	-4.9	-64	12.33
Jun, Jly, Aug 18:00	-15.9	-72.4	0.00
Jun, Jly, Aug 19:00	-27.4	-80.5	0.00
Jun, Jly, Aug 20:00	-39.2	-89	0.00
Jun, Jly, Aug 21:00	-51	-99.1	0.00
Jun, Jly, Aug 22:00	-62.4	-113.3	0.00
Jun, Jly, Aug 23:00	-72	-139.4	0.00

7.9 SCALED circuit schematic



7.10 PCB layout (top layer)



7.11 PCB layout (bottom layer)

